A. Hvatov

Torque Vibration Isolatior

masters project

AALBORG UNIVERSITET
2016

Title: Torque vibration isolator

Theme: Engineering Design of Mechanical Systems Master's Project

Project period:
01/02-2016 - 01/06-2016

Project group:
3.209

AALBORG UNIVERSITY
STUDENT REPORT
Department of Mechanical and Manufacturing Engineering
Fibigerstraede 16
DK 9220 Aalborg Oest
Tlf. 9940 9297
Fax 9815 1675
Web www.ses.aau.dk

Author:

Alexandr Hvatov

Supervisor:
Sergei Sorokin, Alf Soe-Knudsen

Synopsis:

In this project studied properties of complicated periodicity structure in scope of Floquet theory. Bernoulli-Euler beam model of vibration torque isolator is considered. Analytical solution is obtained by using of boundary integrals method, Green's matrix was derived using bi-orthogonality conditions. All solutions are verified with high-order theories and experiments series.

No. printed Copies: 3

No. of Appendix Pages: 30

Completed: 01/06-2016

Table of contents

Introduction

In the course of operation of a windturbine, a large torque, that has constant part and some time-dependent periodic part, is exerted in its gearbox. The periodically alternating part causes vibration of nacelle and tower, which should be reduced as much as possible. Vestas company looks for constructive solution for decreasing of vibration level that does not affect total durability and in same time does not significantly change price and construction of windmill.

Recently, it has become of much interest to consider periodic structures in vibro-isolational scope. It has been shown for different applications see e.g. [1–8], that periodic structures can generate such a vibration isolation. Therefore, the main idea of the master project is:

"Theoretical and experimental study of properties of the torque vibration isolator, which consists of a finite number of periodically alternating segments."

An idea for geometry of such isolator with sufficient static torque stiffness was purposed by Vestas company. It is sketched on Fig.1:

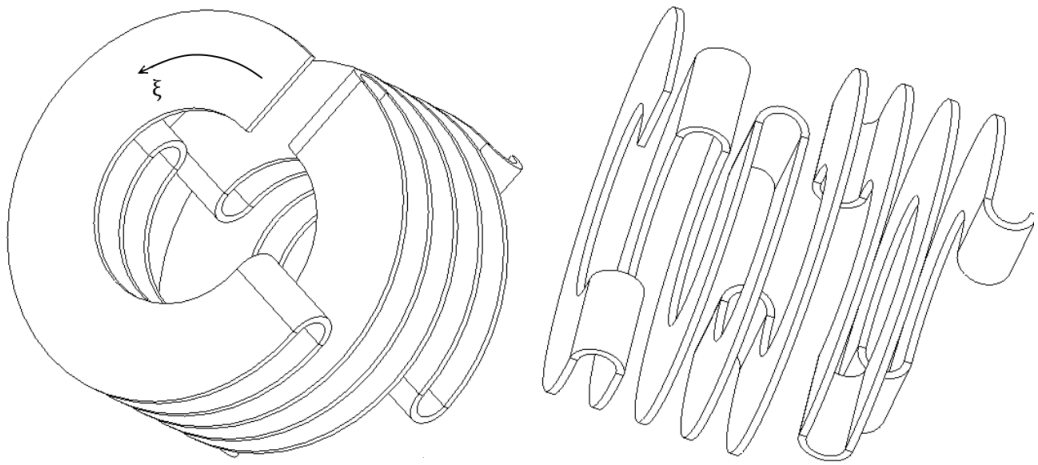

Figure 1: Vibration isolator sketch

In order to conduct experiments in vibration laboratory of Department of Mechanical and Manufacturing Engineering of Aalborg University it was scaled.

Models, considered in this master project are based on differential equations and in order to find solution of these equations following instruments are used:

1. Floquet theory is widely used to study dynamics of periodically alternating infinite structures. As shown for example in [7, 8] the performance of finite structures is in good correspondence with the performance of infinite ones and therefore Floquet theory gives good possibility to analyse both infinite and finite periodic structures and understand mechanisms of wave propagation in these structures.

2.Boundary Integral Equations method is used to find solution of a differential equation, using only information about function and its derivatives on the boundary of domain considered in given problem. In this method Green's matrices are commonly used, which are solution of equation with point force excitation. And in this work, bi-orthogonality conditions (in this work they are

used without detail explanation, because this theory lies out of scope of this work, more detailed description can be found in [9]) are employed to find Green's matrices.

All work divided in following subtasks:

(I) Derivation and evaluation of boundary integral equations for a beam model, based on Bernoulli-Euler theory

(II) Theoretical validation of the Bernoulli-Euler model for the frequency range of interest

(III) Experimental validation of the model and comparison with results obtained in (I)

Project is written in comprehensive way and information in appendices can be used as supply for more clear understanding of methods that are used in this project. Information in appendices is not mandatory for understanding ideas of this project.

Chapter 1

The concept of a periodic structure

In this chapter, all concepts and methods, used to analyse the waveguide properties of a torque vibration isolator, are displayed in full detail. For this purpose, a simple periodic structure is considered. Derivation of Green's function, boundary equations and Floquet equation are presented in an explicit analytical form.

Contents of this chapter are partially covered in the paper [8], co-authored by the author of this thesis. This paper also contains a comprehensive literature survey, which, therefore, is left out of the scope of this project.

1.1 Periodicity cell

Here general definitions for an arbitrary periodic structure considered in this work are introduced. First, an example of infinite periodic structure, which consists from two components and shown on Fig.1.1, can be considered:

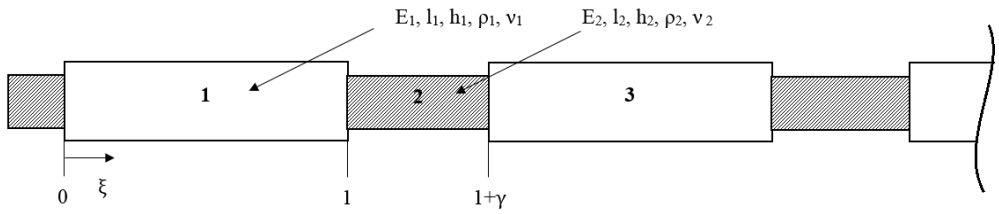

Figure 1.1: Infinite periodical structure scheme

,where ξ is the general coordinate (axial coordinate of a bar, radial coordinate of a circular membrane, natural coordinate of a spring). Each component of a periodic structure can have different material parameters (e.g. Young modulus), geometry parameters (e.g. curvature) and length repeating in periodic alternating manner. In order to use Floquet theory at least one parameter excluding length should be different for two segments. In terms of vibrations, different wavenumbers k_i for each part are required.

The existence of frequency stop- and pass-bands in infinite periodic waveguides is well known and understood since the pioneering work by L.Brillouin [1]. The vibro-acoustics of beams, plates, shells and pipes with periodic attachments or step-wise varying properties has been broadly explored by many authors. Classical works [1, 2] and the modern one [3–8] are just a few of those, which illustrate the classical and recent advances in this area of research. It is of interest to develop methods for various waveguides and make industrial application of theory of periodic structures.

Infinite structure can be considered as built from finite structures called periodicity cell. Here only periodicity cell with one period length are considered. Periodicity cells can be chosen arbitrary, for example as:

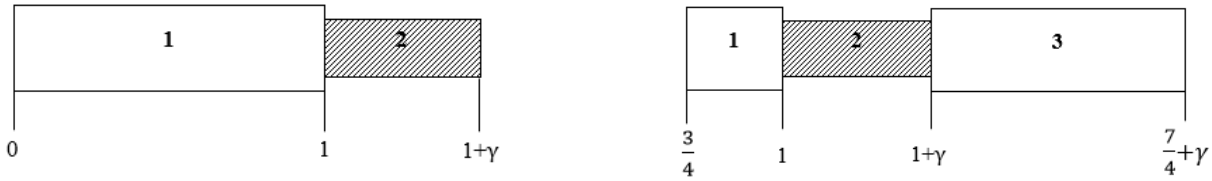

Figure 1.2: Different periodicity cells schemes

To explore the link between properties of finite and infinite periodic structures symmetrical cells should be considered, which can be schematically illustrated as:

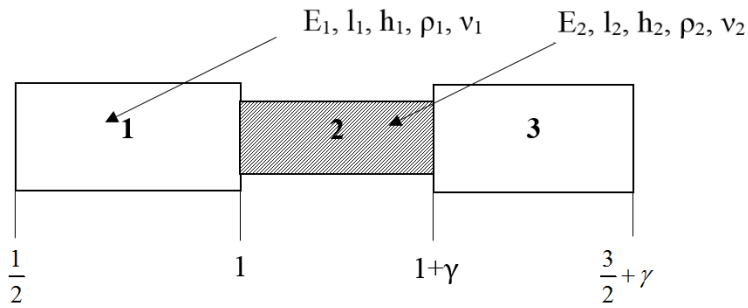

Figure 1.3: Symmetrical periodicity cell scheme (half "white"part - "black"part - half "white"part)

Since infinite structure can not be implemented practically, one can consider also finite structures, built from symmetrical cells. This kind of finite structures has some interesting properties, which will be described below. One can consider non-symmetrical cells as a 'building block' , but they require symmetrization of boundary conditions and will not be considered in this work.

Properties of finite and infinite structures are closely related to each other, and therefore both structures can be considered simultaneously in order to show full picture of wave propagation and vibrations.

1.2 Floquet theorem

Main tool for modelling used in this work is Floquet theorem. Floquet theorem is a powerful tool used in periodical differential operator analysis. Its most general formulation has form:

Let $\dot{x} = A(t)x$ be a system of differential equation, where $A(t+T) = A(t)$ is a periodical operator with period T. If $\Phi(t)$ - fundamental solution, then common solution can be written in form $\forall t \in R \quad \Phi(t+T) = \Phi(t)\Phi^{-1}(0)\Phi(T)$

This theorem also has a statement about Floquet normal form, but it will not be used here and therefore not presented. Main property, that used in this work is that solutions on one period length differs only on a constant multiplier $\Phi^{-1}(0)\Phi(T)$.

1.3 Straight rod example

Since tools used here have very wide scope of implementation it is convenient to show main properties and definitions on a simple example. Such example can be provided by the string equation, which also represents axial vibrations of a straight elastic rod with a uniform cross-section.

Let us consider infinite periodical rod, which schematically can be represented as Fig.1.1. Each part of a rod has an equation of vibration:

$$u_{xx} = \frac{1}{c_i^2} u_{tt} \tag{1.1}$$

Differential operator here can be written as:

$$A(x) = \frac{\partial}{\partial x^2} - \frac{1}{c_i^2(x)} \frac{\partial}{\partial t^2} \tag{1.2}$$

,where

$$c_i(x) = \begin{cases} \sqrt{\frac{E_1}{\rho_1}} & \text{if } x \in \text{'white' part} \\ \sqrt{\frac{E_2}{\rho_2}} & \text{if } x \in \text{'black' part} \end{cases} \tag{1.3}$$

Differential operator Eq.1.2 is obviously periodical with period of sum of lengths of both parts. With following harmonic vibration state considered:

$$u_i(x,t) = \bar{u}_i(x) \exp(-i\omega t) \tag{1.4}$$

Equation Eq.1.1 with Eq.1.4 has the form (bars are omitted):

$$u_i'' + k_i^2 u_i = 0 \tag{1.5}$$

,where $k_i = \frac{\omega}{c_i}$ - wave number.

1.3.1 Green's function

Solution of equation Eq.1.5 can be found in a different ways, but in order to illustrate methods, used in this work, Green's function (as a particular case of Green's matrix for a systems of differential equations) method for solving differential equations is used.

By definition, Green's function of axial vibration equation Eq.1.5 is a solution of following differential equation:

$$\frac{\partial}{\partial x^2} G(x, x_0) + k^2 G(x, x_0) = -\delta(x - x_0) \tag{1.6}$$

,where $\delta(x)$ is Dirac's delta function, x called observation point and x_0 - excitation point.

It can be proven that Green's function should satisfy following properties:

$$\begin{array}{l} G(x, x_0) = G(x_0, x) \\ \frac{\partial}{\partial x} G(x_0, x_0 + \varepsilon) - \frac{\partial}{\partial x} G(x_0, x_0 - \varepsilon) = -1,\ \varepsilon \to 0 \\ G(x_0, x_0 + \varepsilon) = G(x_0, x_0 - \varepsilon),\ \varepsilon \to 0 \end{array} \tag{1.7}$$

Solution of the equation can be written in a following form (if one should consider infinite beam, function $G(x, x_0)$ should satisfy radiation conditions at infinity [10]):

$$\begin{array}{l} G_+(x, x_0) = A\ \exp(ikx)\,, x > x_0 \\ G_-(x, x_0) = B\ \exp(-ikx)\,, x \leq x_0 \end{array} \tag{1.8}$$

Green's function in form Eq.1.8 substituted into two last properties in Eq.1.9 gives:

$$\begin{array}{l} G_+(x_0, x_0) = G_-(x_0, x_0) \\ \frac{d}{dx}(G_+(x, x_0) - G_-(x, x_0))\Big|_{x=x_0} = -1 \end{array} \tag{1.9}$$

or in the explicit form:

$$\begin{aligned} A\ \exp(ikx_0) &= B\ \exp(-ikx_0) \\ ikA\exp(ikx_0) + ikB\exp(-ikx_0) &= -1 \end{aligned} \tag{1.9'}$$

System Eq.1.9' has the unique solution for unknown coefficients A and B:

$$\{A, B\} = \{\frac{i}{2k}\exp(-ikx_0), \frac{i}{2k}\exp(ikx_0)\} \tag{1.10}$$

With constants obtained Green's function can be written as:

$$G(x, x_0) = \begin{cases} \frac{i}{2k}\exp(-ik(x - x_0)) & x \leq x_0 \\ \frac{i}{2k}\exp(ik(x - x_0)) & x > x_0 \end{cases} \tag{1.11}$$

Or in a short form:

$$G(x, x_0) = \frac{i}{2k}\exp(ik\ \mathrm{abs}(x - x_0)) \tag{1.12}$$

If this function plotted it is seen that all properties Eq.1.7 are fulfilled:

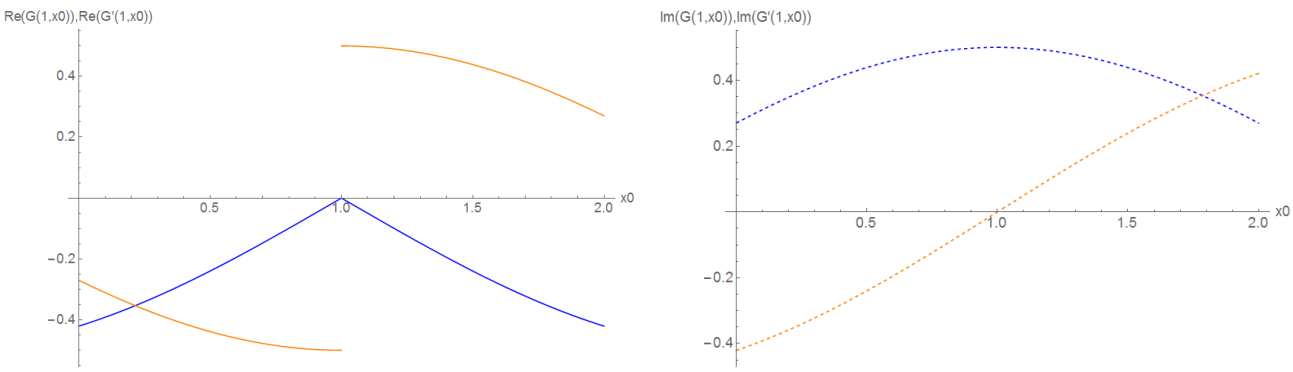

Figure 1.4: Green's function of axial rod vibration equation(blue) and its derivative(orange) real parts(left) and imaginary parts (right)

Green's function can be used in order to obtain solution of a differential equation with arbitrary load. Recalling axial rod vibrations equation:

$$u''(x) + k^2u(x) = -q(x) \tag{1.13}$$

And Green's function definition:

$$\frac{\partial^2}{\partial x^2}G(x, x_0) + k^2G(x, x_0) = -\delta(x - x_0) \tag{1.14}$$

In what follows $\frac{\partial}{\partial x}G(x, x_0) = G'(x, x_0)$
Multiplying equation 1.13 on $G(x, x_0)$ and integrating over beam length:

$$\int_a^b (u''(x) + k^2u(x))G(x, x_0)dx = -\int_a^b q(x)G(x, x_0)dx \tag{1.15}$$

First left hand side of an equation 1.15 considered:

$$I = \int_a^b (u''(x) + k^2u(x))G(x, x_0)dx \tag{1.16}$$

Considering following integral and using by-part integration:

$$I_1 = \int_a^b u''(x)G(x,x_0)dx = u'(x)G(x,x_0) - \int_a^b u'(x)G'(x,x_0)dx = \\ = [u'(x)G(x,x_0) - u(x)G'(x,x_0)]\Big|_a^b + \int_a^b u(x)G''(x,x_0)dx \tag{1.17}$$

And second part of integral just rewritten as:

$$I_2 = \int_a^b k^2 u(x)G(x,x_0)dx \tag{1.18}$$

With using equality $I = I_1 + I_2$ Eq.1.16 can be rewritten:

$$I = [u'(x)G(x,x_0) - u(x)G'(x,x_0)]\Big|_a^b + \int_a^b (G''(x,x_0) + k^2 G(x,x_0))u(x)dx \tag{1.19}$$

With Green's function definition Eq.1.14 one can rewrite Eq.1.19 in form:

$$I = [u'(x)G(x,x_0) - u(x)G'(x,x_0)]\Big|_a^b - \int_a^b \delta(x-x_0)u(x)dx \tag{1.20}$$

Dirac's delta-function has a property:

$$\int_a^b f(x)\delta(x-x_0)dx = f(x_0) \tag{1.21}$$

,which is valid for any range (a,b) that contains x_0 including $(-\infty,+\infty)$.
With property Eq.1.21 and recalling right hand side of Eq.1.15 one can rewrite it as:

$$u(x_0) = [u'(x)G(x,x_0) - u(x)G'(x,x_0)]\Big|_{x=a}^{x=b} + \int_a^b q(x)G(x,x_0)dx \tag{1.22}$$

Therefore, if values of displacements and axial forces on a rod boundaries are known, one can find displacement at any point of the rod. Eq.1.22 is called boundary integral equation for an axial rod vibrations equation.

Equation Eq.1.22 can be used in order to find displacements of a finite rod. After boundary conditions (displacements, forces or their linear combination on both ends) are stated, two boundary integrals with two boundary conditions give four equations for finding four unknowns $u(a), u(b), u'(a), u'(b)$. Obviously that system has unique solution. After unknowns found substituted into Eq.1.22, displacement of each point in range $[a,b]$ can be found.

It should be emphasized, that since $G'(x,x_0)$ has the singularity point $x = x_0$, directional limit should be taken. All limits taken such that points remain in interior of area in which boundary integrals are considered. In what follows it is assumed that limits are taken correctly.

1.3.2 Floquet theory example

Now we can return to a structure, illustrated on the Fig.1.1. Each segment has two unknown boundary displacements $u_i(x_{i1}), u_i(x_{i2})$ and two forces $u_i'(x_{i1}), u_i'(x_{i2})$. Therefore for n consequent segments we should state $4n$ equations in order to fully determine system.

Let us consider three consequent parts. For each we can state two boundary equations in form (to preserve brevity we consider free vibrations (q(x)=0)):

$$\begin{aligned}
u_1(0) &= [u_1'(x)G(x,0) - u_1(x)G'(x,0)]\Big|_{x=0}^{x=1} \\
u_1(1) &= [u_1'(x)G(x,1) - u_1(x)G'(x,1)]\Big|_{x=0}^{x=1} \\
u_2(1) &= [u_2'(x)G(x,1) - u_2(x)G'(x,1)]\Big|_{x=1}^{x=1+\gamma} \\
u_2(1+\gamma) &= [u_2'(x)G(x,1+\gamma) - u_2(x)G'(x,1+\gamma)]\Big|_{x=1}^{x=1+\gamma} \\
u_3(1+\gamma) &= [u_3'(x)G(x,1+\gamma) - u_3(x)G'(x,1+\gamma)]\Big|_{x=1+\gamma}^{x=2+\gamma} \\
u_3(2+\gamma) &= [u_3'(x)G(x,2+\gamma) - u_3(x)G'(x,2+\gamma)]\Big|_{x=1+\gamma}^{x=2+\gamma}
\end{aligned} \tag{1.23}$$

And interfacial conditions:

$$\begin{aligned}
&u_1(1) = u_2(1) \\
&u_1'(1) = \alpha\beta u_2'(1) \\
&u_2(1+\gamma) = u_3(1+\gamma) \\
&\alpha\beta u_2'(1+\gamma) = u_3'(1+\gamma)
\end{aligned} \tag{1.24}$$

,where $\alpha = \frac{E_2}{E_1}, \beta = \frac{A_2}{A_1} = \frac{h_2}{h_1}$

For n consequent cells system of boundary equations and interfacial conditions we have $4n-2$ equations and therefore we need two more equations in order to close the system. Floquet theorem in form "solutions in one period length differ only on a constant multiplier" provides two more equations in form:

$$\begin{aligned}
u_1(0) &= \Lambda u_3(1+\gamma) \\
u_1'(0) &= \Lambda u_3'(1+\gamma)
\end{aligned} \tag{1.25}$$

Equations Eq.1.23-Eq.1.25 give 12 required equations for 3 consequent cells. And, since multiplier Λ is constant it is enough to determine solution at any point of an infinite periodical waveguide.

Equations Eq.1.23-Eq.1.25 also define closed homogenous system of linear algebraic equations with respect to twelve unknown displacement/forces $u_i(x_i), u_i'(x_i)$ and its determinant is equal to:

$$D(\Lambda,\Omega) = \Lambda^2 + \frac{\Lambda\left(\alpha^2\beta^2+\sigma^2\right)\sin(\lambda\Omega)\sin\left(\frac{\gamma\lambda\Omega}{\sigma}\right)}{\alpha\beta\sigma} - 2\Lambda\cos(\lambda\Omega)\cos\left(\frac{\gamma\lambda\Omega}{\sigma}\right) + 1 \tag{1.26}$$

In should be emphasized that free term of this equation is equal to one. That, by Vieta's theorem, means, that we have one pair of roots such that their product is equal to one. That is common property of polynomials, obtained with using Floquet theory in cartesian coordinates. Such pair of roots in this work called Floquet equation branch.

In order to find non-trivial solutions of the system Eq.1.23-Eq.1.25 we use condition $D(\Lambda,\Omega) = 0$ which can be plotted as:

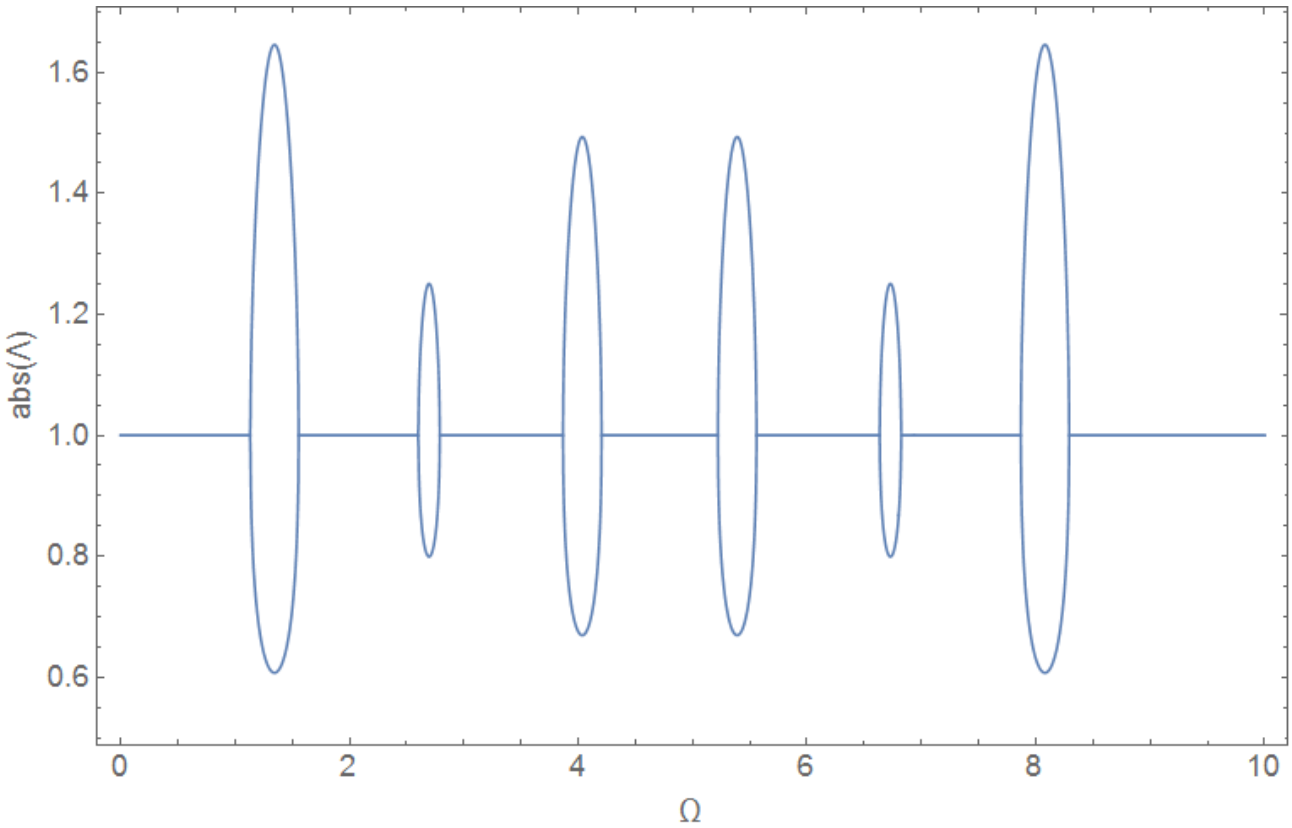

Figure 1.5: Picture of Floquet zones $D(\Lambda, \Omega) = 0$

Zones, where $\text{abs}(\Lambda) = 1$ are called pass-bands and zones with $\text{abs}(\Lambda) \neq 1$ are called stop- or gap-bands respectively. In pass band wave magnitude is not changing throughout period and therefore wave propagating freely. In stop bands we got exponentially decreasing and exponentially increasing wave and therefore energy propagation is fully (or partially in case of several branches, which will be shown later) blocked.

It should be emphasized, that since we consider infinite structure, Floquet theory doesn't depend on a boundary conditions. If one consider energy flow through finite structure (see [8]), it can be shown that Floquet zones are exact limiting case for sufficient number of periodicity cells for any boundary conditions. That proposition allows one to reduce number of experiments or simplify them in case if only Floquet zones are of interest.

One can consider symmetrical periodicity cell, shown on the Fig.1.3 as finite structure. Here instead of Floquet conditions boundary conditions stated. For one periodicity cell one can state A-type conditions:

$$\begin{aligned} u_1(1/2) &= 0 \\ u_3(3/2+\gamma) &= 0 \end{aligned} \tag{1.27}$$

And B-type conditions:

$$\begin{aligned} u_1'(1/2) &= 0 \\ u_3'(3/2+\gamma) &= 0 \end{aligned} \tag{1.28}$$

Boundary and Interfacial conditions Eq.1.23-Eq.1.24 with boundary conditions Eq.1.27 or Eq.1.28 also define homogenous system of algebraical equations. We can find eigenfrequencies of this system and plot them (in order to better comparison eigenfrequencies shown on the line $\text{abs}(\Lambda) = 1$) as:

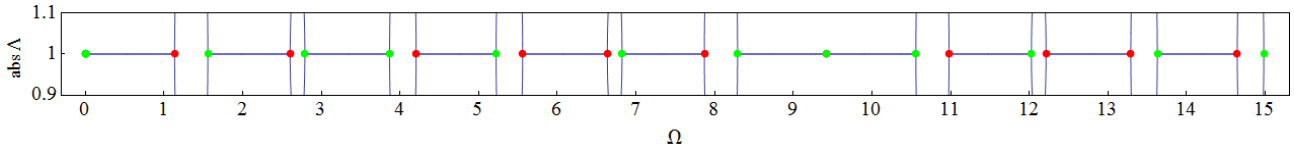

Figure 1.6: Eigenfrequencies of a single periodicity cell A-type conditions (red) and B-type conditions(green)

As seen, eigenfrequencies of A- and B-type boundary problems fully covers gap band borders. Existence of such two types of boundary conditions were predicted by [2] and required theory for obtaining such types was developed in [9]. It should be emphasized that non-symmetrical cell shown on Fig.1.2 can also have such kind of properties but principle of obtaining 'symmetrizing' conditions is not well studied. Therefore it is convenient to consider symmetrical cells.

One can consider finite structure consisting of more than one periodicity cells. In that case eigenfrequencies will appear only in pass-band:

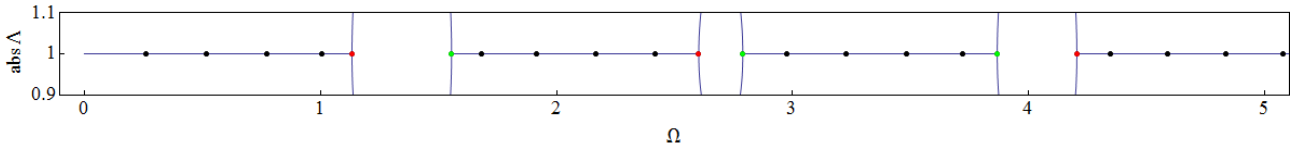

Figure 1.7: Eigenfrequencies of five periodicity cells

In this chapter Green function, boundary integrals method and Floquet theory was introduced, this is main tools, used for modelling of vibration isolator in this work, also some basic definitions, which will be used in following chapters were introduced and illustrated with simple example.

Chapter 2

Mathematical model

In this chapter a mathematical model of a torque vibration isolator is considered. Methods from previous chapter (Floquet theorem, boundary integrals method) have broad range of applicability. In this chapter all these methods are used for more complicated case of system of differential equations. This chapter has theoretical and practical goals. Practical goal is to build model of torque vibration isolator in the form of a system of differential equations, that captures all wave phenomena in the frequency range of interest. Theoretical goal is to show the difference between the structure of Floquet zones of a single differential equation and a system of differential equations. In order to achieve that, methods, considered in Ch.1 are expanded and full range of tools for system of differential equations is obtained.

Torque vibration isolator has following periodicity cell with four different parts illustrated on the Fig. 2.1:

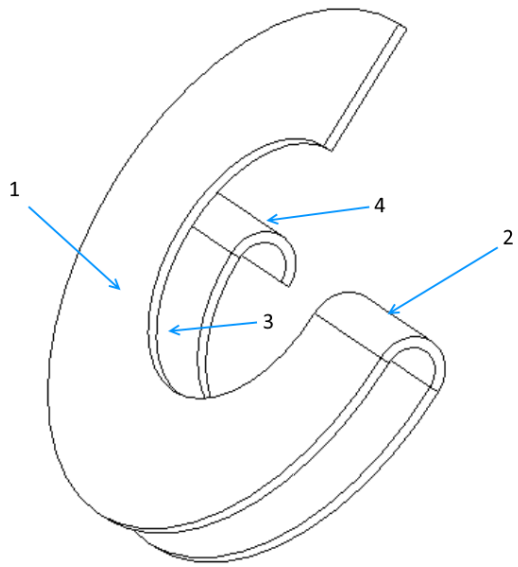

Figure 2.1: Vibration torque part

Parts 1 and 3 are the segments of a circular plate and part 2 and 4 are the segment of a thin cylindrical shell. Each of these elements is much stiffer in transverse direction than in longitudinal. Thus, as first approximation, the curved Bernoulli-Euler beam model can be used. Parts one and three differ with angular lengths whereas parts two and four considered with same shape and parameters in this work.

2.1 Bernoulli-Euler curved beam model

Since Floquet theorem is formulated for a general case of systems of linear differential equations with periodical coefficients, it can be used for more complicated differential operators than one considered in Ch.1. Nevertheless, main ideas, shown in Ch.1 do not change significantly for differential operators with higher number of equations and variables. Vibrations equations and Green's matrix derivation are shown in App.A. In this section differences in application of Floquet theory in higher dimensions are considered.

2.1.1 Infinite periodic structure

Each curved beam segment can have different material, cross-section parameters and geometry. In case of different part materials dimensionless parameters can be introduced as:

$$\alpha_{par} = \frac{E_2}{E_1}; \gamma = \frac{l_2}{l_1};\ \sigma = \frac{c_2}{c_1}; \lambda = \frac{l_1}{h_1};\ \Omega_1 = \Omega;\ \Omega_2 = \frac{\Omega}{\sigma};\ \ \varepsilon_1 = \frac{h_1}{R_1};\ \varepsilon_2 = \frac{h_2}{R_2} \tag{2.1}$$

Since we consider structure, where each segment has the same material and same cross-section parameters, but different curvature radius, hereafter following dimensionless parameters set for computation is considered unless it is stated otherwise (notation α_{par} introduced in order to distinguish $\alpha(s)$ as a rotational angle and α_{par} as a parameter in Ch.1):

$$\alpha_{par} = 1; \gamma = 0.5;\ \sigma = 1; \lambda = 5;\ \varepsilon_1 = 0.2;\ \varepsilon_2 = 0.02 \tag{2.2}$$

It should be emphasized that local coordinates (axes are aligned with respect to principal axes of inertia) are changing for each part as shown on Fig.2.2:

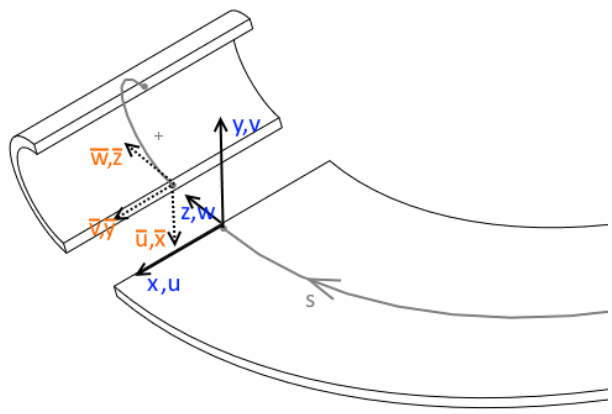

Figure 2.2: Local coordinates for different parts

Coordinate change is rotation on the angle $\pi/2$ with respect to z axis. Therefore, displacements at the interface changing as:

$$\begin{aligned} u = \bar{v},\ v = -\bar{u},\ w = \bar{w} \\ \alpha = -\bar{\beta},\ \beta = -\bar{\alpha},\ \gamma = \bar{\gamma} \end{aligned} \tag{2.3}$$

In order to take local coordinate change into account, following vector notation introduced:

$$\begin{aligned} \vec{d}_{i1}(s) &= \{w_{i1}(s), \beta_{i1}(s), u_{i1}(s), v_{i1}(s), \gamma_{i1}(s), \alpha_{i1}(s)\}^T \\ \vec{f}_{i1}(s) &= \tfrac{1}{E_{i1}I_x^{i1}}\{Q_x^{i1}(s), N_z^{i1}(s), M_y^{i1}(s), Q_y^{i1}(s), M_x^{i1}(s), T_z^{i1}(s)\}^T \\ \vec{d}_{i2}(s) &= \{w_{i2}(s), -\alpha_{i2}(s), v_{i2}(s), -u_{i2}(s), \gamma_{i2}(s), -\beta_{i2}(s)\}^T \\ \vec{f}_{i2}(s) &= \tfrac{1}{E_{i2}I_x^{i2}}\{Q_y^{i2}(s), N_z^{i2}(s), -M_x^{i2}(s), -Q_x^{i2}(s), -M_y^{i2}(s), T_z^{i2}(s)\}^T \end{aligned} \tag{2.4}$$

,where $i1 = 1, 3, 5, ...$ and $i2 = 2, 4, 6, ...$ It should be noted, that normalizing multiplier $\frac{1}{EI_x}$ is used for all forces and moments. Below it is assumed, that all forces and moments are defined correctly and normalized to $\frac{1}{EI_x}$.

Let us consider structure shown on Fig.2.1. For each part of this structure (they shown with a numbers) we define two set of three boundary integrals (see App. A for detailed explanation and boundary integrals derivation) in form Eq.A.23 and Eq.A.28 (totally, 6*8=48 boundary integrals) and additionally interfacial conditions :

$$\begin{aligned}
&w_1(t_1) = w_2(t_1)\,;\beta_1(t_1) = -\alpha_2(t_1)\,;u_1(t_1) = v_2(t_1)\\
&\gamma_1(t_1) = \gamma_2(t_1)\,;v_1(t_1) = -u_2(t_1)\,;\alpha_1(t_1) = -\beta_2(t_1)\\
&N_z^{(1)}(t_1) = \alpha_{par}\,N_z^{(2)}(t_1)\,;M_y^{(1)}(t_1) = -\alpha_{par}\,M_x^{(2)}(t_1)\,;Q_x^{(1)}(t_1) = \alpha_{par}\,Q_y^{(2)}(t_1)\\
&T_z^{(1)}(t_1) = \alpha_{par}\,T_z^{(2)}(t_1)\,;Q_y^{(1)}(t_1) = -\alpha_{par}\,Q_x^{(2)}(t_1)\,;M_x^{(1)}(t_1) = -\alpha_{par}\,M_y^{(2)}(t_1)\\
&...
\end{aligned} \tag{2.4a}$$

Or in vector form (totally 6*6=36 interfacial equations):

$$\begin{aligned}
&\vec{d_1}(t_1) = \vec{d_2}(t_1)\\
&\vec{f_1}(t_1) = \alpha\,\vec{f_2}(t_1)\\
&\vec{d_2}(t_1 + \gamma\,t_2) = \vec{d_3}(t_1 + \gamma\,t_2)\\
&\alpha\vec{f_2}(t1 + \gamma\,t_2) = \vec{f_3}(t_1 + \gamma\,t_2)\\
&\vec{d_3}((t_1 + t_3) + \gamma\,t_2) = \vec{d_4}((t_1 + t_3) + \gamma\,t_2)\\
&\vec{f_3}((t_1 + t_3) + \gamma\,t_2) = \alpha\vec{f_4}((t_1 + t_3) + \gamma\,t_2)
\end{aligned} \tag{2.4b}$$

In this work one turn of larger curvature $2\pi R_1$ taken as a unit length. Since parts of torque vibrational isolator are shorter than one turn it is convenient to consider fractions of whole turn $t_i = \frac{l_i^{(ang)} R_1}{2\pi R_1}$, $l_i^{(ang)}$ – angular length (in radians) of i-th part, i.e. t_i is the fraction of whole turns done by i-th part. With model and parameters used in this work t_1, t_3 are numbers of turns of parts with large curvature (on Fig.2.1 $t_1 = \frac{3}{4} = 0.75, t_3 = 0.5$) and t_2, t_4 are numbers of turns of second part with small curvature ($t_2 = t_4 = 0.5$ on Fig.2.1).

Period of structure is the sum of all turns, but since smaller curvature has smaller arc length (but can have same angular) we use parameter $\gamma = \frac{l_2}{l_1}$ - ratio of arc lengths, and total period is $T = t_1 + t_3 + \gamma(t_2 + t_4)$.

And Floquet periodicity conditions (2*6=12 equations):

$$\begin{aligned}
&u_1(0) = \Lambda\,u_4((t_1 + t_3) + \gamma\,(t_2 + t_4)); \quad v_1(0) = \Lambda\,u_4((t_1 + t_3) + \gamma\,(t_2 + t_4));\\
&w_1(0) = \Lambda\,u_4((t_1 + t_3) + \gamma\,(t_2 + t_4)); \quad \alpha_1(0) = \Lambda\,\alpha_4((t_1 + t_3) + \gamma\,(t_2 + t_4));\\
&\beta_1(0) = \Lambda\,\beta_4((t_1 + t_3) + \gamma\,(t_2 + t_4)); \quad \gamma_1(0) = \Lambda\,\gamma_3((t_1 + t_3) + \gamma\,(t_2 + t_4))\\
&M_x^{(1)}(0) = \Lambda\,M_x^{(4)}((t_1 + t_3) + \gamma\,(t_2 + t_4)); \quad M_y^{(1)}(0) = \Lambda\,M_y^{(4)}((t_1 + t_3) + \gamma\,(t_2 + t_4));\\
&T_z^{(1)}(0) = \Lambda\,T_z^{(4)}((t_1 + t_3) + \gamma\,(t_2 + t_4)); \quad Q_x^{(1)}(0) = \Lambda\,Q_x^{(4)}((t_1 + t_3) + \gamma\,(t_2 + t_4));\\
&Q_y^{(1)}(0) = \Lambda\,Q_y^{(4)}((t_1 + t_3) + \gamma\,(t_2 + t_4)); \quad N_z^{(1)}(0) = \Lambda\,N_z^{(4)}((t_1 + t_3) + \gamma\,(t_2 + t_4))
\end{aligned} \tag{2.5a}$$

Or in vector form:

$$\begin{aligned}
&\vec{d_1}(0) = \Lambda\,\vec{d_4}((t_1 + t_3) + \gamma\,(t_2 + t_4))\\
&\vec{f_1}(0) = \Lambda\,\vec{f_4}((t_1 + t_3) + \gamma\,(t_2 + t_4))
\end{aligned} \tag{2.5b}$$

Total amount of equations is $48 + 36 + 12 = 96$ equations.

Boundary integrals for each part with conditions Eq.2.4a-Eq.2.5b define homogenous system of the algebraical equations with respect to unknown displacements and forces on borders of the isolator parts (each part defined with 2*12=24 constants, for four parts 4*24=96). Let $D(\Lambda, \Omega)$ be the determinant of this system. $D(\Lambda, \Omega)$ is the twelfth order polynomial in Λ , which defines stop- and pass-bands. It should be empathized, that determinant $D(\Lambda, \Omega)$ factorizes in two sixth order polynomials in Λ , i.e. $D(\Lambda, \Omega) = D^{w,u}(\Lambda, \Omega) * D^{\gamma,v}(\Lambda, \Omega) = D^{\bar{w},\bar{v}}(\Lambda, \Omega) * D^{\bar{\gamma},\bar{u}}(\Lambda, \Omega)$. Therefore these two parts can be considered independently.

If we consider flat structure case shown on Fig.2.3, $D^{w,u}$ has meaning of flexural-axial part or in-plane of a Floquet determinant and $D^{\gamma,v}$ has meaning of flexural-torsional or out-of-plane part. In spatial structure case, considered on this project and shown on Fig.2.1 we can't define plane, that contains whole structure and therefore in- and out-of-plane notations lose its meaning.

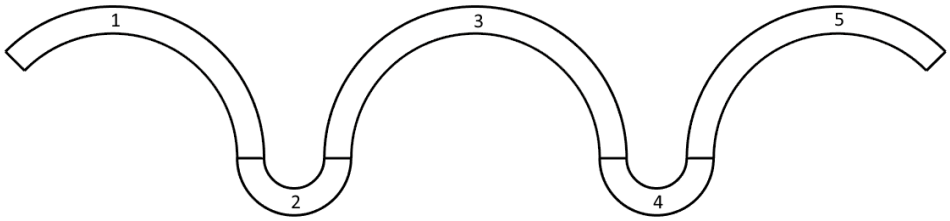

Figure 2.3: Flat structure

It should be noted that both of determinants $D^{w,u}(\Lambda, \Omega)$ and $D^{\gamma,v}(\Lambda, \Omega)$ can be written in form:

$$D^*(\Lambda, \Omega) = \Lambda^6 + a_5\Lambda^5 + a_4\Lambda^4 + a_3\Lambda^3 + a_2\Lambda^2 + a_1\Lambda + 1 \tag{2.7}$$

It has two properties:

1. By Vieta theorem and waveguide symmetry properties, since free term of polynomial $D^*(\Lambda, \Omega)$ is 1, if Λ is a root of polynomial Eq.2.7, then Λ^{-1} is a root of polynomial too.

2. It has only even powers of Ω as coefficients a_i because no damping is considered.

One can plot dependency Λ of Ω, for example from condition $D^{w,u}(\Lambda, \Omega) = 0$. Unlike the cases considered earlier in [8] there exists three pairs with property $\Lambda_1 * \Lambda_2 = 1$, i.e. three branches of solutions $\Lambda_i(\Omega)$: one pair of exponentially increasing and decreasing branches (this couple is not shown below, because it forms stop-band on all frequency range and therefore does not affect on Floquet zones picture) and two pair of branches that defines stop- and pass-bands, it preserves for both determinants $D^{w,u}$ and $D^{\gamma,v}$. Below dependence $\Lambda(\Omega)$ from $D^{w,u}(\Lambda, \Omega) = 0$ is plotted :

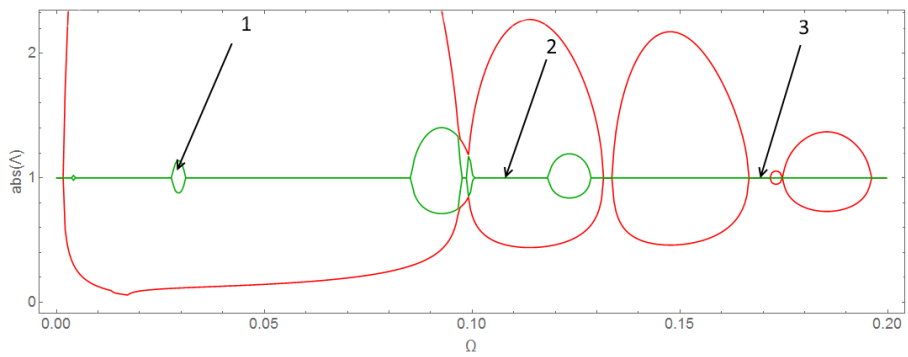

Figure 2.4: Floquet zones for $D^{w,u}(\Lambda, \Omega)$ and different kinds of zones marked with numbers

One can distinct “full” stop-band (marked as 1), where wave propagation is fully blocked, its location is defined by intersection of stop-bands of two branches (overlapping of an green stop band and a red stop band on the Fig.2.4). In zone 1 only exponential increasing-decreasing standing waves are presented. "Partial" stop-band (marked as 2) its location defined by overlapping pass band and stop band of different branches (overlapping of a red stop band and an green pass band and vice versa). In zone 2 appears one propagating wave. And pass-band (marked as 3) its location defined as overlapping of two pass bands of different branches (an green pass band and a red pass band) in zone 3 two propagating waves are presented. All three zones contains one pair of standing exponential increasing-decreasing standing waves, which is described above and not shown on the picture.

Dependence $\Lambda(\Omega)$ from $D^{v,\gamma}(\Lambda,\Omega)=0$ has the similar form:

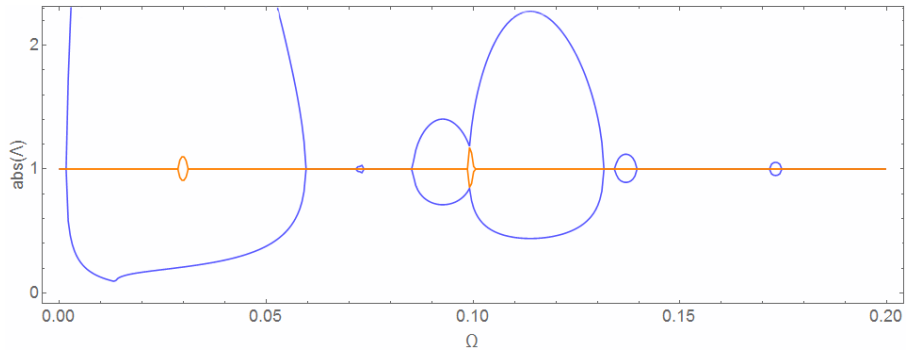

Figure 2.5: Floquet zones for $D^{\gamma,v}(\Lambda,\Omega)$

Since model considered as whole, both pictures for $D^{w,u}$ and $D^{\gamma,v}$ vibrations should be considered simultaneously, but for visual reason they are separated. For comparison, both figures Fig.2.4 and Fig.2.5 shown in one plot:

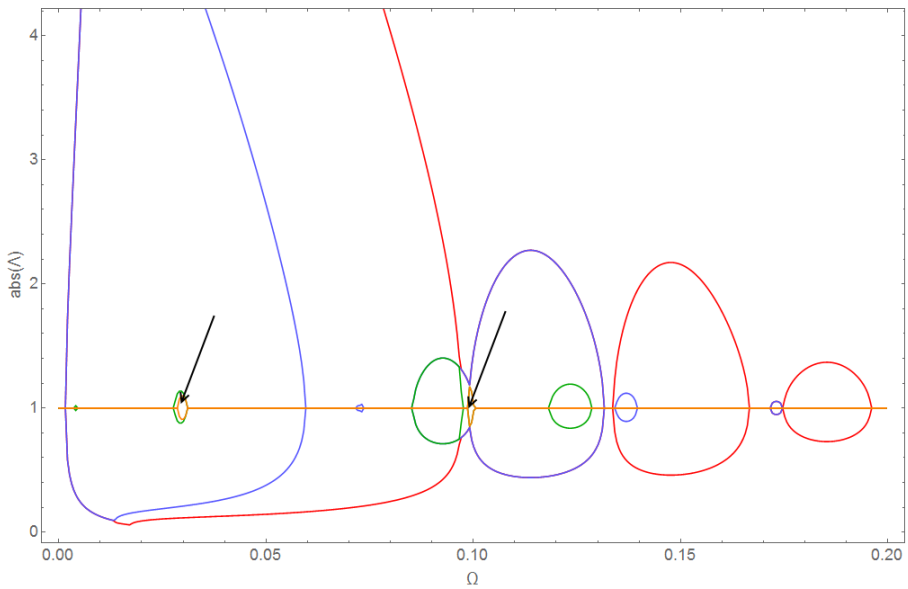

Figure 2.6: Floquet zones for $D(\Lambda,\Omega)$ (with arrow marked "full"stop-bands)

As seen, there are zones (they shown with arrows), where all 6 branches have $\text{abs}(\Lambda)\neq 1$ and therefore wave propagation is fully blocked.

In rod axial vibrations case, considered in Ch.1 all computations can be validated using transfer matrix method, that was done in [7, 8]. In more complicated cases matrices, that are obtained with transfer matrix method are ill conditioned and therefore it can’t be used for validation. Nevertheless,

with transfer matrix method one can obtain displacements (eigenfrequencies) of a single part (for example one, that numbered 1 on Fig.2.1), which works only on initial stages and shown in [11]. Even though there are other methods for finding solution (for example integral transformations like Fourier-Laplace transform) for system of differential equations, their consideration is away from scope of this work and therefore theoretical validation was not done. In this work model will be validated with experiments.

2.1.2 Finite periodic structure

As in previous cases one can introduce concept of a symmetrical periodicity cell. Cell on a Fig.2.1 obviously is not symmetrical one. Therefore we cut first part equally and attach it to the last one, which schematically can be shown as:

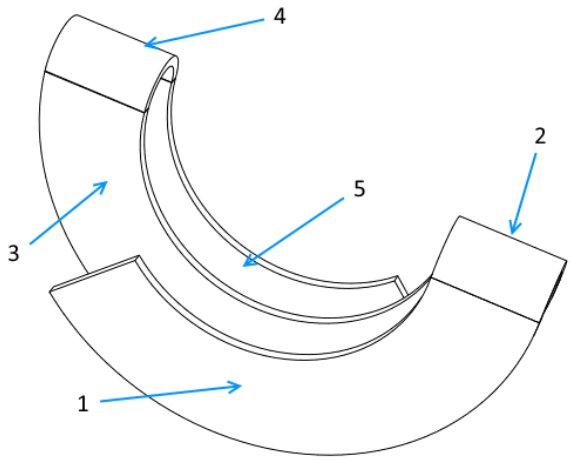

Figure 2.7: Symmetrical periodicity cell

, here length of the first and the fifth parts is $\frac{t_1}{2} = \frac{3}{8}$

One can find eigenfrequencies of this structure. For each part boundary integrals in form A.23 are stated. Also, interfacial conditions are changed as (one part added):

$$\begin{aligned}
&\vec{d_1}(t_1) = \vec{d_2}(t_1)\\
&\vec{f_1}(t_1) = \alpha\,\vec{f_2}(t_1)\\
&\vec{d_2}(t_1 + \gamma\, t_2) = \vec{d_3}(t_1 + \gamma\, t_2)\\
&\alpha\vec{f_2}(t1 + \gamma\, t_2) = \vec{f_3}(t_1 + \gamma\, t_2)\\
&\vec{d_3}((t_1 + t_3) + \gamma\, t_2) = \vec{d_4}((t_1 + t_3) + \gamma\, t_2)\\
&\vec{f_3}((t_1 + t_3) + \gamma\, t_2) = \alpha\vec{f_4}((t_1 + t_3) + \gamma\, t_2)\\
&\vec{d_4}((t_1 + t_3) + \gamma\,(t_2 + t_4)) = \vec{d_5}((t_1 + t_3) + \gamma\,(t_2 + t_4))\\
&\vec{f_4}((t_1 + t_3) + \gamma\,(t_2 + t_4)) = \alpha\vec{f_5}((t_1 + t_3) + \gamma\,(t_2 + t_4))
\end{aligned} \tag{2.4b}$$

Instead of Floquet conditions, boundary conditions are stated. In this case it is two groups of functions Eq.A.16 and Eq.A.24 discussed in App.A. Here Mead [2] A- and B-type boundary conditions terminology, discussed in Ch.1, is preserved.

A-type boundary conditions for one periodicity cell defined as [12]:

$$\begin{aligned}
&\{w(\tfrac{t_1}{2}), \beta(\tfrac{t_1}{2}), Q_x(\tfrac{t_1}{2}), v(\tfrac{t_1}{2}), \gamma(\tfrac{t_1}{2}), M_x(\tfrac{t_1}{2})\} = 0\\
&\{w(\tfrac{t_1}{2} + T), \beta(\tfrac{t_1}{2} + T), Q_x(\tfrac{t_1}{2} + T), v(\tfrac{t_1}{2} + T), \gamma(\tfrac{t_1}{2} + T), M_x(\tfrac{t_1}{2} + T)\} = 0
\end{aligned} \tag{2.8}$$

And B-type boundary conditions as:

$$\begin{aligned}&\{u(\tfrac{t_1}{2}), N_z(\tfrac{t_1}{2}), M_y(\tfrac{t_1}{2}), \alpha(\tfrac{t_1}{2}), Q_y(\tfrac{t_1}{2}), T_z(\tfrac{t_1}{2})\} = 0\\ &\{u(\tfrac{t_1}{2}+T), N_z(\tfrac{t_1}{2}+T), M_y(\tfrac{t_1}{2}+T), \alpha(\tfrac{t_1}{2}+T), Q_y(\tfrac{t_1}{2}+T), T_z(\tfrac{t_1}{2}+T)\} = 0\end{aligned} \tag{2.9}$$

,where $T = (t_1 + t_3) + \gamma_{par}(t_2 + t_4)$ one period length.

Boundary integrals with interfacial conditions Eq.2.4b and boundary conditions Eq.2.8 or Eq.2.9 defines also homogenous system of linear algebraical equations with respect to unknown displacements and forces/moments at the ring parts borders. Final system has order of 120×120. And by equaling determinant of this system to zero we can find eigenfrequencies. Eigenfrequencies of system Eq.2.8 and Eq.2.9 fully covers stop-band borders as in other cases considered in Ch.1 and [8].

Determinant of the system Eq.2.4a, Eq.2.8 or Eq.2.4a, Eq.2.9 also can be factorized into two parts: flexural-axial and flexural-torsional. And also both parts will be shown separately for clarity. Flexural-axial eigenfrequencies can be plotted as:

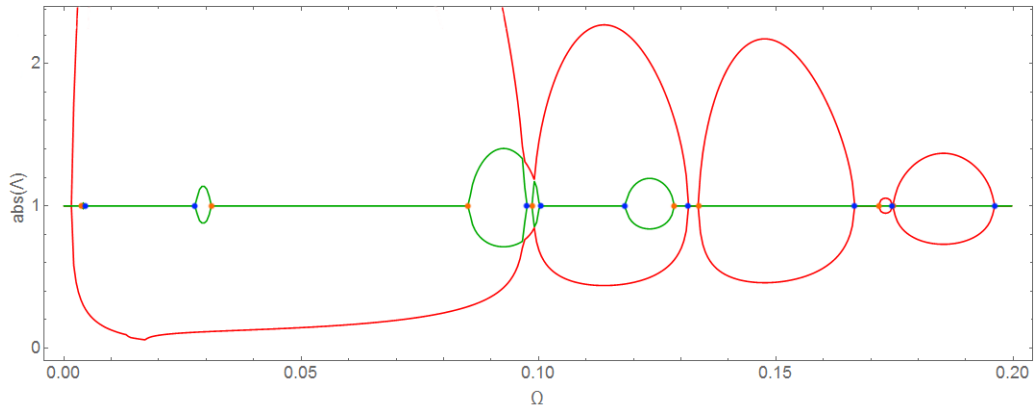

Figure 2.8: Eigenfrequencies of the single periodical cell (flexural-axial part): boundary conditions A (blue) and boundary conditions B (orange)

Picture shown that property of eigenfrequencies of a single periodicity cell is preserved. Eigenfrequency of a single periodicity cell appears only in gap bands borders and covers all borders of gap bands. If one considers $D^{v,\gamma}$, same property can be seen:

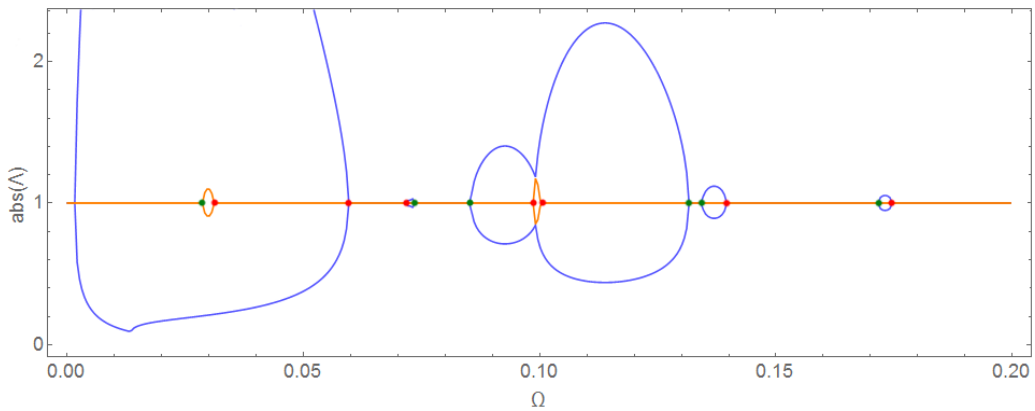

Figure 2.9: Eigenfrequency of single periodicity cell (flexural-torsional part): boundary conditions A (red) and boundary conditions B (green)

As seen, properties of eigenfrequencies, considered in [7], [8] and Ch.1 are preserves for Bernoulli-Euler curved beam case.

2.1.3 Eigenmodes analysis

Eigenmode analysis gives clear understanding of wave propagation picture in infinite waveguide. Form of waves and energy transmission mode (standing or propagating wave) can be easily shown when eigenmodes analysis is performed. More detailed eigenmodes analysis for axial rod vibration case is performed in [8]. Here just main steps are shown.

First same procedure used and determinant $D(\Lambda, \Omega)$ obtained from system Eq.2.4a-Eq.2.5b. As shown above in case of a curved beam second branch of Floquet zones appears. And difference between full and partial gap-band can be considered (see Fig.2.4).

For each root of the polynomial $D^{w,u}(\Lambda, \Omega)$ one can find eigenmodes of in-plane vibrations.For given frequency Ω system Eq.2.4a-Eq.2.5b with parameter Λ substituted has zero determinant. Therefore, one unknown assumed as a constant, for example $u_1(0) = 1$ and one arbitrary equation of the system excluded from consideration. For certainty system Eq.2.4a-Eq.2.5b with first equation changed to $u_1(0) = 1$ called eigenmode of infinite waveguide. In the pure gap-band all waves are standing:

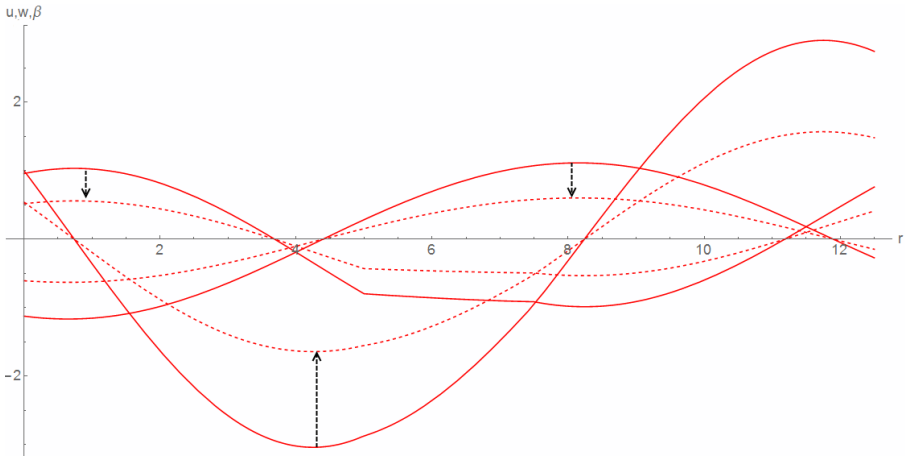

Figure 2.10: Standing waves in pure gap-band $\Omega = 0.037$

In all cases all waved coupled as increasing-evanescent or traveling from left to right and right-left in three groups such that $\Lambda_1 * \Lambda_2 = 1$. In partial gap-band appears one pair of propagating travelling waves, whereas other two pairs are standing and coupled as increasing-evanescent:

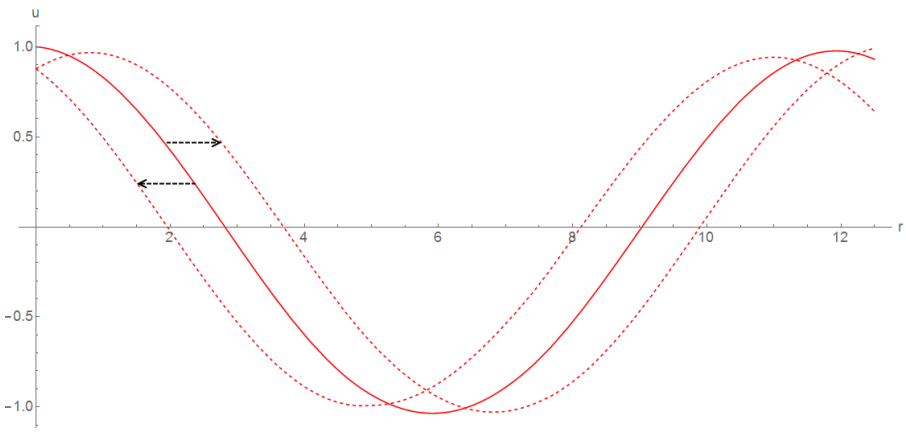

Figure 2.11: One pair of travelling waves in partial gap-band $\Omega = 0.06$

And in pure pass-band appears second couple of travelling propagating waves and one couple standing increasing-evanescent. Waves for pass-band will not be represented here for brevity.

2.2 Higher-order theories

In order to obtain real picture of energy flow and thus picture of Floquet zones, all propagating waves should be considered in each component of a periodic structure shown on Fig.2.1. Therefore it is of interest to check if Bernoulli-Euler curved beam theory captures all propagating waves in a low frequency range, that is considered during experiments.

Increasing number of waves leads to higher-order theories, which are harder to operate. Therefore it is of interest to see how propagating waves predicted by higher order theories are compared with the predictions of Bernoulli-Euler beam theory used in modelling. In this chapter several theories for modelling different parts of vibration isolator are used for this purpose.

2.2.1 Elastic layer (in-plane)

For analysis of in-plane vibration the first part of vibration isolator can be modelled as elastic layer in polar coordinates. Equations derivation can be found in App.B. In order to find eigenvalues of the system one can use potential theory [13]. First, Helmholz decomposition of the displacement field should be introduced (every field can be represented as a sum of conservative and solenoidal fields):

$$u = \nabla\Phi + \nabla \times \mathbf{\Psi} \tag{2.10}$$

,where Φ called scalar field potential and $\mathbf{\Psi}$ called vector field potential. It is required that $\text{div}\mathbf{\Psi} = \nabla\mathbf{\Psi} = 0$, i.e. field $\nabla \times \mathbf{\Psi}$ is solenoidal (field $\nabla\Phi = \text{div}(\Phi)$ is conservative since $\text{curl}(\text{div}(\Phi)) = \nabla \times (\nabla\Phi) \equiv 0$).

In cylindrical coordinates operator ∇ has following actions on a scalar field Φ and vector field $\mathbf{\Psi} = (\Psi_r, \Psi_\theta, \Psi_z)$:

$$\begin{aligned} &\nabla\Phi = (\tfrac{\partial\Phi}{\partial r}, \tfrac{1}{r}\tfrac{\partial\Phi}{\partial\theta}, \tfrac{\partial\Phi}{\partial z}) \\ &\nabla \times \mathbf{\Psi} = (\tfrac{1}{r}\tfrac{\partial\Psi_z}{\partial\theta} - \tfrac{\partial\Psi_\theta}{\partial z}, \tfrac{\partial\Psi_r}{\partial z} - \tfrac{\partial\Psi_z}{\partial r}, \tfrac{1}{r}(\tfrac{\partial(r\Psi_\theta)}{\partial r} - \tfrac{\partial\Psi_r}{\partial\theta})) \end{aligned} \tag{2.11}$$

In case of elastic layer with plane strain (one can use plane stress assumption instead, but effective elastic modulus should be changed to $\frac{E}{1-\nu^2}$) assumptions vector field $\mathbf{\Psi}$ can be replaced with $i_z\Psi_z$, where Ψ_z is the scalar field [14]. With Eq.2.11 we can rewrite Eq.2.10 as:

$$u = (u_r, u_\theta, u_z) = \nabla\Phi + \nabla \times i_z\Psi_z = (\frac{\partial\Phi}{\partial r} + \frac{1}{r}\frac{\partial\Psi_z}{\partial\theta}, \frac{1}{r}\frac{\partial\Phi}{\partial\theta} - \frac{\partial\Psi_z}{\partial r}, \frac{\partial\Phi}{\partial z}) \tag{2.12}$$

Since plane strain state considered $u_z = 0$. After, substituting this into following equations:

$$\begin{pmatrix} \epsilon_{rr} \\ \epsilon_{\theta\theta} \\ \epsilon_{r\theta} \end{pmatrix} = \begin{pmatrix} \frac{\partial u_r}{\partial r} \\ \frac{1}{r}(\frac{\partial}{\partial\theta}u_\theta + u_r) \\ \frac{1}{2}(\frac{1}{r}\frac{\partial}{\partial\theta}u_r + \frac{\partial u_\theta}{\partial r} - \frac{u_\theta}{r}) \end{pmatrix} \tag{2.13}$$

And using constitutive law:

$$\begin{pmatrix} \sigma_{rr} \\ \sigma_{\theta\theta} \\ \sigma_{r\theta} \end{pmatrix} = \begin{bmatrix} 2\mu + \lambda & \lambda & 0 \\ \lambda & 2\mu + \lambda & 0 \\ 0 & 0 & 2\mu \end{bmatrix} \begin{pmatrix} \epsilon_{rr} \\ \epsilon_{\theta\theta} \\ \epsilon_{r\theta} \end{pmatrix} \tag{2.14}$$

Stresses can be formulated in potentials as (index z in Ψ_z is omitted below):

$$\begin{aligned} \sigma_{rr} &= \lambda\nabla^2\Phi + 2\mu(\tfrac{\partial^2\Phi}{\partial r^2} + \tfrac{1}{r}\tfrac{\partial^2\Psi}{\partial r\partial\theta} - \tfrac{1}{r^2}\tfrac{\partial\Psi}{\partial\theta}) \\ \sigma_{r\theta} &= \mu(\tfrac{2}{r}\tfrac{\partial^2\Phi}{\partial r\partial\theta} - \tfrac{2}{r^2}\tfrac{\partial\Phi}{\partial\theta} - \tfrac{\partial^2\Psi}{\partial r^2} + \tfrac{1}{r}\tfrac{\partial\Psi}{\partial r} + \tfrac{1}{r^2}\tfrac{\partial^2\Psi}{\partial\theta^2}) \\ \sigma_{\theta\theta} &= \lambda\nabla^2\Phi + 2\mu(\tfrac{1}{r^2}\tfrac{\partial\Psi}{\partial\theta} + \tfrac{1}{r^2}\tfrac{\partial^2\Phi}{\partial\theta^2} + \tfrac{1}{r}\tfrac{\partial\Phi}{\partial r} - \tfrac{1}{r}\tfrac{\partial^2\Psi}{\partial r\partial\theta}) \end{aligned} \tag{2.15}$$

After substitution into equations of vibration Eq.B.15 (see App.B for derivation and equations) we get following equations for potential:

$$\begin{aligned} \nabla^2\Phi - \frac{1}{c_1^2}\frac{\partial\Phi}{\partial t^2} = 0 \\ \nabla^2\Psi - \frac{1}{c_2^2}\frac{\partial\Psi}{\partial t^2} = 0 \end{aligned} \tag{2.16}$$

With dimensionless parameters $\bar{r} = \frac{r}{h}$, $\bar{s} = \frac{\theta r_0}{h}$, $\xi = \frac{\omega r_0}{c_1}$ we can employ following expression for potentials (bars are omitted):

$$\begin{aligned} \Phi(r,\theta,t) = \phi(r)\exp(i\xi s - i\omega t) \\ \Psi(r,\theta,t) = \psi(r)\exp(i\xi s - i\omega t) \end{aligned} \tag{2.17}$$

Eq.2.17 substituted into 2.16 gives form for functions $\phi(r), \psi(r)$ (they should satisfy Bessel equation):

$$\begin{aligned} \phi(r,\theta,t) = A_1 J_{\xi r_0}(\Omega r) + B_1 Y_{\xi r_0}(\Omega r) \\ \psi(r,\theta,t) = A_2 J_{\xi r_0}(\eta\Omega r) + B_2 Y_{\xi r_0}(\eta\Omega r) \end{aligned} \tag{2.18}$$

,where $\eta = \frac{c_1}{c_2} = \sqrt{2 + \frac{\lambda}{\mu}}$

In order to obtain dispersion diagrams we consider traction-free boundary conditions at $r = r_0$ and $r = r_0 + b/h$, from Eq.B.17 they are:

$$\begin{aligned} \sigma_{rr} = 0 \\ \sigma_{r\theta} = 0 \end{aligned} \tag{2.19}$$

After substitution Eq.2.17 into Eq.2.19 with expressions Eq.2.15 we get boundary conditions in $\phi(r), \psi(r)$:

$$\begin{aligned} -\Omega^2\phi + (\phi'' + \frac{i\xi r_0}{r}\psi' - \frac{i\xi r_0}{r^2}\psi)2\frac{\mu}{\lambda} = 0 \\ 2i\xi r_0(\frac{1}{r}\phi' - \frac{1}{r^2}\phi) - \psi'' + \frac{1}{r}\psi' - \frac{\xi^2 r_0^2}{r^2}\psi = 0 \end{aligned} \tag{2.20}$$

After substitution Eq.2.18 into Eq.2.20 and evaluation at the points $r = r_0$ and $r = r_0 + b/h$ we get four linear algebraical equations with respect to unknowns $A_i, B_i \;\; i = 1, 2$. Determinant of this system is the transcendent dispersion equation for in-plane elastic layer vibrations in polar coordinates:

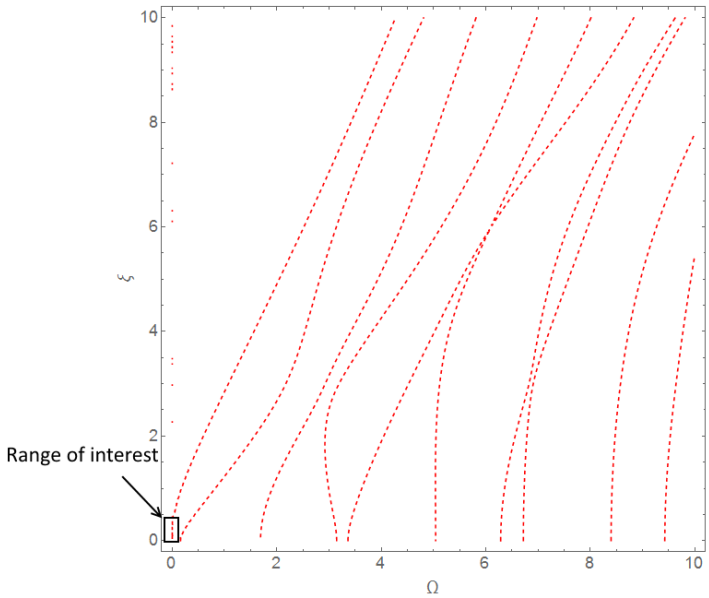

Figure 2.12: In-plane elastic layer dispersion equation

Solution, obtained with theory, used in this chapter can be used for a wide frequency range. The Bernoulli-Euler theory works only for frequencies $\Omega < \Omega_2^{cut-on} \approx 0.3$, when the second branch of elastic layer dispersion equation appears. Frequency range, considered in this work for experiments, 0-1500 Hz which corresponds to $\Omega \approx 10^{-3}$ allows one to use both theories for approximation. Comparison with the beam theory in the low frequency range is shown below.

2.2.2 Kirchhoff plate equation (out-of-plane)

As shown in App.C elastic layer free out-of-plane vibrations can be represented as Eq.C.19, which is Kirchhoff-Love plate equation (assuming harmonic vibration state $w(r,\theta,t) = w(r,\theta)\exp(-i\omega t))$:

$$(\Delta^2 - k^2)w = 0 \tag{2.21}$$

Therefore, solution in polar coordinates has a form ($\xi = kr_0$ as in previous case):

$$w(r) = A_1 J_\xi(\sqrt{\Omega}r) + A_2 Y_\xi(\sqrt{\Omega}r) + A_3 I_\xi(\sqrt{\Omega}r) + A_4 K_\xi(\sqrt{\Omega}r) \tag{2.22}$$

,where $\Omega^2 = 12(1-\nu^2)(\frac{\omega h}{c})^2$

In order to obtain dispersion diagrams we consider traction-free boundary conditions at $r = r_0$ and $r = r_0 + b/h$, from Eq.C.21 they are:

$$\begin{aligned} &\frac{\partial w^2}{\partial r^2} + \nu(\frac{1}{r^2}\frac{\partial w^2}{\partial \theta^2} + \frac{1}{r}\frac{\partial w}{\partial r}) = 0 \\ &\frac{\partial w^3}{\partial r^3} + (2-\nu)(\frac{1}{r}\frac{\partial w^2}{\partial r^2} - \frac{1}{r^2}\frac{\partial w}{\partial r} + \frac{1}{r^2}\frac{\partial^3 w}{\partial r \partial \theta^2} - \frac{2}{r^3}\frac{\partial w^2}{\partial \theta^2}) = 0 \end{aligned} \tag{2.23}$$

After substitution Eq.2.22 into Eq.2.23 and evaluation at the points $r = r_0$ and $r = r_0 + b/h$ we get four linear algebraical equations with respect to unknowns A_i , $i = 1,2,3,4$. Determinant of this system is dispersion equation for out-of-plane elastic plate vibrations in polar coordinates:

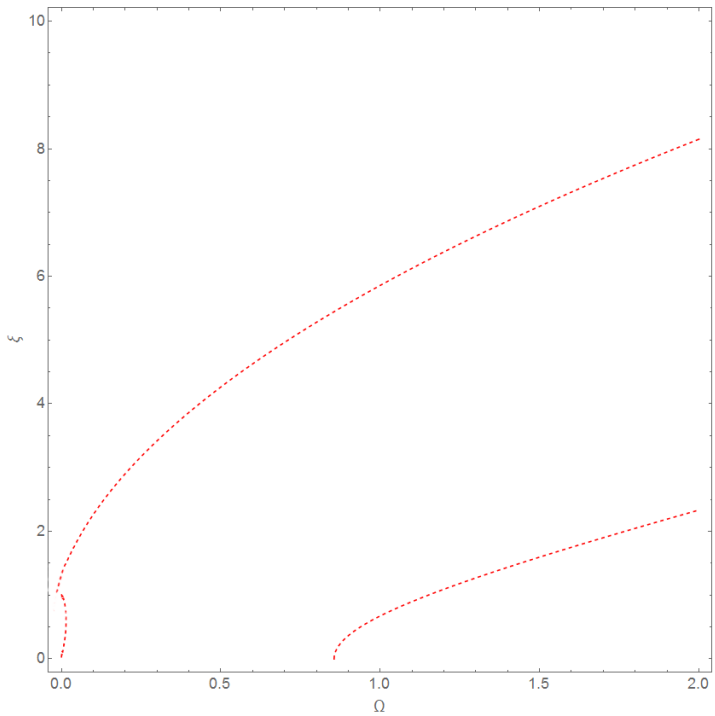

Figure 2.13: Out-of-plane elastic layer dispersion equation

As in previous case, Bernoulli-Euler theory works only for frequencies $\Omega < \Omega_2^{cut-on}$ (they are different for in-plane and out-of-plane vibrations). But frequency range considered in this work is way below cut-on frequency.

With assumptions, taken in App.C this theory valid for a lesser frequency range then one taken for in-plane, but still it is wider than Bernoulli-Euler beam theory range. In scope of this work taken very small frequency range and therefore all theories are valid for modelling torque vibrational isolator.

In order to compare dispersion diagrams, we will use low frequency range 0-1500 Hz, which was used during experiments (see App.A for Bernoulli-Euler curved beam dispersion equation):

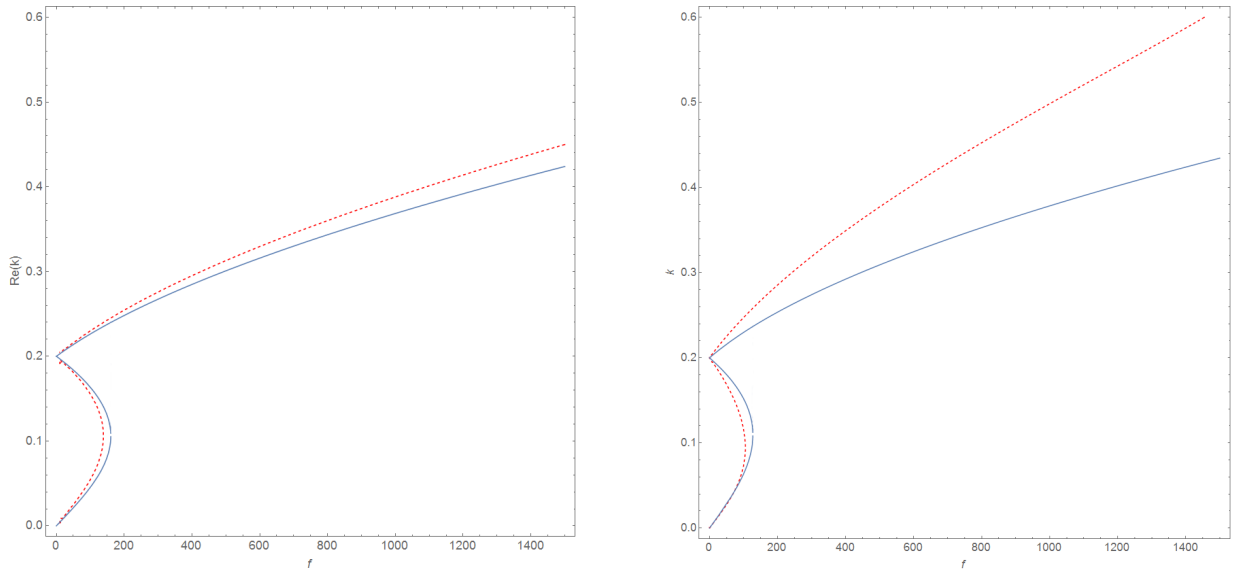

Figure 2.14: Dispersion diagram (propagating waves only) blue - Bernoulli-Euler curved beam, red - high-order theories, left - in-plane, right - out-of-plane

Comparison shows, that two propagating waves at the low frequency range present in elastic layer and in Bernoulli-Euler curved beam dispersion equation. Therefore, curved beam model can be used for Floquet analysis of parts 1,3 at the low frequency range without significant losses in accuracy. Using high-order theories in that case affects only on stop-band borders, but not on existing (absenting) of Floquet zones.

As seen, in-plane and out-of-plane factorization of Bernoulli-Euler curved beam are corresponding to elastic layer vibration with plain strain assumptions and Kirchhoff-Love plate out-of-plane vibration respectively. That means, that factorization into two parts is also presenting in higher order theories.

2.2.3 Cylindrical shell

Parts 2 and 4 of a structure, shown on a Fig.2.1 can be represented as a thin cylindrical shell. Equations derivation with Hamilton's principle can be found in App.D. Final system of cylindrical shell vibration equations have form (Eq.D.25):

$$\begin{gathered}
-\frac{\partial^2 u}{\partial x^2} - \frac{1-\nu}{2}\frac{1}{R^2}\frac{\partial^2 u}{\partial \theta^2} - \frac{1+\nu}{2}\frac{1}{R}\frac{\partial^2 v}{\partial x \partial \theta} - \frac{\nu}{R}\frac{\partial w}{\partial x} + \frac{\rho}{E(1-\nu^2)}\frac{\partial^2 u}{\partial t^2} = 0 \\
-\frac{1+\nu}{2}\frac{1}{R}\frac{\partial^2 u}{\partial x \partial \theta} - \frac{1-\nu}{2}\frac{\partial^2 v}{\partial x^2} - \frac{1}{R^2}\frac{\partial^2 v}{\partial \theta^2} - \frac{h^2}{12}\frac{1-\nu}{R^2}\frac{\partial^2 v}{\partial x^2} - \frac{h^2}{12}\frac{1}{R^4}\frac{\partial^2 v}{\partial \theta^2} - \\
-\frac{1}{R^2}\frac{\partial w}{\partial \theta} + + \frac{h^2}{12}\frac{1}{R^4}\frac{\partial^3 w}{\partial \theta^3} + \frac{h^2}{12}\frac{1}{R^2}\frac{\partial^3 w}{\partial x^2 \partial \theta} + \frac{\rho}{E(1-\nu^2)}\frac{\partial^2 v}{\partial t^2} = 0 \\
\frac{\nu}{R}\frac{\partial u}{\partial x} + \frac{1}{R^2}\frac{\partial v}{\partial \theta} - \frac{h^2}{12}\frac{1}{R^4}\frac{\partial^3 v}{\partial \theta^3} - \frac{h^2}{12}\frac{1}{R^2}\frac{\partial^3 v}{\partial x^2 \partial \theta} + \frac{1}{R^2}w + \frac{h^2}{12}\frac{\partial w^4}{\partial x^4} + \\
+\frac{h^2}{12}\frac{1+\nu}{R^2}\frac{\partial^4 w}{\partial x^2 \partial \theta^2} + \frac{h^2}{12}\frac{1}{R^4}\frac{\partial^4 w}{\partial \theta^4} + \frac{\rho}{E(1-\nu^2)}\frac{\partial^2 w}{\partial t^2} = 0
\end{gathered} \tag{2.24}$$

Usually in references (e.g. [15]) full cylindrical shell is considered and wave propagation in the axis of symmetry direction is considered. In that case it can be fully factorized and equations are separated for each circumferential wave m. Torque vibration isolator parts don't have closed

shape as shown on a Fig.2.15. For vibration isolator it is of interest to consider propagating wave in circumferential direction and standing in longitudinal.

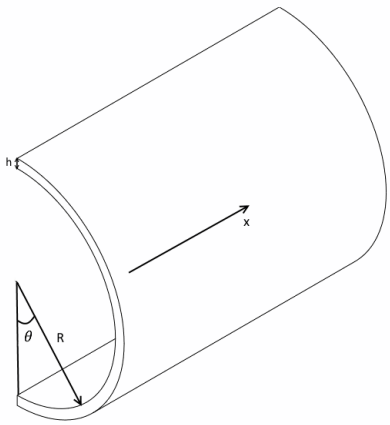

Figure 2.15: Cylindrical shell in vibrational isolator

Following coordinate dependance is used:

$$\begin{aligned} u(x,\theta) &= U\exp(ik_x\,x + ik_\theta\,\theta - i\omega t) \\ v(x,\theta) &= V\exp(ik_x\,x + ik_\theta\,\theta - i\omega t) \\ w(x,\theta) &= W\exp(ik_x\,x + ik_\theta\,\theta - i\omega t) \end{aligned} \tag{2.25}$$

After Eq.2.25 substituted into equations Eq.2.24, one obtain system of three equations with respect to three unknown amplitudes U, V, W. By equating determinant of that system to zero, relation between k_θ , k_x and Ω (here $\Omega = \frac{\omega h}{c}$ - non-dimensional frequency parameter) can be found. That relation is eight order polynomial both in k_x and k_θ :

$$\begin{aligned} &\frac{1}{288R^{10}}(k_\theta^2(h^2(k_\theta^2+k_x^2R^2)+12R^2)((h^2(k_\theta^2+k_x^2R^2)+12R^2)(k_\theta^2(\nu-1)+2R^2(\Omega^2-k_x^2)) \\ &\quad + 12k_x^2\nu(\nu+1)R^4) + 12k_x^2\nu R^4(h^2(k_\theta^4(\nu+1)+k_\theta^2(k_x^2(\nu+1)R^2-2\nu)+2k_x^2(\nu-1)\nu R^2) \\ &\quad + 12R^2(\nu R^2(k_x^2(\nu-1)+2\Omega^2)-k_\theta^2(\nu-1))) + (h^2(k_\theta^4+k_x^4R^4+k_\theta^2k_x^2(\nu+1)R^2) \\ &\quad - 12R^2(R^2\Omega^2-1))((2R^2(k_x^2-\Omega^2)-k_\theta^2(\nu-1))(h^2(k_\theta^2-k_x^2(\nu-1)R^2) \\ &\quad + 6R^2(2k_\theta^2+R^2(k_x^2(-\nu)+k_x^2-2\Omega^2))) - 6k_\theta^2k_x^2(\nu+1)^2R^4)) = 0 \end{aligned} \tag{2.26}$$

It should be emphasized, that if $k_\theta = m$, $m \in \mathbb{N}$ one can obtain classical dispersion equation, which used in full cylindrical shell analysis.

With solving Eq.2.26 with respect to k_x we can find explicit dependance $k_x^{(i)}(k_\theta)$, $i = 1, ..., 8$ (since eight order polynomial solution is very cumbersome it is not represented here).

Also, it is convenient to introduce modal coefficients $m_v = \frac{V}{U}$, $m_w = \frac{W}{U}$, which can be found from, for example two first equations Eq.2.24. Modal coefficients depend on particular wave number $k_x^{(i)}$ taken. They have form:

$$\begin{aligned} m_v(k) &= \frac{k_\theta\left(h^2\left(k_\theta^2+k_x^2R^2\right)\left(k_\theta^2(\nu-1)+2R^2\left(\Omega^2-k_x^2\right)\right)+12(\nu-1)R^2\left(k_\theta^2+k_x^2(\nu+2)R^2\right)+24R^4\Omega^2\right)}{k_xR\left(h^2\left(k_\theta^4(\nu+1)+k_\theta^2(k_x^2(\nu+1)R^2-2\nu)+2k_x^2(\nu-1)\nu R^2\right)-12k_\theta^2(\nu-1)R^2+12\nu R^4(k_x^2(\nu-1)+2\Omega^2)\right)} \\ m_w(k) &= i\frac{h^2\left(\mathrm{k}\theta^2-k_x^2(\nu-1)R^2\right)\left(k_\theta^2(\nu-1)+2R^2\left(\Omega^2-k_x^2\right)\right)}{k_xR\left(h^2\left(k_\theta^4(\nu+1)+k_\theta^2(k_x^2(\nu+1)R^2-2\nu)+2k_x^2(\nu-1)\nu R^2\right)-12k_\theta^2(\nu-1)R^2+12\nu R^4(k_x^2(\nu-1)+2\Omega^2)\right)} \\ &+i\frac{12R^2\left(-(\nu-3)R^2\Omega^2\left(k_\theta^2+k_x^2R^2\right)+(\nu-1)\left(k_\theta^2+k_x^2R^2\right)^2-2R^4\Omega^4\right)}{k_xR\left(h^2\left(k_\theta^4(\nu+1)+k_\theta^2(k_x^2(\nu+1)R^2-2\nu)+2k_x^2(\nu-1)\nu R^2\right)-12k_\theta^2(\nu-1)R^2+12\nu R^4(k_x^2(\nu-1)+2\Omega^2)\right)} \end{aligned} \tag{2.27}$$

After dependance $k_x(k_\theta)$ is found, we can represent solution as:

$$\begin{aligned} u(x,\theta) &= u(x)\exp(ik_\theta\,\theta) \\ v(x,\theta) &= v(x)\exp(ik_\theta\,\theta) \\ w(x,\theta) &= w(x)\exp(ik_\theta\,\theta) \end{aligned} \tag{2.28}$$

,where

$$\begin{aligned} u(x) &= \sum_{j=1}^{j=8} U_i \exp(ik_x^{(j)}\,x) \\ v(x) &= \sum_{j=1}^{j=8} U_i m_v^{(j)} \exp(ik_x^{(j)}\,x) \\ w(x) &= \sum_{j=1}^{j=8} U_i m_w^{(j)} \exp(ik_x^{(j)}\,x) \end{aligned} \tag{2.29}$$

,where $m_v^{(j)} = m_v(k_x^{(j)})$ - modal coefficient with substituted value $k_x^{(j)}$.

Equation Eq.2.28 can now be substituted into boundary conditions. For correspondence between 1st and 2nd part shown on Fig.2.1 axial coordinate traction-free boundary conditions Eq.D.26. After θ coordinate is factorized and cancelled they have form:

$$\begin{aligned} &\tfrac{1}{R}(-ik_\theta\nu v(x) + \nu w(x)) + u'(x) = 0 \\ &\tfrac{1-\nu}{12R^2}(6ik_\theta R u(x) - (h^2+6R^2)v'(x) + ih^2k_\theta w'(x)) = 0 \\ &\tfrac{h^2}{12R^2}(ik_\theta\nu v(x) - k_\theta^2\nu w(x) + R^2 w''(x)) = 0 \\ &-\tfrac{h^2}{12}(ik_\theta v'(x) - k_\theta^2 w'(x) + R^2 w'''(x)) = 0 \end{aligned} \tag{2.30}$$

When functions in Eq.2.29 are substituted into Eq.2.30 at points $x = 0$ and $x = l$ we obtain homogenous linear algebraical system with respect to unknowns U_i , $i = 1, ..., 8$. Determinant of this system is dispersion equation from which dependance $k_\theta(\Omega)$ can be found. It should be emphasized that cylindrical shell dispersion equation has 8 roots whereas Bernoulli-Euler curved beam has 12 (6 for both in-plane and out-of-plane parts) and therefore there is no complete correspondence between Bernoulli-Euler curved beam model and a thin cylindrical shell model. Dependance $k_\theta(\Omega)$ can be compared now with Bernoulli-Euler dispersion equation:

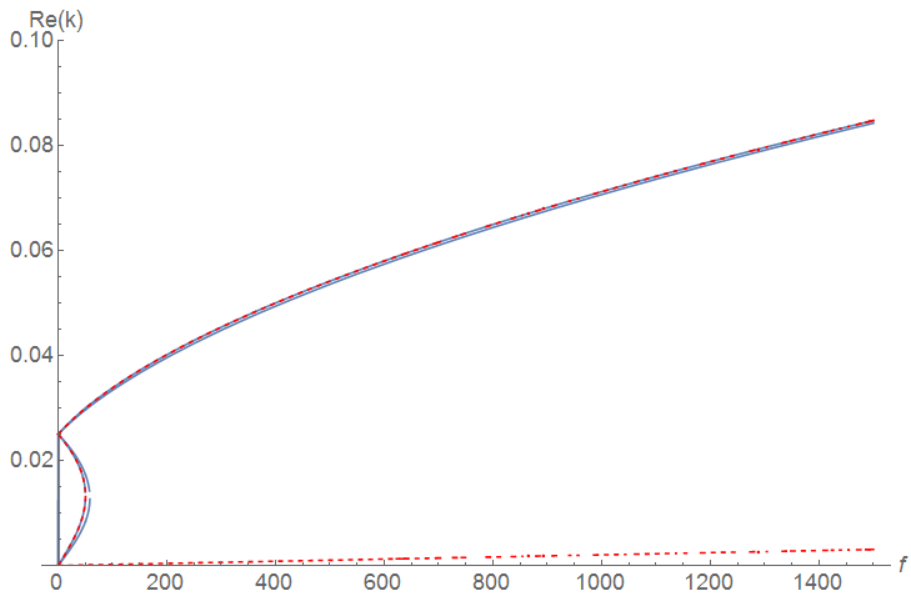

Figure 2.16: Dispersion diagrams(propagating(pure real) waves only): Bernoulli-Euler curved beam(blue) and cylindrical shell(red), $h = 1$mm, $R = 40$mm, $L = 20h$

Cylindrical shell dispersion equation factorizes into two parts sixth degree "in-plane" and second degree anti-plane part. Therefore, in order to capture Bernoulli-Euler beam model out-of-plane part, it is necessary (as in elastic layer in-plane case above) to formulate a refined theory, which is more complicated in this case and therefore out of scope of this work.

Nevertheless, for in-plane branches of Bernoulli-Euler curved beam dispersion equation and cylindrical shell is almost fully matching and therefore it may be concluded, that approximation with Bernoulli-Euler beam is chosen correctly.

2.3 Model for experiments

As shown above, Bernoulli-Euler curved beam model gives decent prediction on a low frequency range, but producing prototype, shown on Fig.2.1, is difficult technically and requires advanced tools. Since a prototype with the circular cross-section is much easier to produce, a periodic curved Bernoulli-Euler beam model with circular cross-section will be considered:

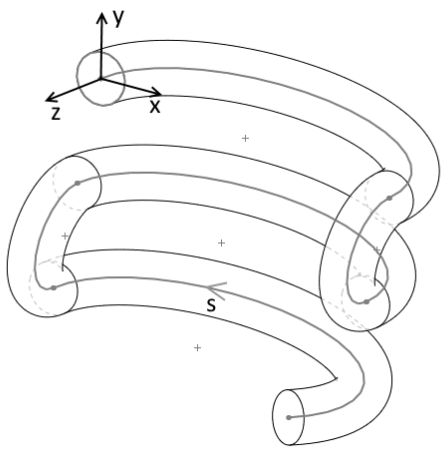

Figure 2.17: Model with a circular cross-section

This kind of structure has been used as prototype for an experimental setup.

In theoretical point of view, we don't change waveguide properties, because dispersion diagrams are very close to each other:

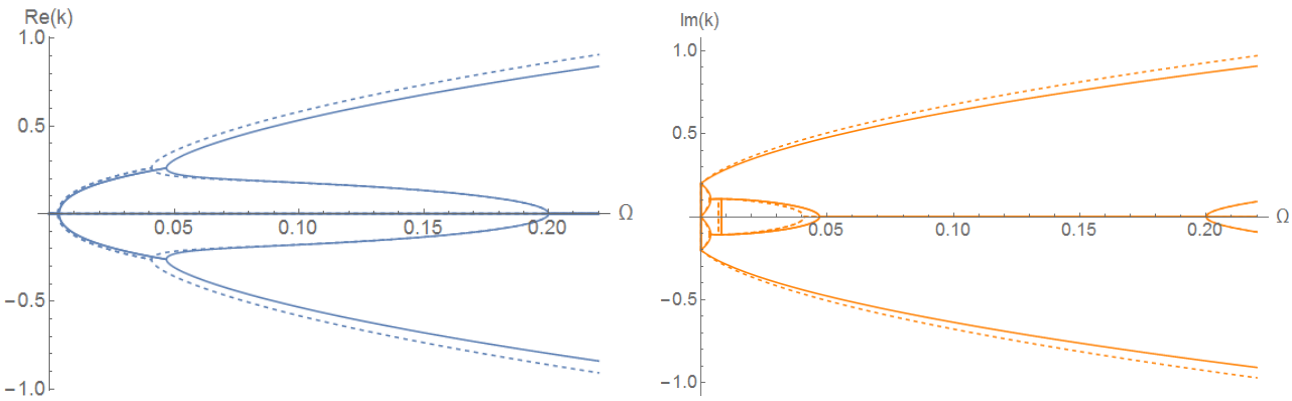

Figure 2.18: Dispersion diagrams ($\epsilon_1 = 0.2, \epsilon_2 = 0.02$) for rectangular cross-section ($\frac{h}{b} = \frac{1}{20}$) and circular cross-section (dashed) real parts(blue) and imaginary parts (orange)

Therefore, a model with a circular cross-section is pretty good replacement of a model with a rectangular one and all waveguide properties, that are presenting in circular one, preserved

in rectangular. Nevertheless, model with a circular cross-section is more symmetrical than with rectangular and therefore they have different durability properties. Thus, durability tests were not conduced during this work.

Also, for comparison with experimental sample following dimensionless parameters (calculated with using parameters, that used in experiments part) will be used:

$$\alpha_{par} = 1; \gamma = 7.08;\ \sigma = 1; \lambda = 25.13;\ \varepsilon_1 = 0.25;\ \varepsilon_2 = 0.0352 \tag{2.31(a)}$$

$$\alpha_{par} = 1; \gamma = 3.17;\ \sigma = 1; \lambda = 25.13;\ \varepsilon_1 = 0.25;\ \varepsilon_2 = 0.0789 \tag{2.31(b)}$$

With those schematics and steel parameters following gap-band picture obtained:

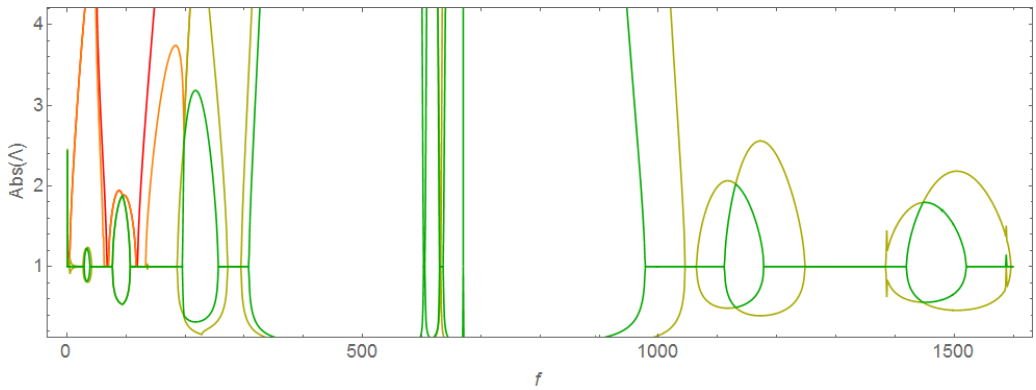

Figure 2.19: Final model scheme for parameters Eq.2.31(a)

Even though parameters ϵ_1, ϵ_2 are close to one used above, parameters γ and λ are significantly larger than considered above. λ here has the meaning of a scale parameter, and with its increasing more gap-bands appearing. Parameters study are partially covered in [11] for parameters ϵ_1, ϵ_2 and γ.

It should be noted that all results reported in Sect.2.1 are exact in the framework of Bernoulli-Euler beam model. The Green's matrices and boundary integral equations are as accurate as the governing equations and unlike any numerical methods do not contaminate the end results with discretisation errors.

Another advantage of this solutions is its non-dimensional form, which facilitates its adjustment to any dimensional parameters.

Chapter 3

Experimental setup

In this chapter series of experiments are described, that were conducted in order to validate mathematical model, built in previous chapters. Also, it is of interest to build real experimental prototype and study its properties in a small scale before it can be produced in a real size.

3.1 Spring equipment

Following equipment was produced in order to preserve the same periodical pattern in each vibration isolator prototype (for technical sketch see App.E):

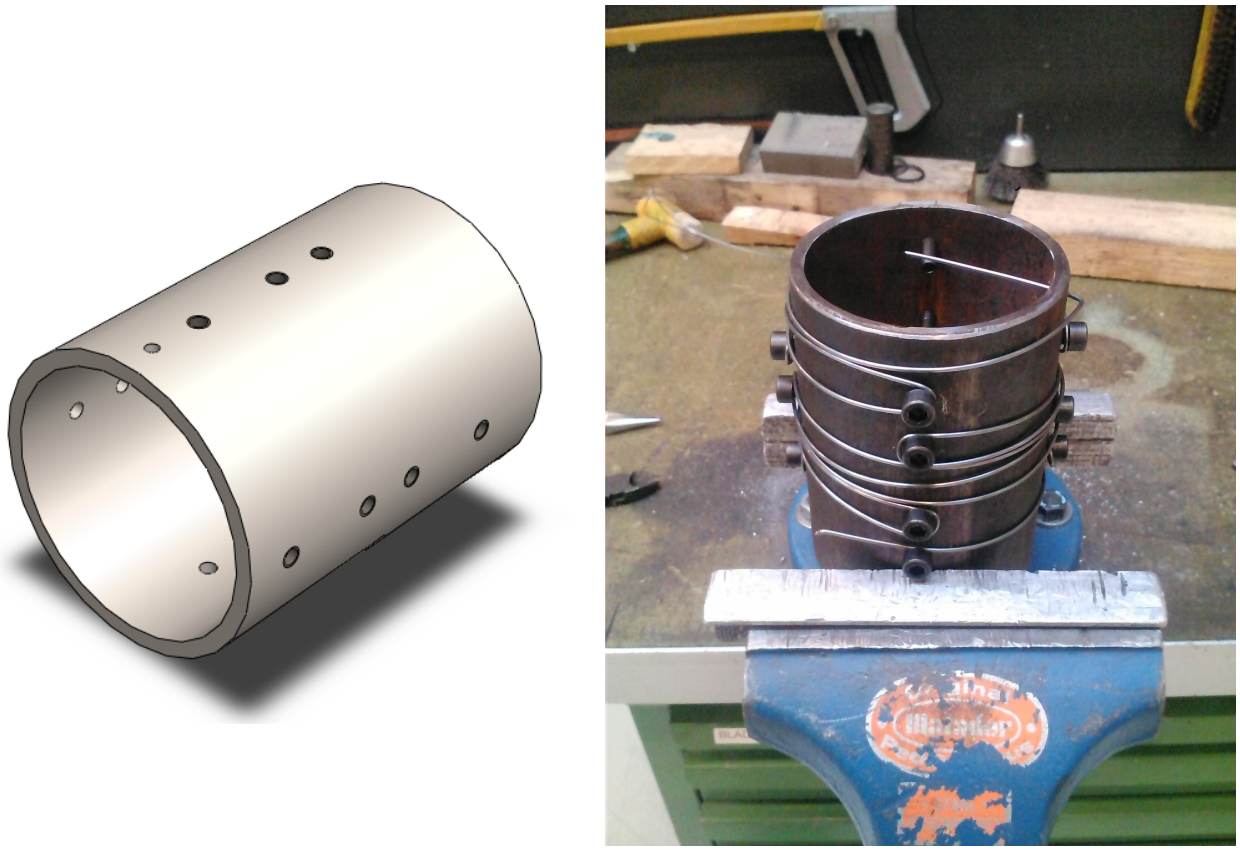

Figure 3.1: Spring equipment: sketch(left), produced prototype with wire(right)

In threaded technical holes, M6 bolts are attached. Cylinder diameter provides large curvature radius and bolt diameter provides small curvature radius. Holes are placed such that 3/4 large-1/2 small-1/2 large-1/2 small turns of curvature can be completed and therefore isolator will have form as on the Fig.2.17.

3.2 Experimental setup

In order to conduct experiments two experimental setups were built: experimental setup for axial loading (I) and for torque loading (II). Each setup contains rig for fixating isolator and following set of Brüel&Kjær equipment:

Unit	Model
Data Acquisition System	Type 3560c
Power Amplifier	Type 2706
Vibration Exciter	Type 4809
Charge to DeltaTron® Converter (preamplifier)	Type 2647a
Accelerometer(I)	Type 4321
Accelerometer(II)	Type 4374

Table 3.1: Equipment set

In first setup shaker is connected to a freely suspended isolator and other end of isolator is fixed into the fixture plate with tri-axial accelerometer(I). Plate is suspended with a system of rubber bands as shown on a Fig.3.2.

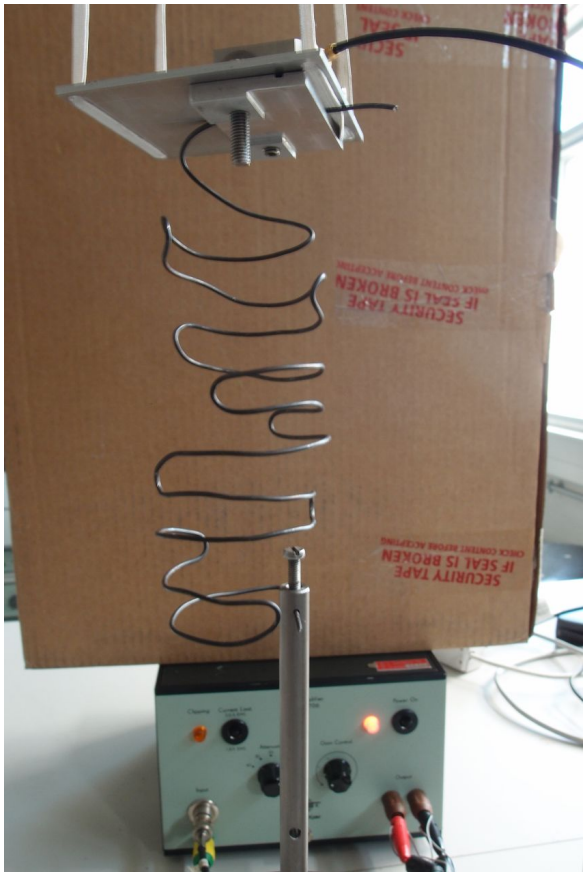

Figure 3.2: Uni-axial loading setup

The uni-axial shaker excitation is performed parallel to the large curvature plane. The acceleration is measured in z-direction, i.e. perpendicular to the fixture plate plane.

In second setup shaker is connected to an transition arm such that uni-axial vibrations of shaker are transmitted to shaft torque vibrations. One end of the isolator is connected to a shaft and other one is laterally fixed. Uni-axial accelerometer is fixed near fixed end of the isolator such that axis of an accelerometer is parallel to a shaker axis of vibration as shown on a Fig.3.3.

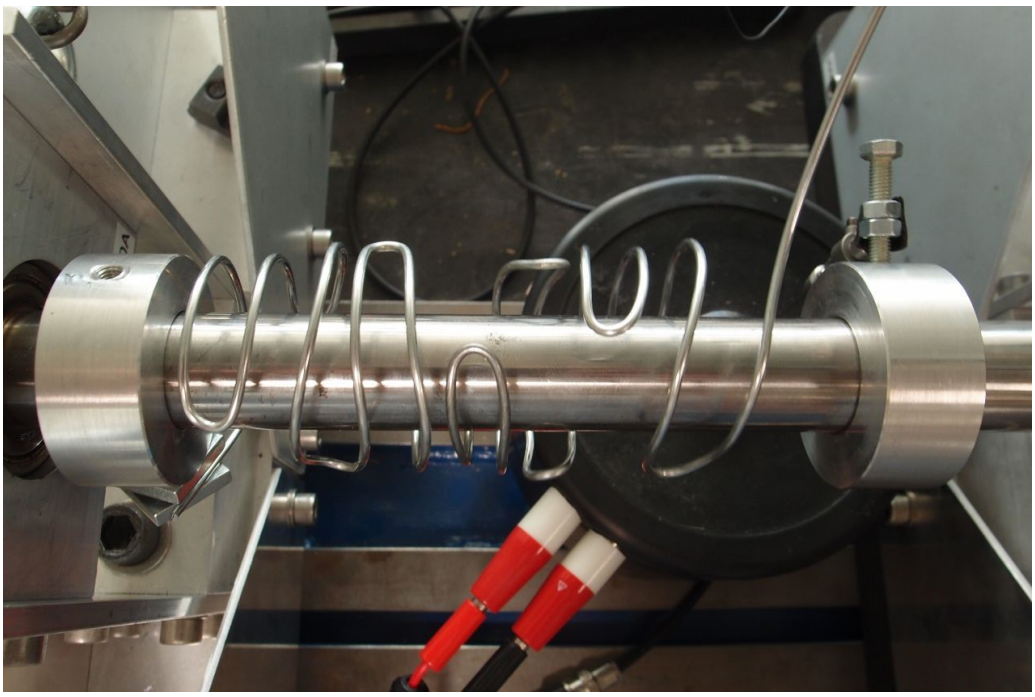

Figure 3.3: Torque loading setup

3.3 Experimental data

During experiments sessions four prototypes made of two different materials, magnesium-lithium alloy and steel, were used. For all experiments same experimental setups, described above, are used.

Since it was of interest to experimentally identify only location of gap-bands in order to compare it with Floquet zones, obtained theoretically, power supply was not calibrated. Reference force is taken such that it has same value for experiments, where same force amplitude is assumed.

3.3.1 Lithium-magnesium prototypes

First material, magnesium-lithium alloy, is taken because it is relatively soft material and was available in the laboratory. For magnesium-lithium alloy material parameters were unknown and therefore standard tests to measure the density and Young's modulus were conducted. All wire parameters shown on the following table:

Notation	Value	Description
d	1.5 mm	Wire diameter
ρ_2	1700 kg/m^3	Magnesium-Lithium alloy wire density
E_2	64 GPa	Magnesium-Lithium alloy wire Young's modulus

Table 3.2: Lithium-magnesium model parameters

These parameters are used in order to obtain dimensionless parameters Eq.2.28 mathematical model.

In order to check scale effect two prototypes made of lithium-magnesium alloy, but with different larger curvature radius, were used. For all prototypes used same geometrical parameters $R_1^{(1)} = 45\text{mm}, R_2^{(1)} = 6\text{mm}$ and $R_1^{(2)} = 19\text{mm}, R_2^{(2)} = 6\text{mm}$. Hereafter, they called large radius spring or 'LR' and small radius spring or 'SR' respectively. Following picture was obtained for LR and SR:

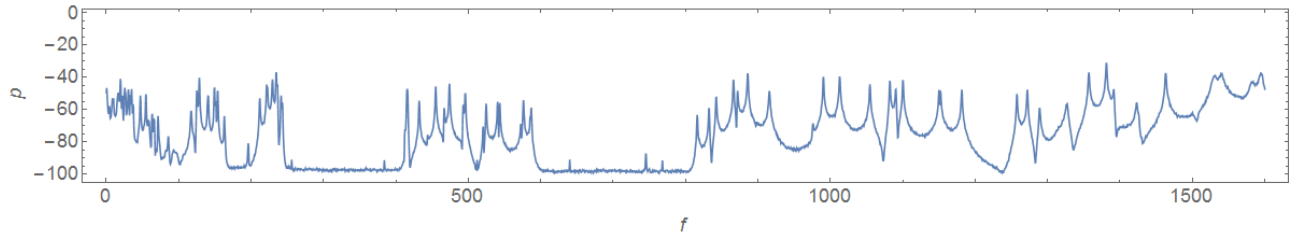

Figure 3.4: Magnesium-lithium alloy, uni-axial loading, LR

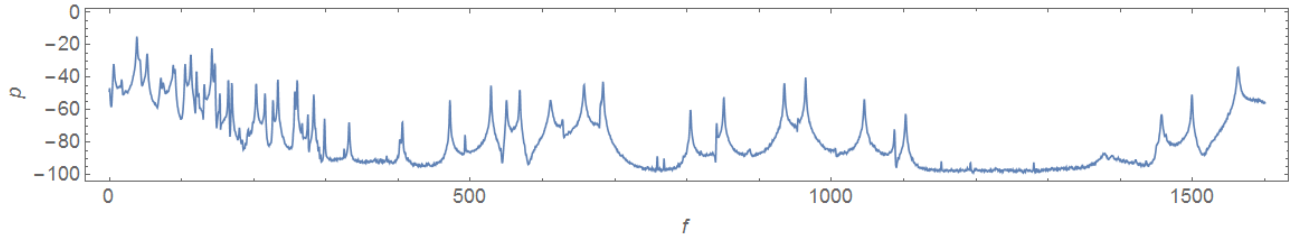

Figure 3.5: Magnesium-lithium alloy, uni-axial loading, SR

Ordinate axis in this diagrams represents acceleration level in dB. It is assumed that $p = 10\lg(\frac{a}{a_0})$, where a_0 is unknown reference acceleration level. a_0 is taken such that is it has same value for experiments with same reference acceleration level.

On Fig.3.4-Fig.3.5 zones with high attenuation are observed. These zones are correspond to a theoretical Floquet stop-band zones, which are shown in the Ch.2.

Since it was stated in Ch.1 that boundary conditions should not affect Floquet zones picture it was of interest to check two different loading scenarios. Uni-axial loading is shown on a Fig.3.4-Fig.3.5, for torque loading:

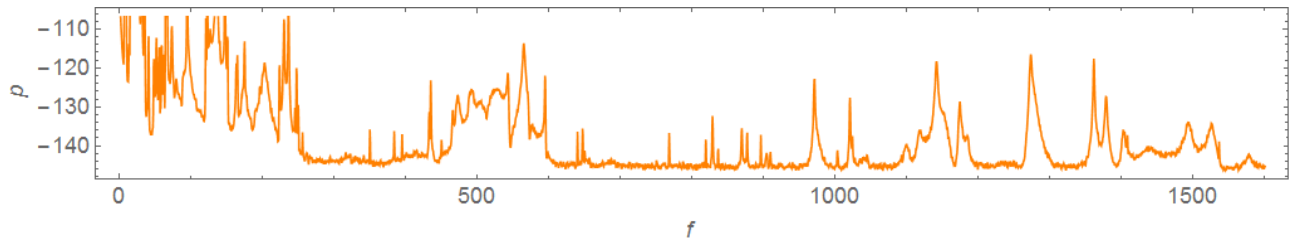

Figure 3.6: Magnesium-lithium alloy, torque loading, LR

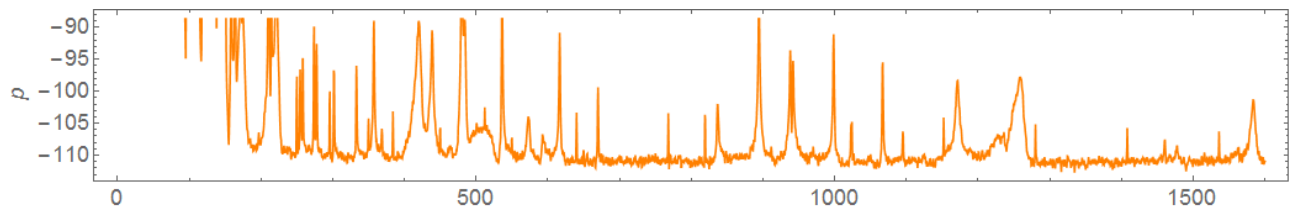

Figure 3.7: Magnesium-lithium alloy, torque loading, SR

In scope was also non-linearity effect and therefore it was of interest to see picture with force amplitude increased. It should be noted that experiments with higher force amplitude were conduced only for several cases:

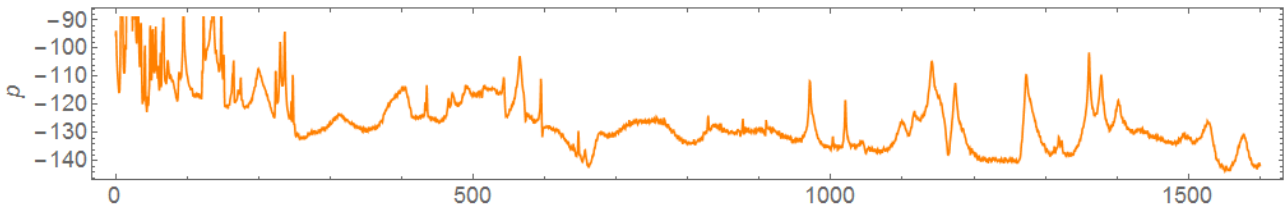

Figure 3.8: Magnesium-lithium alloy, torque loading, LR, higher force amplitude

In order to contrast performance of periodical vibration isolator, helical spring also was tested for small radius. Criterions for producing spring were same coil radius $R = 19$mm and same height:

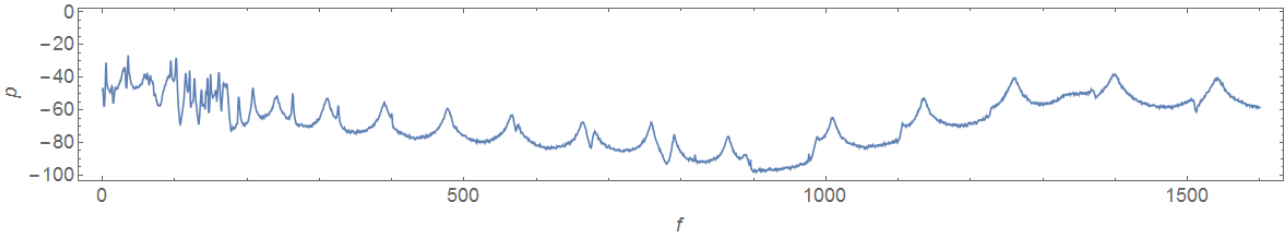

Figure 3.9: Helical spring, magnesium-lithium alloy, uni-axial loading, SR

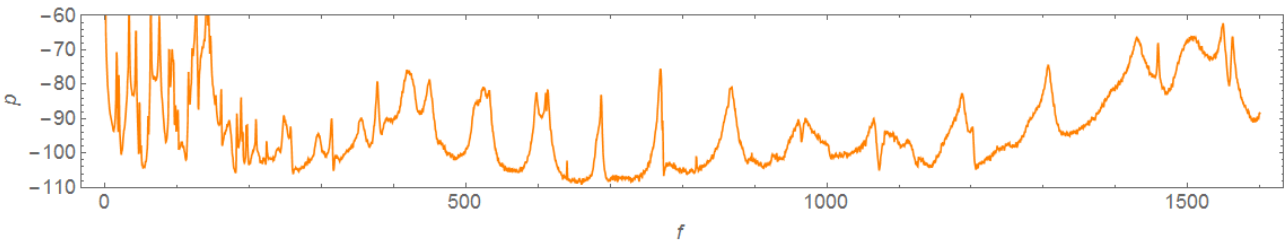

Figure 3.10: Helical spring, magnesium-lithium alloy, torque loading, SR

In springs experiments no stop-bands are observed, what is expected, because there is no periodic wavenumber changes within ordinary spring. Peaks that are represent eigenfrequencies are different for different loading cases. It is shown on Fig.A.1 and Fig.A.4 that in-plane and out-of-plane parts have different wave guide properties, axial loading affects more on the 'out-of plane' part and torque loading affects more on the 'in-plane' part, what explains difference in eigenfrequencies.

3.3.2 Steel prototypes

Second material, steel was taken as relatively stiff material. Same experimental setup as in first series is used. For large and small radius different steels are taken, for large radius spring steel was used. Practice shows, that for isolator better to use heat processed steel. Both steels have almost same Young's modulus and density which is shown in [16] and stated by wire producers.

Notation	Value	Description
$d^{(1)}$	1.5 mm	Spring steel wire diameter
$d^{(2)}$	2 mm	Heat processed steel wire diameter
ρ	7800 kg/m^3	Steel wire density
E	210 GPa	Steel wire Young's modulus

Table 3.3: Steel model parameters

Experimental structure repeats one, that used in magnesium-lithium experiment series and therefore it will not be reproduced here. All results of experiments can be found in App.G.

Chapter 4

Comparison of results

In this chapter results that obtained in Ch.2-Ch.3 are compared. In first part only experimental results from Ch.3 are considered. It is of interest to check, how experimental data are compared with theoretical statements shown in Ch.1. In second part experimental data compared with theoretical data, obtained in Ch.2.

4.1 Experimental results

In order to prove, that experiments were done correctly it is of interest to check if physical properties, that stated for theoretical isolator, are present in real structures.

First, statement from Ch.1 that loading scenario does not affect stop-band picture is considered:

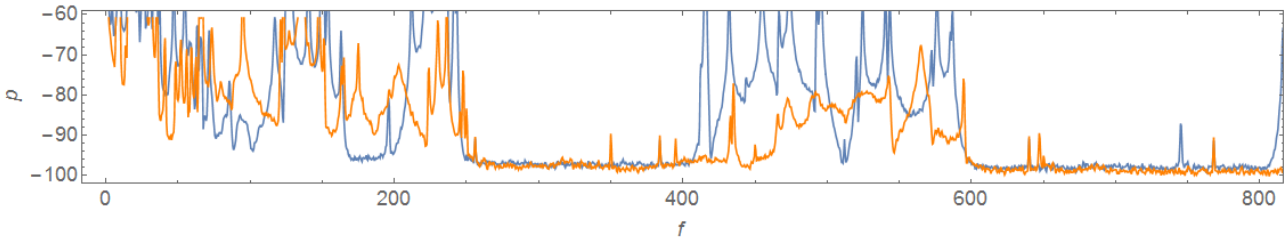

Figure 4.1: Two experiments with uni-axial loading (blue) with torque loading (orange), steel, LR

On Fig.4.1 perfect correspondence between stop-bands obtained from different loading scenarios. Therefore it may be concluded, that experimentally we obtain close pictures of stop-bands with different loading cases.

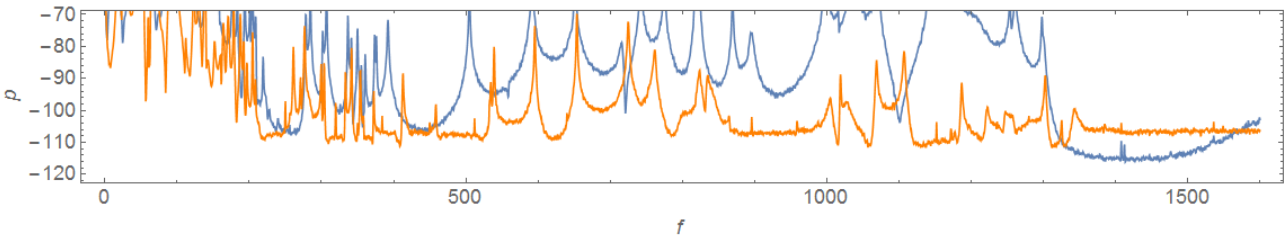

Figure 4.2: Two experiments with uni-axial loading (blue) and torque loading (orange), steel, SR

On Fig.4.2 correspondence is not such clear, but stop-band begins at frequency of 1300 Hz and stop-bands are matching for both loading cases.

Experiments show that steel structure has non-linear behaviour in sense that force amplitude affects on a gap-band picture. Higher amplitude gives less clear picture of gap bands:

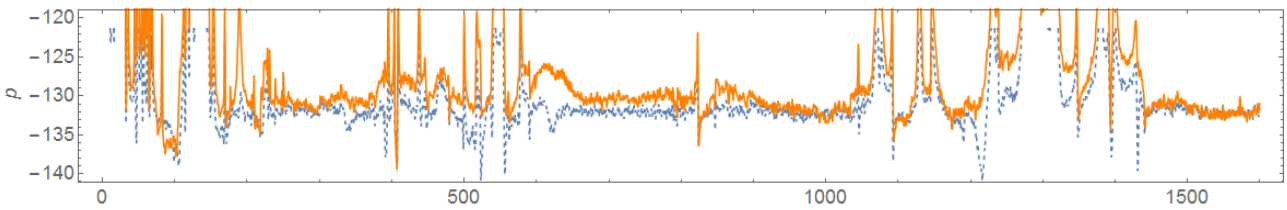

Figure 4.3: Two experiments with loading(II) medium force amplitude (blue) and large force amplitude(orange), steel, LR

For smaller structures non-linear effects vanishing and stop-band picture is the same for any loading amplitude:

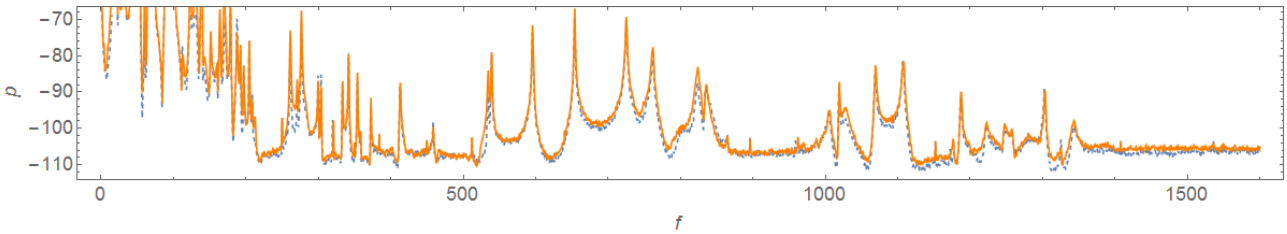

Figure 4.4: Two experiments with loading(II) medium force amplitude (blue) and large force amplitude(orange), steel, SR

Two samples of ordinary helical spring were produced for smaller curvature radius $R_1 = 19mm$. They have same length and curvature radius as prototype of isolator used during experiments. Experiments were conduced with same reference force and shown on the Fig.4.5:

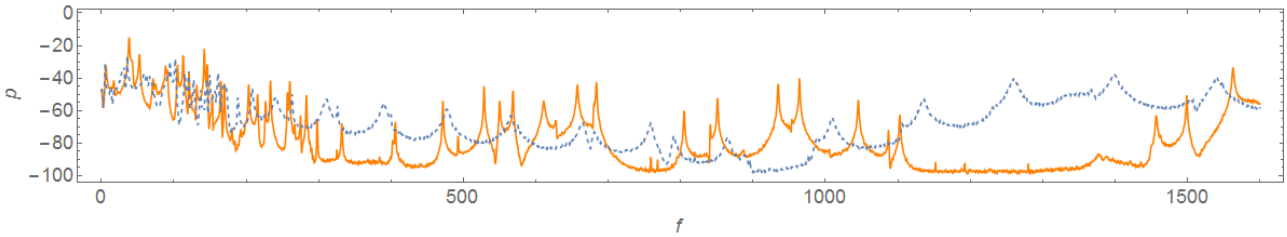

Figure 4.5: Two experiments with loading(I) ordinary spring (Fig.3.9) (blue) and vibration isolator (Fig.3.5) (orange), magnesium-lithium alloy, SR

Comparison shows, that experimental rig and setup is chosen correctly and stop-bands which are shown for vibration isolator are not present in ordinary helical spring. Also, it is shown in contrast, that vibration isolator has attenuation zones, which are not presenting in helical spring.

Experiments show that scale effect present in vibration isolator. Vibration isolator with smaller curvature radius has stop-bands at the higher frequencies as shown on the Fig.4.6:

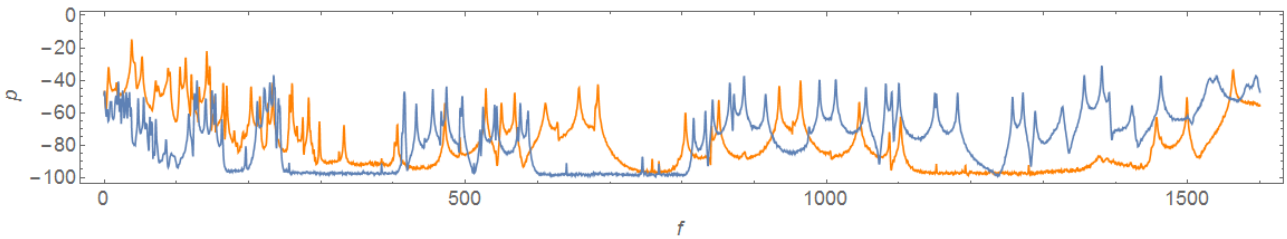

Figure 4.6: Uni-axial loading LR (blue) (Fig.3.4) and SR (orange) (Fig.3.5), magnesium-lithium

Experiments show that stop-bands shown in theoretical part are existing in real prototypes made of two different materials and under two different loading scenarios. It should be emphasized that all prototypes were produced manually and therefore they contain imperfections. Since wavelengths of order 100m are considered, small imperfections do not affect waveguide properties. For more precise experiments required several samples produced mechanically. But even though experiments made with rough samples, they show good correspondence to the theory and it gives reason, that more precise experiments will just give more solid theory proof.

4.2 Comparison with theoretical results

For material and geometry parameters listed in Tab.3.2 Floquet theory gives the following result:

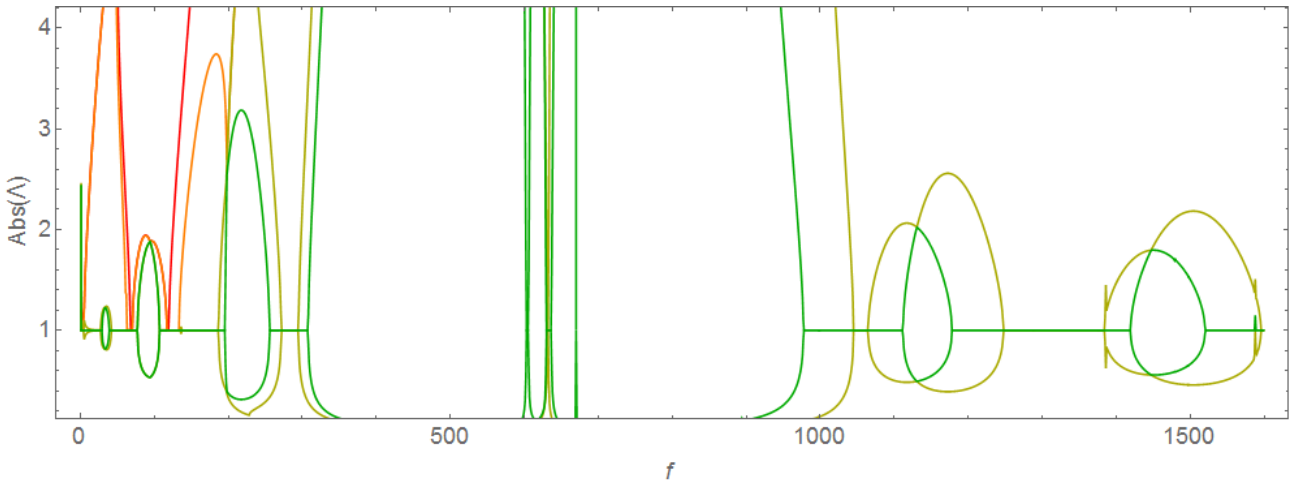

Figure 4.7: Floquet zones for experimental parameters (Tab.3.2), magnesium-lithium alloy, $R_1 = 45$mm

Also for comparison, experimental data obtained from experiments in Ch.3 for parameters used in model is taken (Fig.3.4 represented here for illustrative matters):

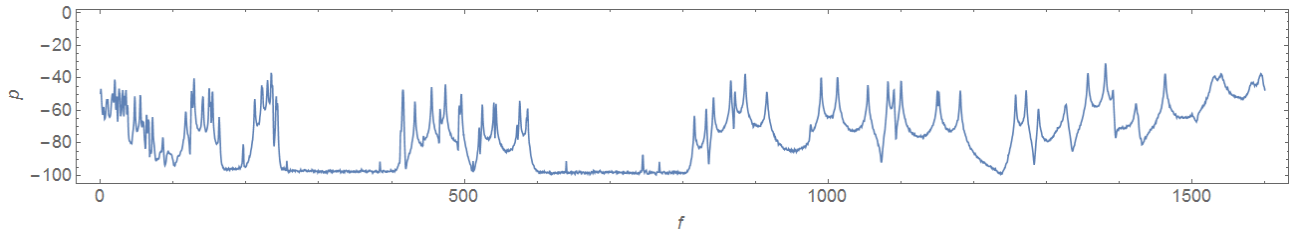

Figure 4.8: Experimental data: uni-axial loading, magnesium-lithium alloy, LR

From Fig.4.7-Fig.4.8 one can obtain stop-band positions. Data from both pictures in comparison can be shown as:

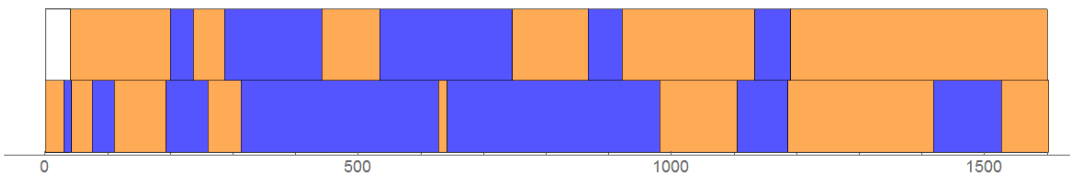

Figure 4.9: Full stop-bands(blue) and pass-bands(orange). Below - Floquet theory,above-experiments

Frequency range 0-40 Hz in experiments is out of scope because test rig is not able to fully capture response of the system. Fig.4.9 shows that Floquet theory have good correlation with experimental data. Thus, it can give good a priori characteristics of vibro-isolation properties and can be used for initial stages of projecting of real structure.

In order to check if correlation preserves for all structures, Floquet zones For material and geometry parameters listed in Tab.3.3 is taken:

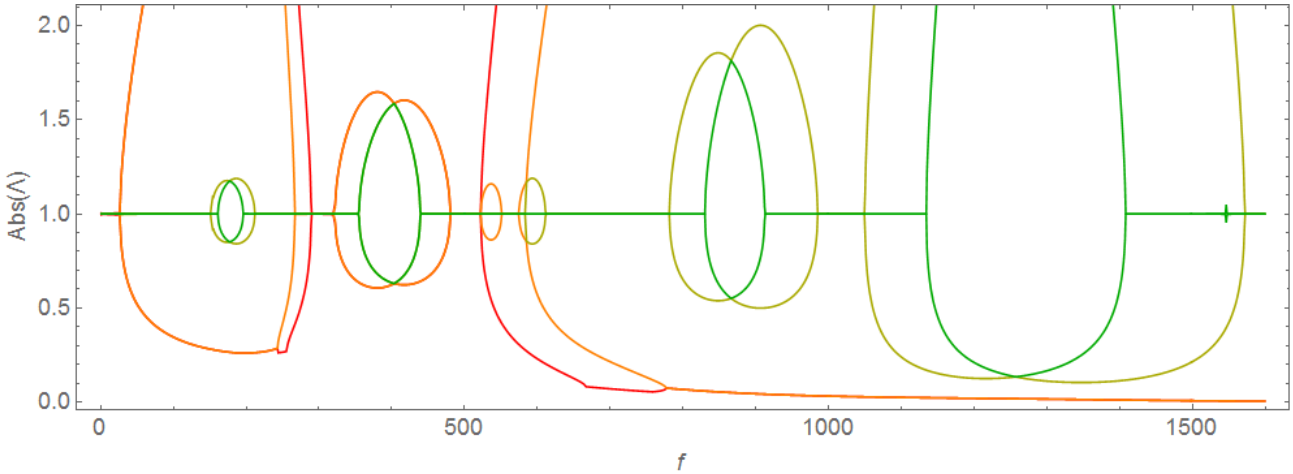

Figure 4.10: Floquet zones for experimental parameters (Tab.3.2), magnesium-lithium alloy, $R_1 = 19$mm

And experimental data for small curvature radius is taken for comparison (Fig.3.5 represented here for illustrative matters):

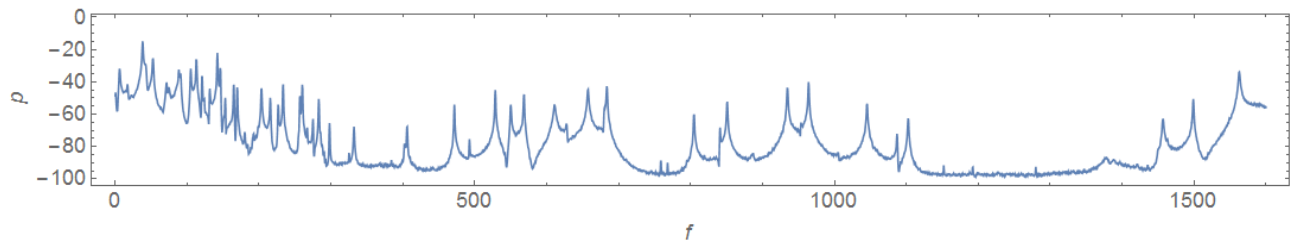

Figure 4.11: Experimental data: uni-axial loading, magnesium-lithium alloy, SR

Both data can be shown in one diagram as :

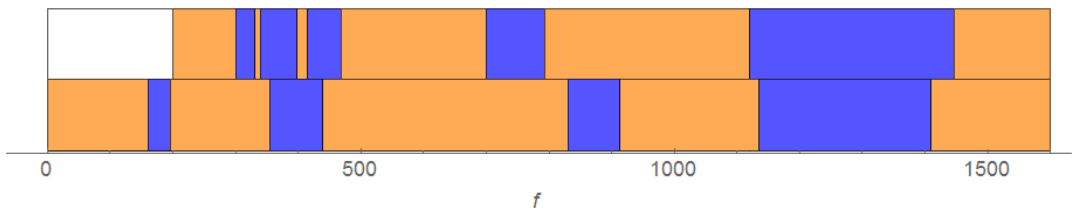

Figure 4.12: Full stop-bands(blue) and pass-bands(orange). Below - Floquet theory,above-experiments

Some frequency range on a Fig.4.12 is also out of scope, but due to scaling effect it is larger (0-200 Hz).

Comparison shows good correlation between Floquet theory, obtained theoretically and experimental data. Difference between theory and experiments can be explained by imperfection of experiments: prototypes were done manually and contain shape and length imperfections. Also,

material data can be obtained more precise. Fig.4.2 and Fig.4.4 show that Floquet theory, developed in Ch.2 can be used as first estimation of Floquet zones, present in real structures.

Both theory and experiments show, that scaling effect are present in vibration isolator and structure with lesser curvature radius have stop-bands at higher frequencies.

Conclusion

In order to conclude, let us reproduce the main idea of this project, stated in the introduction:

"Theoretical and experimental study of properties of the torque vibration isolator, which consists of a finite number of periodically alternating segments."

As an outcome of the master project, the functional model based on the Bernoulli-Euler theory was built. By means of the Floquet theory, existence of stop-bands in periodic torque vibration isolator and connection between dynamics of infinite and finite structures was shown. Theoretical results are proved with experimental data, which shows existence of theoretical stop-bands in real structure, even though number of cells is relatively small. In that way the desired properties of the isolator were predicted theoretically and obtained practically.

The Bernoulli-Euler beam model is relatively simple for computations and with Green's matrices and boundary integrals method used in this project the analysis is numerically stable. Since no discretisation is used the model's accuracy is controlled only by a theory used, so the only restriction on its applicability is the theory validity range. Model is formulated in dimensionless quantities, so it can be used for different scales, also it gives a room for parametric studies.

Wolfram Mathematica language is very illustrative and universal and therefore all codes developed in this project can be rewritten in any other programming language in order to speed up the computations. Also, it is good for large analytical systems and most results in this project are obtained in the closed, although very cumbersome, analytical form.

With all its advantages, the Bernoulli-Euler beam theory has limitations, it is valid for relatively low frequency range. However, it was shown, that the Bernoulli-Euler theory is valid in frequency range used in the industrial applications of the torque vibration isolator and high order theories in that frequency range do not alternate its waveguide properties. Specifically, these theories do not introduce additional propagating waves. Rather, they validate parameters of propagating waves, predicted by the Bernoulli-Euler model. Also, dimensions of large structures can be compared with wavelength, predicted by all theories. Therefore, additional wave phenomena such as diffraction are introduced.

This project has also contributed to the general theory of periodic structures. Specifically, correspondence between eigenfrequencies of a finite structure, consisting of symmetrical spatial multi-segment cells and stop-band borders was shown. Before it was proved only for simple structures in [8]. Existence of pairs of A-type and B-type boundary conditions was predicted by D.J.Mead in [2]. In this work, following [9], it was shown that A-type and B-type boundary conditions can be defined with bi-orthogonality conditions for Bernoulli-Euler curved beam. Another theoretical contribution is the derivation of dispersion equation and analysis of waveguide properties of an opened strip of a cylindrical shell in the circumferential direction.

During experimental sessions it was shown, that loading scenario does not affect picture of stop-bands. That gives possibility to reduce number of experiments, which should be conducted for studying waveguide properties of a periodic structure. Scale effect was shown. Also, it was shown that theoretically obtained with the Floquet theory stop-bands correspond to practical ones and therefore we can conclude that the Floquet theory is a good tool for studying waveguide properties of a periodic structure. Theory shows existence of partial gap-bands, but their consideration was out of scope of this project and also requires more advanced experiment tools and technique.

Future work

Summing all theoretical and practical results, obtained in this project , following directions for future projects and research can be purposed:

- Design, manufacturing and experiments with vibrational isolator with rectangular cross-section
- Finite element modelling and studying of dynamics of a real-sized structure with the emphasis on the influence of interfacial condition between the isolator and adjacent components
- Studying and modelling of additional wave effects (e.g. diffraction) in real-sized structure
- Studying of partial stop-bands
- Developing of a high-order cylindrical shell theory to capture ’bending-twist’ deformation of an opened cylindrical shell
- Formulation of a high-order isolator model in scope of Floquet theory valid for low- and mid-frequency ranges, comparison with Bernoulli-Euler beam
- Studying of non-symmetrical periodicity cells eigenfrequency distribution. Search for set of "symmetrizing" boundary conditions, such that eigenfrequencies will be located on gap band borders.
- Deep parametric studies and deep investigation of scale effects
- Design of different types of vibration isolators, based on theoretical tools and practical data, obtained in this master project

Literature

1. L.Brillouin. Wave Propagation in Periodic Structures second ed. Dover Publications New York, 1953.

2. D.J.Mead. Wave propagation in continuous periodic structures. Research contributions from Southampton 1964-1995 // Journal of Sound and Vibration. 1996. Vol. 190. P. 495–524.

3. A.Søe-Knudsen, R.Darula, Sorokin S. Theoretical and experimental analysis of the stop-band behavior of elastic springs with periodically discontinuous of curvature // Journal of the Acoustical Society of America. 2012. Vol. 132. P. 1378–1383.

4. A.Søe-Knudsen, Sorokin S. Modelling of linear wave propagation in spatial fluid filled pipe systems consisting of elastic curved and straight elements // Journal of Sound and Vibration. 2010. Vol. 329. P. 5116–5146.

5. A.Søe-Knudsen. Design of stop-band filter by use of curved pipe segments and shape optimization // Structural and Multidisciplinary Optimization. 2011. Vol. 44. P. 863–874.

6. A.Søe-Knudsen. Design of stop-band filters by use of compound curved pipe segments and shape optimization // 10th International Conference on Recent Advances in Structural Dynamics. Institute of Sound and Vibration Research, 2010.

7. A.Hvatov, S.Sorokin. Analysis of eigenfrequencies of finite periodic structures in view of location of frequency pas- and stop-bands // Proceedings of 20th International Congress on Sound and Vibration. 2013.

8. A.Hvatov, S.Sorokin. Free vibrations of finite periodic structures in pass- and stop-bands of the counterpart infinite waveguides // Journal of Sound and Vibration. 2015. Vol. 347. P. 200–217.

9. S.Sorokin. On the bi-orthogonality conditions for multi-modal elastic waveguides. // Journal of Sound and Vibration. 2013. Vol. 332. P. 5606–5617.

10. Skudrzyk E. The Foundations of Acoustics. Basic mathematics and basic acoustics. Springer-Verlag, 1971.

11. A.Hvatov. Torque Vibrational Isolator. 9th semester DMS3 study project, 2016.

12. S.Sorokin. The Green's matrix and the boundary integral equations for analysis of time-harmonic dynamics of elastic helical springs. // Journal of the Acoustical Society of America. 2011. Vol. 129. P. 1315–1323.

13. L.D.Landau, E.M.Lifshitz. The Classical Theory of Fields. Pergamon Press, 1971.

14. L.I.Slepyan. Non-steady-state Elastic Waves (in Russian). Sudostroenie, Leningrad, 1972.

15. S.V.Sorokin, J.B.Nielsen, N.Olhoff. Green's matrix and the boundary integral equation method for the analysis of vibration and energy flow in cylindrical shells with and without internal fluid loading // Journal of Sound and Vibration. 2004. Vol. 271. P. 815–847.

16. Materials Data Book. Cambridge University Engineering Department, 2003.

17. Achenbach J. D. Reciprocity in Elastodynamics. Cambridge University Press, 2003.

18. S.P.Timoshenko, J.M.Gere. Theory of Elastic Stability, 2nd edition. Dover Publication, 2003.

19. Dym C. L., I.H.Shames. Energy and finite element methods in structural mechanics. Taylor&Francis, 2003.

20. A.L.Goldenweiser. Theory of Thin Elastic Shells. Pergamon Press, 1961.

Appendix A

Bernoulli-Euler curved beam vibrations

A.1 Equations of motion

A.1.1 In-plane vibrations

Equations of motion of flat ring in-plane vibrations have the form [12]:

$$\begin{array}{l} \rho A\frac{\partial^2 u}{\partial t^2} = \frac{\partial Q_x}{\partial s} + \frac{1}{R}N_z + p_u - \frac{\partial p_\beta}{\partial s} \\ \rho A\frac{\partial^2 w}{\partial t^2} = \frac{\partial N_z}{\partial s} - \frac{1}{R}Q_x + p_w + \frac{1}{R}p_\beta \end{array} \tag{A.1}$$

,where u - x-axis displacement, w - z-axis displacement, β - rotation with respect to y axis, Q_i, N_i - components of force vector, M_i, T_i-components of moment vector, R is the radius of curvature. Generalized forces and rotation with Bernoulli-Euler assumptions have form:

$$\begin{array}{l} \frac{M_y}{EI_y} = \frac{\partial \beta}{\partial s}\,, Q_x = -\frac{\partial M_y}{\partial s} \\ \frac{N_z}{EA} = \frac{\partial w}{\partial s} - \frac{1}{R}u\,, \beta = \frac{\partial u}{\partial s} + \frac{1}{R}w \end{array} \tag{A.2}$$

For brevity no external loading considered, i.e. $p_u = p_w = p_\beta \equiv 0$

Time and space dependence for both in-plane and out-plane vibration has the form:

$$\{u(\bar{s},t), v(\bar{s},t), w(\bar{s},t), \gamma(\bar{s},t)\}^T = \{\bar{U}, \bar{V}, \bar{W}, \Gamma\}^T exp(k_{\dim}\bar{s} - i\omega t) \tag{A.3}$$

For rectangular cross-section $I_y = \frac{hb^3}{12}$.

Following dimensionless parameters used:

$$\Omega = \frac{\omega h}{c}, k = k_{\dim}h, s = \frac{\bar{s}}{h}, U = \frac{\bar{U}}{h}, V = \frac{\bar{V}}{h}, W = \frac{\bar{W}}{h}, \varepsilon = \frac{h}{R} \tag{A.4}$$

With time and space dependence Eq.A.3, moments of inertia and dimensionless parameters Eq.A.4substituted into the system Eq.A.1-Eq.A.2 following system is obtained:

$$\begin{array}{l} W(12k\varepsilon - k^3\varepsilon) + U(-k^4 + 12\Omega^2 - 12\varepsilon^2) \\ W(12k^2 + k^2\varepsilon^2 + 12\Omega^2) + U(-12\mathrm{k}\varepsilon + k^3\varepsilon) = 0 \end{array} \tag{A.5}$$

Determinant of system of algebraical linear equations Eq.A.5 gives 6th order polynomial in k, which is called dispersion relation:

$$k^6 + k^4\Omega^2 + 2k^4\varepsilon^2 - 12k^2\Omega^2 + k^2\varepsilon^4 - k^2\Omega^2\varepsilon^2 - 12\Omega^4 + 12\Omega^2\varepsilon^2 \tag{A6'}$$

For circular cross-section $I_y = \frac{\pi d^4}{64}$.

Following dimensionless parameters used:

$$\Omega = \frac{\omega d}{c}, k = k_{\dim}d, s = \frac{\bar{s}}{d}, U = \frac{\bar{U}}{d}, V = \frac{\bar{V}}{d}, W = \frac{\bar{W}}{d}, \varepsilon = \frac{d}{R} \tag{A.6}$$

With time and space dependence Eq.A.3 ,moments of inertia and dimensionless parameters Eq.A.6 substituted into the system Eq.A.1-Eq.A.2 following system is obtained:

$$\begin{aligned} W\left(16\mathrm{k}\varepsilon - \mathrm{k}^3\varepsilon\right) + U\left(-\mathrm{k}^4 - 16\varepsilon^2 + 16\Omega^2\right) = 0 \\ U\left(-16\mathrm{k}\varepsilon + \mathrm{k}^3\varepsilon\right) + W\left(16\mathrm{k}^2 + \mathrm{k}^2\varepsilon^2 + 16\Omega^2\right) = 0 \end{aligned} \tag{A.7}$$

Determinant of system of algebraical linear equations Eq.A.7 gives 6th order polynomial in k:

$$k^6 + k^4\Omega^2 + 2k^4\varepsilon^2 - 16k^2\Omega^2 + k^2\varepsilon^4 - k^2\Omega^2\varepsilon^2 - 16\Omega^4 + 16\Omega^2\varepsilon^2 \tag{A9'}$$

Both equations Eq.A6' and Eq.A9' when solved with respect to k give 6 wavenumbers $k_i^{(in)}$:

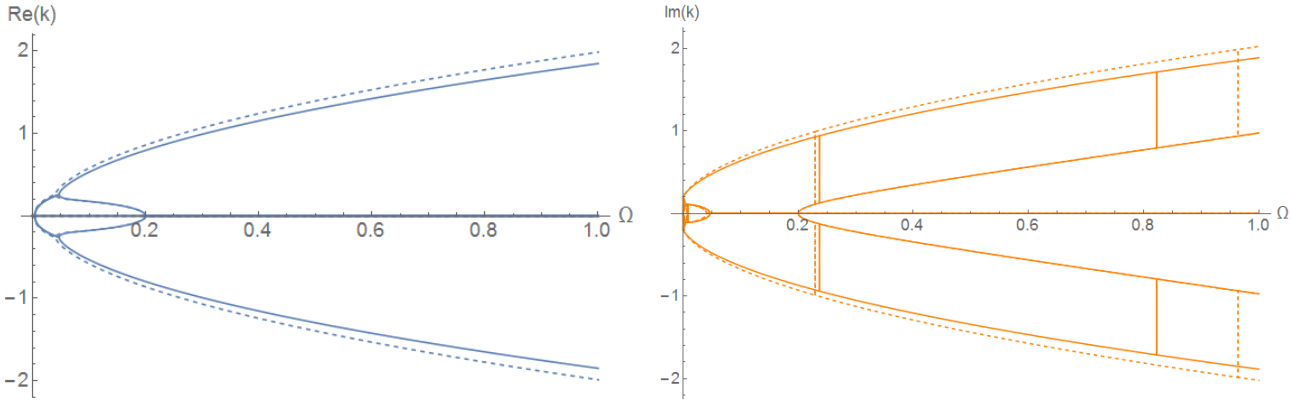

Figure A.1: $k^{(in)}$ for rectangular cross-section and circular cross-section (dashed) real parts(blue) and imaginary parts (orange), ($\epsilon_1 = 0.2, \epsilon_2 = 0.02$, $\frac{h}{b} = \frac{1}{20}$)

Different forms of wave number k_i represents different form of waves. At the given frequency Ω, value $k(\Omega)$ can be pure real, pure imaginary and complex number. Since space dependence $\exp(k\,s)$ considered, pure imaginary $k(\Omega)$ represents propagating wave (wave that does not change its absolute value when s is changing). Since dispersion equation has only even powers of k one can state that if ik_{im} is the root of dispersion relation, then $-ik_{im}$ also the root. Root ik_{im} defines wave propagating from left to right (with time dependence $\exp(-i\omega t)$) and root $-ik_{im}$ defines wave propagating from right to left. Pure real value k_{re} represents evanescent waves (waves that exponentially decreasing from left to right or from right to left):

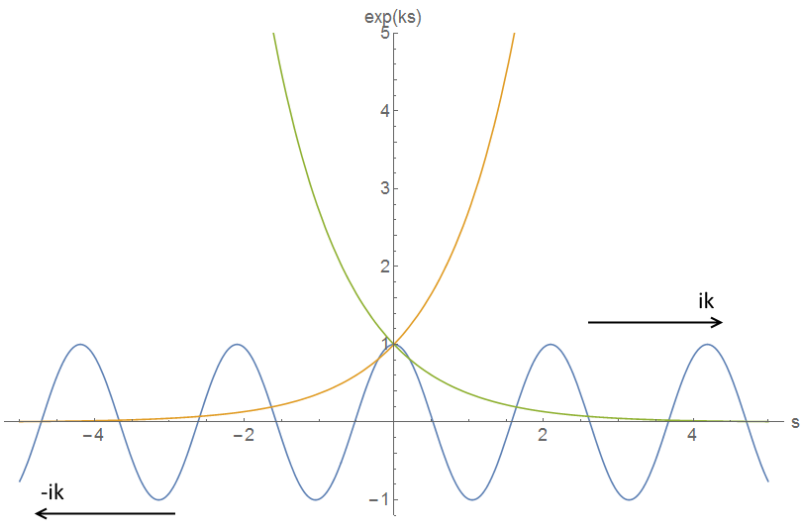

Figure A.2: Different form of waves: pure imaginary ik_{im} (blue), pure real $k_{re} > 0$ (orange), pure real $k_{re} < 0$ (green)

Complex value represents wave $k_{comp} = k_{comp}^{(re)} + ik_{comp}^{(im)}$, propagating from left to right or from right to left (depends on a sign of imaginary part $k_{comp}^{(im)}$) modulated by $\exp(k_{comp}^{(re)}s)$,i.e. oscillating between two curves $\exp(k_{comp}^{(re)}s)$ and $-\exp(k_{comp}^{(re)}s)$ (shown dashed on the following figure) :

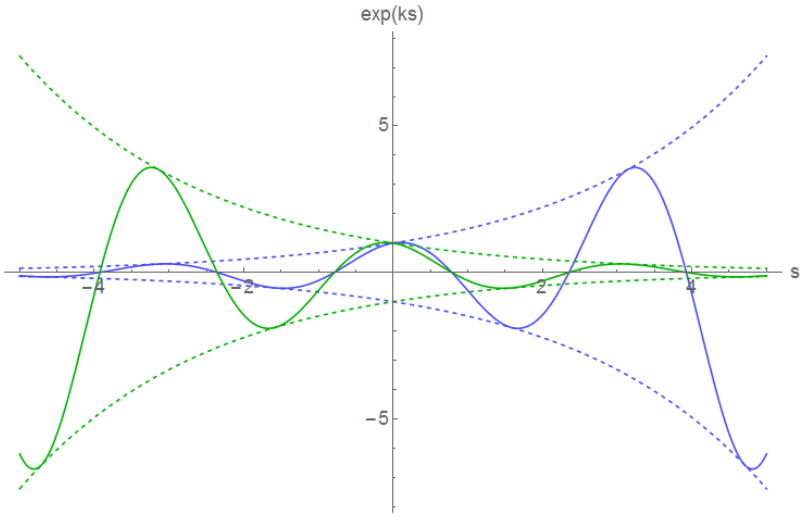

Figure A.3: Different form of waves $k_{comp} = k_{comp}^{(re)} + ik_{comp}^{(im)}$: $k_{comp}^{(re)} > 0$ (blue), $k_{comp}^{(re)} < 0$ (green)

It is also convenient to introduce modal coefficient $m_w = \frac{W}{U}$, which is found from equations Eq.A.5 and Eq.A.7 for each wave number individually. In that case $m_u = \frac{U}{U} = 1$. Also, modal coefficients for forces, moments and rotation for rectangular cross-section are introduced as:

$$\begin{aligned} m_\beta &= (k\, m_u + \varepsilon\, m_w) \\ m_{My} &= k\, m_\beta \\ m_{Nz} &= 12\,(k\, m_w - \varepsilon\, m_u) \\ m_{Qx} &= -k\, m_{My} \end{aligned} \tag{A.10(a)}$$

And for circular cross-section:

$$\begin{aligned} m_\beta &= (k\, m_u + \varepsilon\, m_w) \\ m_{My} &= k\, m_\beta \\ m_{Nz} &= 16\,(k\, m_w - \varepsilon\, m_u) \\ m_{Qx} &= -k\, m_{My} \end{aligned} \tag{A.10(b)}$$

A.1.2 Out-plane vibrations

Equations of motion of flat ring out-of-plane vibrations have the form:

$$\begin{aligned} \rho I_p \frac{\partial^2 \gamma}{\partial t^2} &= \frac{\partial T_z}{\partial s} - \frac{1}{R} M_x + p_\gamma \\ \rho A \frac{\partial^2 v}{\partial t^2} &= \frac{\partial Q_y}{\partial s} + p_v + \frac{\partial p_\alpha}{\partial s} \end{aligned} \tag{A.9}$$

With generalized forces and rotation with Bernoulli-Euler assumptions in form:

$$\begin{aligned} \frac{M_x}{EI_x} &= \frac{\partial \alpha}{\partial s} + \frac{1}{R}\gamma\,,\ \frac{T_z}{GI_p} = \frac{\partial \gamma}{\partial s} - \frac{1}{R}\alpha \\ Q_y &= \frac{\partial M_x}{\partial s} + \frac{1}{R} T_z\,,\ \alpha = -\frac{\partial v}{\partial s} \end{aligned} \tag{A.10}$$

Where, v - y-axis displacement, α - rotation with respect to x-axis, γ - rotation with respect to z-axis. For rectangular cross-section $I_x = \frac{bh^3}{12}, I_p = \kappa bh^3$,where κ is the shear coefficient, in this work $\kappa = \frac{1}{3}(1 - 0.63\frac{h}{b})$

With time and space dependence Eq.A.3, moments of inertia, and dimensionless parameters Eq.A.4 (Eq.A.6) substituted into the system Eq.A.9-Eq.A.10 following systems are obtained:

$$\Gamma(\tfrac{6\kappa}{\nu+1}k^2 + 12\kappa\Omega^2 + -\varepsilon^2) + V(\tfrac{6\kappa\epsilon}{\nu+1}k^2 + k^2\varepsilon) = 0$$
$$\Gamma(\tfrac{6\kappa k^2\epsilon}{\nu+1} + k^2\epsilon) + V(-k^4 + \tfrac{6\kappa\varepsilon^2}{\nu+1}k^2 + 12\Omega^2) = 0 \qquad \text{(A.13(rectangular))}$$

For circular cross-section $I_x = \frac{\pi d^4}{64}, I_p = \frac{\pi d^4}{32}$.

$$\Gamma\left(\tfrac{k^2}{\nu+1} + 2\Omega^2 - \varepsilon^2\right) + V\left(\tfrac{k^2\varepsilon}{\nu+1} + k^2\varepsilon\right) = 0$$
$$\Gamma\left(\tfrac{k^2\varepsilon}{\nu+1} + k^2\varepsilon\right) + V\left(-k^4 + \tfrac{k^2\varepsilon^2}{\nu+1} + 16\Omega^2\right) = 0 \qquad \text{(A.13(circular))}$$

Determinants of the systems Eq.A.13(rectangular) and Eq.A.13(circular):

$$-k^6 - 2k^4\nu\Omega^2 - 2k^4\Omega^2 - 2k^4\varepsilon^2 + 12k^2\Omega^2 - k^2\varepsilon^4 + 12\kappa k^2\Omega^2\varepsilon^2 + 24\nu\Omega^4 + 24\Omega^4 - \frac{2\nu\Omega^2\varepsilon^2}{\kappa} - \frac{2\Omega^2\varepsilon^2}{\kappa} \qquad \text{(A.14(rectangular))}$$

$$-k^6 - 2k^4\nu\Omega^2 - 2k^4\Omega^2 - 2k^4\varepsilon^2 + 16k^2\Omega^2 - k^2\varepsilon^4 + 2k^2\Omega^2\varepsilon^2 + 32\nu\Omega^4 + 32\Omega^4 - 16\nu\Omega^2\varepsilon^2 - 16\Omega^2\varepsilon^2 \qquad \text{(A.14(circular))}$$

Also gives 6 wavenumbers $k_i^{(out)}$:

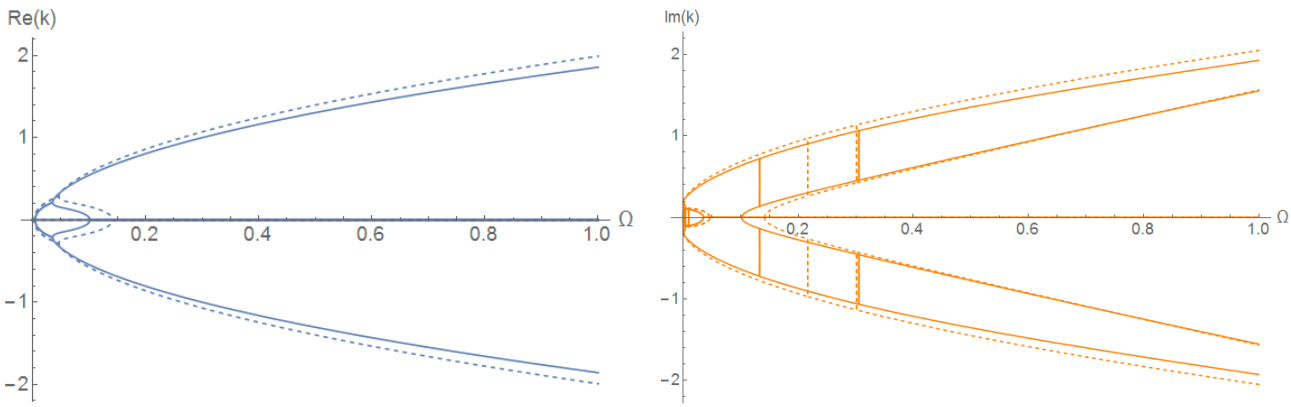

Figure A.4: $k^{(out)}$ for rectangular cross-section and circular cross-section (dashed) real parts(blue) and imaginary parts (orange) ($\epsilon_1 = 0.2, \epsilon_2 = 0.02, \frac{h}{b} = \frac{1}{20}$)

Modal coefficients in this case have form:

$$\begin{aligned} m_\gamma &= 1 & m_v &= \tfrac{V}{\Gamma} \\ m_\alpha &= -km_v & m_{My} &= (k\,m_\alpha + \varepsilon m_\gamma) \\ m_{Tz} &= \tfrac{6\kappa}{1+\nu}\,(k\,m_\gamma - \varepsilon\,m_\alpha) & m_{Qy} &= k\,m_{Mx} + \varepsilon m_{Tz} \end{aligned} \qquad \text{(A.15(rectangular))}$$

$$\begin{aligned} m_\gamma &= 1 & m_v &= \tfrac{V}{\Gamma} \\ m_\alpha &= -km_v & m_{My} &= (k\,m_\alpha + \varepsilon m_\gamma) \\ m_{Tz} &= \tfrac{1}{1+\nu}\,(k\,m_\gamma - \varepsilon\,m_\alpha) & m_{Qy} &= k\,m_{Mx} + \varepsilon m_{Tz} \end{aligned} \qquad \text{(A.15(circular))}$$

A.2 Boundary integrals method

Definition of Green's matrix for a system of a differential equation is the same as for Green's function for a single equation, but in case of n equations with m variable functions n load cases should be considered. In each case one load is represented by delta-function whereas other are zero. Therefore, Green's matrix has dimensions $n \times m$.

Since in boundary integrals method Green's matrix for infinite structure considered, Green's matrix should satisfy radiation and decay conditions at the infinity [10]. Therefore, not all wavenumbers can be considered. Detailed explanation of principle of choice and all necessary references contained in [12]. Among six roots of both dispersion relations we choose one complex with negative real part ($Re(k) < 0$) and two purely imaginary roots with $c_{group} = \frac{dk_{din}}{d\omega} > 0$ for each in-plane and out-plane equations.

For Green's matrix derivation bi-orthogonality condition will be used. It can be derived from reciprocity theorem, which is well known for most commonly used linear differential equations and for elastic helical spring is described in [17]. Derivation of all bi-orthogonality conditions used here can be found in [9].

A.2.1 In-plane vibrations

Bi-orthogonality condition for this case has the form:

$$M_y^A(s)\beta^B(s) + N_z^A(s)w^B(s) - u^A(s)Q_x^B(s) = 0 \tag{A.14}$$

Or with modal coefficients introduced in Eq. A.15(rectangular)-Eq.A.15(circular):

$$m_{My}^{(i)}\, m_{\beta}^{(j)} + m_{Nz}^{(i)}\, m_{w}^{(j)} - m_{u}^{(i)}\, m_{Qx}^{(j)} = 0 \ (i \neq j) \tag{A.15}$$

Equations Eq.A.14-Eq.A.15 are called bi-orthogonality conditions for flat ring in-plane vibrations. And with reciprocity theorem they are widely used in Green's functions theory and for boundary integral equations derivation.

In in-plane ring vibrations case each string of Green's matrix represents solution for each of a loading case $p_i = \delta(s)$, $p_j = 0\,(i \neq j\ ;\ i, j \in \{u, w, \beta\})$

In order to find Green's matrix, property of force unit jump of Green's function also used. Three load cases considered: load case 1 $N_z(0) = -\frac{1}{2}sign(s)$ (it represents case $p_w = \delta(s)$), load case 2 $M_y(0) = -\frac{1}{2}sign(s)$ ($p_\beta = \delta(s)$) and load case 3 $Q_x(0) = -\frac{1}{2}sign(s)$ ($p_u = \delta(s)$). With that loading cases introduced it is convenient to split Forces/Moments and displacements into two groups:

$$\begin{array}{l} \{w(s), \beta(s), Q_x(s)\} \\ \{u(s), N_z(s), M_y(s)\} \end{array} \tag{A.16}$$

If functions of first group are even, then functions of second group are odd and vice versa. Since Heaviside theta-function is odd function, only continuity of functions should be considered. Even functions have property of continuity at zero, and therefore, functions of second group are continuous.

Let us consider loading case 1. Significant part of Green's matrix has a following form:

$$\{u(s), N_z(s), M_y(s)\} = \sum_{i=1}^{3} \{m_u^{(i)}, m_{Nz}^{(i)}, m_{My}^{(i)}\}\Gamma_i^{(1)} \exp(k_i\, abs(s))sign(s) \tag{A.17}$$

Properties of Green's matrix have following form:

$$
\begin{aligned}
&u(0) = 0 \\
&M_y(0) = 0 \\
&N_z(0) = -\tfrac{1}{2} sign(s)
\end{aligned}
\tag{A.18}
$$

Substituting A.17 to A.18 and multiplying each string to $m_{Qx}^{(j)}$, $m_{\beta}^{(j)}$, $m_{w}^{(j)}$ $(j = 1, 2, 3)$ respectively:

$$
\begin{aligned}
&\sum_{i=1}^{3} \Gamma_i^{(1)} m_u^{(i)} m_{Qx}^{(j)} = 0 \\
&\sum_{i=1}^{3} \Gamma_i^{(1)} m_{My}^{(i)} m_{\beta}^{(j)} = 0 \\
&\sum_{i=1}^{3} \Gamma_i^{(1)} m_N z^{(i)} m_w^{(j)} = -\tfrac{1}{2}
\end{aligned}
\tag{A.19}
$$

Summing all equations in A.19:

$$
\sum_{i=1}^{3} \Gamma_i^{(1)} (m_u^{(i)}\, m_{Qx}^{(j)} + m_{My}^{(i)}\, m_{\beta}^{(j)} + m_{Nz}^{(i)}\, m_w^{(j)}) = -\frac{1}{2}
\tag{A.20}
$$

Expression in brackets is exactly bi-orthogonal condition A.15 and it is not zero only when $i = j$. Thus one can obtain explicit form of each coefficient $\Gamma_i^{(1)}$.

In same way all Green's matrix coefficient entries can be found as:

$$
\begin{aligned}
\Gamma(in)_i^{(1)} &= -\tfrac{1}{2} \frac{m_w^{(i)}}{m_{My}^{(i)}\, m_{\beta}^{(i)} + mNz_i\, m_w^{(i)} - m_u^{(i)}\, m_{Qx}^{(i)}} \\
\Gamma(in)_i^{(2)} &= -\tfrac{1}{2} \frac{m_{\beta}^{(i)}}{m_{My}^{(i)}\, m_{\beta}^{(i)} + mNz_i\, m_w^{(i)} - m_u^{(i)}\, m_{Qx}^{(i)}} \\
\Gamma(in)_i^{(3)} &= \tfrac{1}{2} \frac{m_u^{(i)}}{m_{My}^{(i)}\, m\beta_i + mNz_i\, m_w^{(i)} - m_u^{(i)}\, m_{Qx}^{(i)}}
\end{aligned}
\tag{A.21}
$$

After coefficients found green matrix formed as (on example of loading case 1):

$$
\begin{aligned}
&G_1^{in}(s, s_0) = \{u^{(n)}(s), w^{(n)}(s), \beta^{(n)}(s), Q_x^{(n)}(s), N_z^{(n)}(s), M_y^{(n)}(s)\} = \\
&\sum_{i=1}^{3} \{sign(s)\, m_u^{(i)}, m_w^{(i)}, m_{\beta}^{(i)}, m_{Qx}^{(i)}, sign(s)\, mNz_i, sign(s)\, m_{My}^{(i)}\} \Gamma(in)_i^{(1)} \exp(k_i^{in}\, abs(s - s_0))
\end{aligned}
\tag{A.22}
$$

After Green's matrix found, one can obtain displacement, expressed in terms of Green's matrix (analogous to 1.22) in same way as it done in Ch.1. It can be written as ([17]):

$$
\delta_{1n} w(s_0) + \delta_{2n} \beta(s_0) + \delta_{3n} u(s_0) = \left[G_n^{in}(s, s_0). \{Q_x(s), Nz(s), My(s), -u(s), -w(s), -\beta(s)\} \right]_{s=a}^{s=b}
\tag{A.23}
$$

,where δ_{ij} -Kronecker's delta and $\{\}.\{\}$ - dot product of two vectors. Equations Eq.A.23 called boundary integrals for ring in-plane vibrations.

A.2.2 Out-plane vibrations

In same way, with three loading cases: load case 1 $Q_y(0) = -\frac{1}{2} sign(s)$ ($p_u = \delta(s)$), load case 2 $T_z(0) = -\frac{1}{2} sign(s)$ ($p_{\gamma} = \delta(s)$) and load case 3 $M_x(0) = -\frac{1}{2} sign(s)$ ($p_{\alpha} = \delta(s)$).

Two groups of functions:

$$
\begin{aligned}
&\{v(s), \gamma(s), M_x(s)\} \\
&\{\alpha(s), T_z(s), Q_y(s)\}
\end{aligned}
\tag{A.24}
$$

And bi-orthogonality condition:

$$m_{Tz}^{(i)}\, m_{\gamma}^{(j)} + m_{Qy}^{(i)}\, m_{v}^{(j)} - m_{\alpha}^{(i)}\, m_{Mx}^{(j)} = 0 \ (i \neq j) \tag{A.25}$$

One can obtain Green's matrix coefficients in form:

$$\begin{aligned} \Gamma(out)_i^{(1)} &= -\tfrac{1}{2}\tfrac{m_v^{(i)}}{m_{Tz}^{(i)}\, m_{\gamma}^{(i)} + m_{Qy}^{(i)}\, m_v^{(i)} - m_{\alpha}^{(i)}\, m_{Mx}^{(i)}} \\ \Gamma(out)_i^{(2)} &= -\tfrac{1}{2}\tfrac{m_{\gamma}^{(i)}}{m_{Tz}^{(i)}\, m_{\gamma}^{(i)} + m_{Qy}^{(i)}\, m_v^{(i)} - m_{\alpha}^{(i)}\, m_{Mx}^{(i)}} \\ \Gamma(out)_i^{(3)} &= \tfrac{1}{2}\tfrac{m_{\alpha}^{(i)}}{m_{Tz}^{(i)}\, m_{\gamma}^{(i)} + m_{Qy}^{(i)}\, m_v^{(i)} - m_{\alpha}^{(i)}\, m_{Mx}^{(i)}} \end{aligned} \tag{A.26}$$

Green's matrix in form:

$$\begin{aligned} &G_1^{out}(s, s_0) = \{v^{(n)}(s), \alpha^{(n)}(s), \gamma^{(n)}(s), Q_y^{(n)}(s), M_z^{(n)}(s), T_z^{(n)}(s)\} = \\ &\sum_{i=1}^{3} \{m_v^{(i)}, sign(s)\, m_{\alpha}^{(i)}, m\gamma_i, sign(s)\, m_{Qy}^{(i)}, m_{Mx}^{(i)}, sign(s)\, m_{Tz}^{(i)}\} \Gamma(out)_i^{(1)} \exp(k_i^{out}\, abs(s - s_0)) \end{aligned} \tag{A.27}$$

And boundary equations in form:

$$\delta_{1n} v(s_0) + \delta_{2n}\gamma(s_0) + \delta_{3n}\alpha(s_0) = \left[G_n^{out}(s, s_0).\, \{Q_y(s), Mx(s), Tz(s), -u(s), -\alpha(s), -\gamma(s)\}\right]_{s=a}^{s=b} \tag{A.28}$$

Appendix B

Elastic layer in-plane vibrations

We consider plane strain state and therefore following constitutive law can be used [18]:

$$\begin{pmatrix}\sigma_{rr}\\ \sigma_{\theta\theta}\\ \sigma_{r\theta}\end{pmatrix} = \begin{bmatrix}2\mu+\lambda & \lambda & 0\\ \lambda & 2\mu+\lambda & 0\\ 0 & 0 & 2\mu\end{bmatrix}\begin{pmatrix}\epsilon_{rr}\\ \epsilon_{\theta\theta}\\ \epsilon_{r\theta}\end{pmatrix} \tag{B.1}$$

With following strain definition:

$$\begin{pmatrix}\epsilon_{rr}\\ \epsilon_{\theta\theta}\\ \epsilon_{r\theta}\end{pmatrix} = \begin{pmatrix}\frac{\partial u_r}{\partial r}\\ \frac{1}{r}(\frac{\partial}{\partial\theta}u_\theta + u_r)\\ \frac{1}{2}(\frac{1}{r}\frac{\partial}{\partial\theta}u_r + \frac{\partial u_\theta}{\partial r} - \frac{u_\theta}{r})\end{pmatrix} \tag{B.2}$$

Energy potential has a form:

$$U = \frac{1}{2}\iint\limits_S \sigma_{rr}\epsilon_{rr} + 2\sigma_{r\theta}\epsilon_{r\theta} + \sigma_{\theta\theta}\epsilon_{\theta\theta}dS \tag{B.3}$$

In this appendix, following references, equations in statics are considered. Equating first variation of energy potential to zero:

$$\delta U = \frac{1}{2}\iint\limits_S \delta\sigma_{rr}\epsilon_{rr} + \sigma_{rr}\delta\epsilon_{rr} + 2\delta\sigma_{r\theta}\epsilon_{r\theta} + 2\sigma_{r\theta}\delta\epsilon_{r\theta} + \delta\sigma_{\theta\theta}\epsilon_{\theta\theta} + \sigma_{\theta\theta}\delta\epsilon_{\theta\theta}dS = 0 \tag{B.4}$$

Let us now find first variation by using by-part integration:

$$I_1 = \iint\limits_S \epsilon_{rr}\delta\sigma_{rr}dS = \iint\limits_S \epsilon_{rr}\delta((2\mu+\lambda)\frac{\partial u_r}{\partial r} + \lambda\frac{1}{r}(\frac{\partial}{\partial\theta}u_\theta + u_r))dS \tag{B.5}$$

$$\begin{aligned}
I_{11} &= \iint\limits_S (2\mu+\lambda)\epsilon_{rr}\delta(\tfrac{\partial u_r}{\partial r})dS = \int\limits_{\theta_1}^{\theta_2}(2\mu+\lambda)\epsilon_{rr}r\delta u_r\Big|_{r=a}^{r=b}d\theta - \iint\limits_S (2\mu+\lambda)\tfrac{\partial\epsilon_{rr}}{\partial r}\delta u_r dS\\
I_{12} &= \iint\limits_S \tfrac{\lambda}{r}\epsilon_{rr}\delta(\tfrac{\partial u_\theta}{\partial\theta})dS = \int\limits_a^b \tfrac{\lambda}{r}r\epsilon_{rr}\delta u_\theta\Big|_{\theta=\theta_1}^{\theta=\theta_2}dr - \iint\limits_S \tfrac{\lambda}{r}\tfrac{\partial\epsilon_{rr}}{\partial\theta}\delta u_\theta dS\\
I_{13} &= \iint\limits_S \tfrac{\lambda}{r}\epsilon_{rr}\delta u_r dS
\end{aligned} \tag{B.6}$$

$$I_2 = \iint\limits_S \sigma_{rr}\delta\epsilon_{rr}dS = \iint\limits_S \sigma_{rr}\delta(\frac{\partial u_r}{\partial r})dS = \int\limits_{\theta_1}^{\theta_2}\sigma_{rr}r\delta u_r\Big|_{r=a}^{r=b}d\theta - \iint\limits_S \frac{\partial\sigma_{rr}}{\partial r}\delta u_r dS \tag{B.7}$$

$$I_3 = \iint\limits_S \epsilon_{r\theta}\delta\sigma_{r\theta}dS = I_4 = \iint\limits_S \sigma_{r\theta}\delta\epsilon_{r\theta}dS = 2\mu\iint\limits_S \epsilon_{r\theta}\delta\epsilon_{r\theta}dS = \mu\iint\limits_S \epsilon_{r\theta}\delta(\frac{1}{r}\frac{\partial}{\partial\theta}u_r + \frac{\partial u_\theta}{\partial r} - \frac{u_\theta}{r})dS \tag{B.8}$$

$$\begin{aligned}
I_{31} &= \iint\limits_S \tfrac{\mu}{r}\epsilon_{r\theta}\delta(\tfrac{\partial u_r}{\partial\theta})dS = \int\limits_a^b \tfrac{\mu}{r}r\epsilon_{r\theta}\delta u_r\Big|_{\theta=\theta_1}^{\theta=\theta_2}dr - \iint\limits_S \tfrac{\mu}{r}\tfrac{\partial\epsilon_{r\theta}}{\partial\theta}\delta u_r dS \\
I_{32} &= \iint\limits_S \mu\epsilon_{r\theta}\delta(\tfrac{\partial u_\theta}{\partial r})dS = \int\limits_{\theta_1}^{\theta_2} \mu r\epsilon_{r\theta}\delta u_\theta\Big|_{r=a}^{r=b}dr - \iint\limits_S \mu\tfrac{\partial\epsilon_{r\theta}}{\partial r}\delta u_\theta dS \\
I_{33} &= \iint\limits_S -\tfrac{\mu}{r}\epsilon_{r\theta}\delta u_\theta dS
\end{aligned} \tag{B.9}$$

$$I_5 = \iint\limits_S \epsilon_{\theta\theta}\delta\sigma_{\theta\theta}dS = \iint\limits_S \epsilon_{\theta\theta}\delta(\lambda\frac{\partial u_r}{\partial r} + (2\mu+\lambda)\frac{1}{r}(\frac{\partial}{\partial\theta}u_\theta + u_r))dS \tag{B.10}$$

$$\begin{aligned}
I_{51} &= \iint\limits_S \lambda\epsilon_{\theta\theta}\delta(\tfrac{\partial u_r}{\partial r})dS = \int\limits_{\theta_1}^{\theta_2} \lambda\epsilon_{\theta\theta}r\delta u_r\Big|_{r=a}^{r=b}d\theta - \iint\limits_S \lambda\tfrac{\partial\epsilon_{\theta\theta}}{\partial r}\delta u_r dS \\
I_{52} &= \iint\limits_S \tfrac{(2\mu+\lambda)}{r}\epsilon_{\theta\theta}\delta(\tfrac{\partial u_\theta}{\partial\theta})dS = \int\limits_a^b \tfrac{(2\mu+\lambda)}{r}r\epsilon_{\theta\theta}\delta u_\theta\Big|_{\theta=\theta_1}^{\theta=\theta_2}dr - \iint\limits_S \tfrac{(2\mu+\lambda)}{r}\tfrac{\partial\epsilon_{\theta\theta}}{\partial\theta}\delta u_\theta dS \\
I_{53} &= \iint\limits_S \tfrac{(2\mu+\lambda)}{r}\epsilon_{\theta\theta}\delta u_r dS
\end{aligned} \tag{B.11}$$

$$I_6 = \iint\limits_S \sigma_{\theta\theta}\delta\epsilon_{\theta\theta}dS = \iint\limits_S \epsilon_{\theta\theta}\delta\tfrac{1}{r}(\tfrac{\partial}{\partial\theta}u_\theta + u_r)dS \tag{B.12}$$

$$\begin{aligned}
I_{61} &= \iint\limits_S \tfrac{1}{r}\sigma_{\theta\theta}\delta(\tfrac{\partial u_\theta}{\partial\theta})dS = \int\limits_a^b \tfrac{1}{r}r\sigma_{\theta\theta}\delta u_\theta\Big|_{\theta=\theta_1}^{\theta=\theta_2}dr - \iint\limits_S \tfrac{1}{r}\tfrac{\partial\sigma_{\theta\theta}}{\partial\theta}\delta u_\theta dS \\
I_{62} &= \iint\limits_S \tfrac{1}{r}\sigma_{\theta\theta}\delta u_r dS
\end{aligned} \tag{B.13}$$

Finally, $\delta U = I_1 + I_2 + 2(I_3 + I_4) + I_5 + I_6$ and using Eq.B.5-Eq.B.13 it can be rearranged as:

$$\begin{aligned}
\delta U = &-\iint\limits_S((2\mu+\lambda)\tfrac{\epsilon_{rr}}{r} - \tfrac{\lambda}{r}\epsilon_{rr} + \tfrac{\partial\sigma_{rr}}{\partial r} + \tfrac{1}{r}\tfrac{\partial\epsilon_{r\theta}}{\partial\theta} + \lambda\tfrac{\partial\epsilon_{\theta\theta}}{\partial r} - \tfrac{2\mu+\lambda}{r}\epsilon_{\theta\theta} - \tfrac{1}{r}\sigma_{\theta\theta})\delta u_r + \\
&+(\tfrac{\lambda}{r}\tfrac{\partial\epsilon_{rr}}{\partial\theta} + 2\mu\tfrac{\partial\epsilon_{r\theta}}{\partial r} + 2\tfrac{\mu}{r}\epsilon_{r\theta} + \tfrac{2\mu+\lambda}{r}\tfrac{\partial\epsilon_{\theta\theta}}{\partial\theta} + \tfrac{1}{r}\tfrac{\partial\sigma\theta\theta}{\partial r})\delta u_\theta dS + \\
&+\int\limits_{\theta_1}^{\theta_2}(2\mu+\lambda)\epsilon_{rr}r + \sigma_{rr}r + \lambda\epsilon_{rr}r\delta u_r\Big|_{r=a}^{r=b}d\theta + \int\limits_{\theta_1}^{\theta_2}2\mu\epsilon_{r\theta}r\delta u_\theta\Big|_{r=a}^{r=b}d\theta + \\
&+\int\limits_a^b 2\mu\epsilon_{r\theta}\delta u_r\Big|_{\theta=\theta_1}^{\theta=\theta_2}dr + \int\limits_a^b(\lambda\epsilon_{rr} + (2\mu+\lambda)\epsilon_{\theta\theta} + \sigma_{\theta\theta})\delta u_\theta\Big|_{\theta=\theta_1}^{\theta=\theta_2}dr
\end{aligned} \tag{B.14}$$

From equality $\delta U = 0$ we get two differential equation in stresses:

$$\begin{aligned}
&\tfrac{\partial\sigma_{rr}}{\partial r} + \tfrac{1}{r}\tfrac{\partial\sigma_{r\theta}}{\partial\theta} + \tfrac{1}{r}(\sigma_{rr} - \sigma_{\theta\theta}) = 0 \\
&\tfrac{1}{r}\tfrac{\partial\sigma_{\theta\theta}}{\partial\theta} + \tfrac{\partial\sigma_{r\theta}}{\partial r} + \tfrac{2}{r}\sigma_{r\theta} = 0
\end{aligned} \tag{B.15}$$

After substitution Eq.B.1 and Eq.B.2 into Eq.B.15 one can obtain Lame equations for an elastic layer. These equations are cumbersome and therefore not reproduced here.

Pair of boundary conditions at $r = a$ and $r = b$:

$$\begin{aligned} u_r = 0 \quad &\text{or} \quad \sigma_{rr} = 0 \\ u_\theta = 0 \quad &\text{or} \quad \sigma_{r\theta} = 0 \end{aligned} \tag{B.16}$$

Pair of boundary conditions at $\theta = \theta_1$ and $\theta = \theta_2$:

$$\begin{aligned} u_r = 0 \quad &\text{or} \quad \sigma_{r\theta} = 0 \\ u_\theta = 0 \quad &\text{or} \quad \sigma_{\theta\theta} = 0 \end{aligned} \tag{B.17}$$

In order to fully define system we need to state boundary conditions only at $r = a, r = b$ or $\theta = \theta_1, \theta = \theta_2$

Appendix C

Elastic layer out-of-plane vibrations

C.1 Equation in cartesian coordinates

We consider plane strain state in cartesian coordinates and therefore following constitutive law can be used [18]:

$$\begin{pmatrix} \sigma_{xx} \\ \sigma_{yy} \\ \sigma_{xy} \end{pmatrix} = \begin{bmatrix} \frac{E}{1-\nu^2} & \frac{\nu E}{1-\nu^2} & 0 \\ \frac{\nu E}{1-\nu^2} & \frac{E}{1-\nu^2} & 0 \\ 0 & 0 & 2G \end{bmatrix} \begin{pmatrix} \epsilon_{xx} \\ \epsilon_{yy} \\ \epsilon_{xy} \end{pmatrix} \tag{C.1}$$

With following strain definition:

$$\begin{pmatrix} \epsilon_{rr} \\ \epsilon_{\theta\theta} \\ \epsilon_{r\theta} \end{pmatrix} = \begin{pmatrix} \frac{\partial u}{\partial x} - z\frac{\partial^2 w}{\partial x^2} \\ \frac{\partial v}{\partial y} - z\frac{\partial^2 w}{\partial y^2} \\ \frac{1}{2}(\frac{\partial u}{\partial y} + \frac{\partial v}{\partial x}) - z\frac{\partial^2 w}{\partial x \partial y} \end{pmatrix} \tag{C.2}$$

Energy potential has a form:

$$U = \frac{1}{2} \iint\limits_S \int\limits_{-h/2}^{h/2} \sigma_{xx}\epsilon_{xx} + 2\sigma_{xy}\epsilon_{xy} + \sigma_{yy}\epsilon_{yy} dz dS \tag{C.3}$$

With constitutive law Eq.C.1 it can be rewritten as:

$$U = \frac{1}{2} \iint\limits_S \int\limits_{-h/2}^{h/2} \epsilon_{xx}^2 + 2\nu\epsilon_{xx}\epsilon_{yy} + \epsilon_{yy}^2 + 2(1-\nu)\epsilon_{xy}^2 dz dS \tag{C.4}$$

And with strain definition Eq.C.2:

$$U = \frac{1}{2} \iint\limits_S \int\limits_{-h/2}^{h/2} (\frac{\partial u}{\partial x} - z\frac{\partial^2 w}{\partial x^2})^2 + 2\nu(\frac{\partial u}{\partial x} - z\frac{\partial^2 w}{\partial x^2})(\frac{\partial v}{\partial y} - z\frac{\partial^2 w}{\partial y^2}) + (\frac{\partial v}{\partial y} - z\frac{\partial^2 w}{\partial y^2})^2 +$$
$$+ 2(1-\nu)(\frac{1}{2}(\frac{\partial u}{\partial y} + \frac{\partial v}{\partial x}) - z\frac{\partial^2 w}{\partial x \partial y})^2 dz dS \tag{C.5}$$

Since we consider out-of-plane vibrations $u, v = 0$ and $\int\limits_{-h/2}^{h/2} z^2 dz = 2\frac{z^3}{3}\Big|_{z=0}^{z=h/2} = \frac{h^3}{12}$ energy potential finally has a form:

$$U = \frac{D}{2}\iint\limits_S (\frac{\partial^2 w}{\partial x^2})^2 + 2\nu\frac{\partial^2 w}{\partial x^2}\frac{\partial^2 w}{\partial y^2} + (\frac{\partial^2 w}{\partial y^2})^2 + 2(1-\nu)(\frac{\partial^2 w}{\partial x \partial y})^2 dS \tag{C.6}$$

,where $D = \frac{Eh^3}{12(1-\nu^2)}$

Let us now find first variation by using by-part integration:

$$\delta I_1 = \delta\iint\limits_S (\frac{\partial^2 w}{\partial x^2})^2 dS = 2\iint\limits_S \frac{\partial^2 w}{\partial x^2}\delta\frac{\partial^2 w}{\partial x^2}dS = 2\int\limits_a^b (\frac{\partial^2 w}{\partial x^2}\delta\frac{\partial w}{\partial x} - \frac{\partial^3 w}{\partial x^3}\delta w)\Big|_{x=a}^{x=b} dy + 2\iint\limits_S \frac{\partial^4 w}{\partial x^4}\delta w dS \tag{C.7}$$

$$\delta I_2 = \delta\iint\limits_S (\frac{\partial^2 w}{\partial y^2})^2 dS = 2\iint\limits_S \frac{\partial^2 w}{\partial y^2}\delta\frac{\partial^2 w}{\partial y^2}dS = 2\int\limits_a^b (\frac{\partial^2 w}{\partial y^2}\delta\frac{\partial w}{\partial y} - \frac{\partial^3 w}{\partial y^3}\delta w)\Big|_{y=a}^{y=b} dx + 2\iint\limits_S \frac{\partial^4 w}{\partial y^4}\delta w dS \tag{C.8}$$

Using chain rule for variations $\delta(uv) = u\delta v + v\delta u$ we can write $\delta(\frac{\partial^2 w}{\partial x^2}\frac{\partial^2 w}{\partial y^2}) = \frac{\partial^2 w}{\partial x^2}\delta\frac{\partial^2 w}{\partial y^2} + \frac{\partial^2 w}{\partial y^2}\delta\frac{\partial^2 w}{\partial x^2}$:

$$\delta I_{31} = \iint\limits_S \frac{\partial^2 w}{\partial x^2}\delta\frac{\partial^2 w}{\partial y^2}dS = \int\limits_a^b (\frac{\partial^2 w}{\partial x^2}\delta\frac{\partial w}{\partial y} - \frac{\partial^3 w}{\partial x^2 \partial y}\delta w)\Big|_{y=a}^{y=b} dx + \iint\limits_S \frac{\partial^4 w}{\partial x^2 \partial y^2}\delta w dS \tag{C.9}$$

$$\delta I_{32} = \iint\limits_S \frac{\partial^2 w}{\partial y^2}\delta\frac{\partial^2 w}{\partial x^2}dS = \int\limits_a^b (\frac{\partial^2 w}{\partial y^2}\delta\frac{\partial w}{\partial x} - \frac{\partial^3 w}{\partial y^2 \partial x}\delta w)\Big|_{x=a}^{x=b} dy + \iint\limits_S \frac{\partial^4 w}{\partial x^2 \partial y^2}\delta w dS \tag{C.10}$$

$$\delta I_4 = \delta\iint\limits_S (\frac{\partial^2 w}{\partial x \partial y})^2 dS = \iint\limits_S 2\frac{\partial^2 w}{\partial x \partial y}\delta\frac{\partial^2 w}{\partial x \partial y}dS = \int\limits_a^b 2\frac{\partial^2 w}{\partial x \partial y}\delta\frac{\partial w}{\partial x}\Big|_{y=a}^{y=b} dx - \iint\limits_S 2\frac{\partial^3 w}{\partial x \partial y^2}\delta\frac{\partial w}{\partial x}dS =$$

$$= 2\frac{\partial^2 w}{\partial x \partial y}\delta w\Big|_{y=a}^{y=b}\Big|_{x=a}^{x=b} - \int\limits_a^b 2\frac{\partial^2 w}{\partial x^2 \partial y}\delta w\Big|_{y=a}^{y=b} dx - \int\limits_a^b 2\frac{\partial^3 w}{\partial x \partial y^2}\delta w\Big|_{x=a}^{x=b} dy + \iint\limits_S 2\frac{\partial^4 w}{\partial y^2 \partial x^2}\delta w \tag{C.11}$$

Term $\frac{\partial^2 w}{\partial x \partial y}\delta w\Big|_{y=a}^{y=b}\Big|_{x=a}^{x=b}$ represents "corner" forces. Existence of this kind of forces is purely mathematical phenomena and considered and discussed in references (for example, for rectangular plate in [19]). Consideration of these forces is out of scope of this work and therefore it is assumed that they are not affecting on a value of a total energy potential.

Variation of energy potential δU using Eq.C.7-Eq.C.11 as:

$$\delta U = \frac{D}{2}(\delta I_1 + \delta I_2 + 2\nu(\delta I_{31} + \delta I_{32}) + 2(1-\nu)(\delta I_{41} + \delta I_{42})) \tag{C.12}$$

Variation δU can be rearranged as:

$$\delta U = \frac{D}{2}\iint\limits_S (2\frac{\partial^4 w}{\partial x^4} + 2\frac{\partial^4 w}{\partial y^4} + 4\nu\frac{\partial^4 w}{\partial x^2\partial y^2} + 4(1-\nu)\frac{\partial^4 w}{\partial x^2\partial y^2})\delta w dS +$$

$$+\frac{D}{2}\int\limits_a^b (2\frac{\partial^2 w}{\partial y^2} + 2\nu\frac{\partial^2 w}{\partial x^2})\delta(\frac{\partial w}{\partial y}) + (-2\frac{\partial^3 w}{\partial y^3} - 2\nu\frac{\partial^3 w}{\partial x^2\partial y} - 4(1-\nu)\frac{\partial^3 w}{\partial x^2\partial y})\delta w\Big|_{y=a}^{y=b} dx +$$

$$+\frac{D}{2}\int\limits_a^b (2\frac{\partial^2 w}{\partial x^2} + 2\nu\frac{\partial^2 w}{\partial y^2})\delta(\frac{\partial w}{\partial x}) + (-2\frac{\partial^3 w}{\partial x^3} - 2\nu\frac{\partial^3 w}{\partial y^2\partial x} - 4(1-\nu)\frac{\partial^3 w}{\partial y^2\partial x})\delta w\Big|_{x=a}^{x=b} dy =$$

$$= D\iint\limits_S (\frac{\partial^4 w}{\partial x^4} + 2\frac{\partial^4 w}{\partial x^2\partial y^2} + \frac{\partial^4 w}{\partial y^4})\delta w dS +$$

$$+ D\int\limits_a^b (\frac{\partial^2 w}{\partial y^2} + \nu\frac{\partial^2 w}{\partial x^2})\delta(\frac{\partial w}{\partial y}) - (\frac{\partial^3 w}{\partial y^3} + (2-\nu)\frac{\partial^3 w}{\partial x^2\partial y})\delta w\Big|_{y=a}^{y=b} dx +$$

$$+ D\int\limits_a^b (\frac{\partial^2 w}{\partial x^2} + \nu\frac{\partial^2 w}{\partial y^2})\delta(\frac{\partial w}{\partial x}) - (\frac{\partial^3 w}{\partial x^3} + (2-\nu)\frac{\partial^3 w}{\partial y^2\partial x})\delta w\Big|_{x=a}^{x=b} dy \quad \text{(C.13)}$$

From equality $\delta U = 0$ we can obtain following differential equation:

$$\frac{\partial^4 w}{\partial x^4} + 2\frac{\partial^4 w}{\partial x^2\partial y^2} + \frac{\partial^4 w}{\partial y^4} = (\frac{\partial^2}{\partial x^2} + \frac{\partial^2}{\partial y^2})^2 w = \Delta^2 w = 0 \quad \text{(C.14)}$$

Kinetic energy potential has a form $T = \frac{\rho}{E}\frac{1}{2}\iint\limits_S (\frac{\partial w}{\partial t})^2 dS$. Lets consider following variation:

$$\delta\frac{1}{2}\frac{\rho}{E}\int\limits_{t_1}^{t_2}\iint (\frac{\partial w}{\partial t})^2 dt dS = \frac{\rho}{E}\int\limits_{t_1}^{t_2}\iint \frac{\partial w}{\partial t}\delta\frac{\partial w}{\partial t} dt dS =$$

$$= \frac{\rho}{E}\iint \frac{\partial w}{\partial t}\delta w\Big|_{t=t_1}^{t=t_2} dS - \frac{\rho}{E}\int\limits_{t_1}^{t_2}\iint \frac{\partial^2 w}{\partial t^2}\delta w dt dS = -\frac{\rho}{E}\int\limits_{t_1}^{t_2}\iint \frac{\partial^2 w}{\partial t^2}\delta w dt dS \quad \text{(C.15)}$$

Variation $\frac{\rho}{E}\iint \frac{\partial w}{\partial t}\delta u\Big|_{t=t_1}^{t=t_2} dS$ is equal to zero because variation δw can be taken arbitrary and function increment is not dependent on t.

From Hamilton's principle $\delta H = \delta\int\limits_{t_1}^{t_2}(T-V)dt = 0$ and Eq.C.14-Eq.C.15 we can obtain final equation:

$$D\Delta^2 w + \rho h\frac{\partial^2 w}{\partial t^2} = 0 \quad \text{(C.16)}$$

And boundary conditions at $y = a, b$:

$$\begin{array}{lll} \frac{\partial^2 w}{\partial y^2} + \nu\frac{\partial^2 w}{\partial x^2} = 0 & \text{or} & \frac{\partial w}{\partial y} = 0 \\ \frac{\partial^3 w}{\partial y^3} + (2-\nu)\frac{\partial^3 w}{\partial x^2\partial y} = 0 & \text{or} & w = 0 \end{array} \quad \text{(C.17)}$$

At $x = a, b$:

$$\begin{array}{lll} \frac{\partial^2 w}{\partial x^2} + \nu \frac{\partial^2 w}{\partial y^2} = 0 & \text{or} & \frac{\partial w}{\partial x} = 0 \\ \frac{\partial^3 w}{\partial x^3} + (2-\nu) \frac{\partial^3 w}{\partial y^2 \partial x} = 0 & \text{or} & w = 0 \end{array} \tag{C.18}$$

C.2 Equation in polar coordinates

As known transition from cartesian to polar coordinates (r, θ) preserves Laplace Δ operator, so equation stays the same:

$$D(\frac{\partial^2}{\partial r^2} + \frac{1}{r}\frac{\partial}{\partial r} + \frac{1}{r^2}\frac{\partial^2}{\partial \theta^2})^2 w + \rho h \frac{\partial^2 w}{\partial t^2} = D\Delta^2 w + \rho h \frac{\partial^2 w}{\partial t^2} = 0 \tag{C.19}$$

But boundary equations change to:
And boundary conditions at $\theta = \theta_1, \theta_2$:

$$\begin{array}{lll} \frac{1}{r^2}\frac{\partial^2 w}{\partial \theta^2} + \frac{1}{r}\frac{\partial w}{\partial r} + \nu \frac{\partial^2 w}{\partial r^2} = 0 & \text{or} & \frac{\partial w}{\partial \theta} = 0 \\ \frac{1}{r}(\frac{1}{r^2}\frac{\partial^3 w}{\partial \theta^3} + \frac{1}{r}\frac{\partial^2 w}{\partial r \partial \theta}) + (2-\nu)\frac{1}{r}\frac{\partial^3 w}{\partial^2 r \partial \theta} = 0 & \text{or} & w = 0 \end{array} \tag{C.20}$$

At $r = a, b$:

$$\begin{array}{lll} \frac{\partial^2 w}{\partial r^2} + \nu(\frac{1}{r^2}\frac{\partial^2 w}{\partial \theta^2} + \frac{1}{r}\frac{\partial w}{\partial r}) = 0 & \text{or} & \frac{\partial w}{\partial r} = 0 \\ \frac{\partial^3 w}{\partial r^3} + (2-\nu)(\frac{1}{r}\frac{\partial^2 w}{\partial r^2} - \frac{1}{r^2}\frac{\partial w}{\partial r} + \frac{1}{r^2}\frac{\partial^3 w}{\partial r \partial \theta^2} - \frac{2}{r^3}\frac{\partial^2 w}{\partial \theta^2}) = 0 & \text{or} & w = 0 \end{array} \tag{C.21}$$

Appendix D

Cylindrical shell vibrations

Potential energy of a segment of a cylindrical shell has a form [20]:

$$V = \frac{1}{2}\int_0^l \int_0^{2\pi} (\epsilon_1 T_1 + \epsilon_2 T_2 + \omega S + \kappa_1 M_1 + \kappa_2 M_2 + \tau H) R d\theta dx \tag{D.1}$$

,where $(\epsilon_1, \epsilon_2, \omega, \kappa_1, \kappa_2, \tau)$ are components of mid-plane deformation and $(T_1, T_2, S, M_1, M_2, H)$ are in-plane force resultants and moment resultants:

$$\begin{array}{ll}
\epsilon_1 = \frac{\partial u}{\partial x} & \text{strain in the axial direction} \\
\epsilon_2 = \frac{1}{R}\frac{\partial v}{\partial \theta} + \frac{w}{R} & \text{strain in the circumferential direction} \\
\omega = \frac{1}{R}\frac{\partial u}{\partial \theta} + \frac{\partial v}{\partial x} & \text{shear strain} \\
\kappa_1 = -\frac{\partial^2 w}{\partial x^2} & \text{bending curvature in the axial direction} \\
\kappa_2 = -\frac{1}{R^2}\frac{\partial^2 w}{\partial \theta^2} + \frac{1}{R^2}\frac{\partial v}{\partial \theta} & \text{bending curvature in the circumferential direction} \\
\tau = -\frac{1}{R}\frac{\partial^2 w}{\partial x \partial \theta} + \frac{1}{R}\frac{\partial v}{\partial x} & \text{twisting}
\end{array} \tag{D.2}$$

$$\begin{array}{ll}
T_1 = \frac{Eh}{1-\nu^2}(\frac{\partial u}{\partial x} + \nu(\frac{1}{R}\frac{\partial v}{\partial \theta} + \frac{w}{R})) & \text{axial membrane force} \\
T_1 = \frac{Eh}{1-\nu^2}(\nu\frac{\partial u}{\partial x} + \frac{1}{R}\frac{\partial v}{\partial \theta} + \frac{w}{R}) & \text{circumferential membrane force} \\
S = \frac{Eh}{1-\nu^2}\frac{1-\nu}{2}(\frac{1}{R}\frac{\partial u}{\partial \theta} + \frac{\partial v}{\partial x}) & \text{shear force} \\
M_1 = \frac{h^2}{12}\frac{Eh}{1-\nu^2}(-\frac{\partial^2 w}{\partial x^2} + \nu(-\frac{1}{R^2}\frac{\partial^2 w}{\partial \theta^2} + \frac{1}{R^2}\frac{\partial v}{\partial \theta})) & \text{axial bending moment} \\
M_2 = \frac{h^2}{12}\frac{Eh}{1-\nu^2}(-\nu\frac{\partial^2 w}{\partial x^2} - \frac{1}{R^2}\frac{\partial^2 w}{\partial \theta^2} + \frac{1}{R^2}\frac{\partial v}{\partial \theta}) & \text{circumferential bending moment} \\
H = \frac{h^2}{12}\frac{Eh}{1-\nu^2}(1-\nu)(-\frac{1}{R}\frac{\partial^2 w}{\partial x \partial \theta} + \frac{1}{R}\frac{\partial v}{\partial x}) & \text{twisting moment}
\end{array} \tag{D.3}$$

Let us consider following integrals and variations (below multiplier $\frac{Eh}{1-\nu^2}R$ is omitted):

$$I_1 = \epsilon_1 T_1 = \frac{\partial u}{\partial x}(\frac{\partial u}{\partial x} + \nu(\frac{1}{R}\frac{\partial v}{\partial \theta} + \frac{w}{R})) = (\frac{\partial u}{\partial x})^2 + \frac{\nu}{R}\frac{\partial u}{\partial x}(\frac{\partial v}{\partial \theta} + w) \tag{D.4}$$

$$\delta I_{11} = \delta \iint \frac{1}{2}(\frac{\partial u}{\partial x})^2 dx d\theta = \iint \frac{\partial u}{\partial x}\delta\frac{\partial u}{\partial x} dx d\theta = \int_0^{2\pi} \frac{\partial u}{\partial x}\delta u\Big|_{x=0}^{x=l} d\theta - \iint \frac{\partial^2 u}{\partial x^2}\delta u dS \tag{D.5}$$

$$\delta I_{12} = \iint \frac{1}{2}\frac{\nu}{R}(\frac{\partial v}{\partial \theta} + w)\delta\frac{\partial u}{\partial x} dx d\theta = \int_0^{2\pi} \frac{1}{2}\frac{\nu}{R}(\frac{\partial v}{\partial \theta} + w)\delta u\Big|_{x=0}^{x=l} d\theta - \iint \frac{1}{2}\frac{\nu}{R}(\frac{\partial^2 v}{\partial \theta \partial x} + \frac{\partial w}{\partial x})\delta u dS \tag{D.6}$$

$$\delta I_{13} = \iint \frac{1}{2}\frac{\nu}{R}\frac{\partial u}{\partial x}\delta(\frac{\partial v}{\partial \theta}+w)dxd\theta = \int\limits_0^l \frac{1}{2}\frac{\nu}{R}\frac{\partial u}{\partial x}\delta v\Big|_{\theta=0}^{\theta=2\pi}dx - \iint \frac{1}{2}\frac{\nu}{R}\frac{\partial^2 u}{\partial x\partial\theta}\delta v dS + \iint \frac{1}{2}\frac{\nu}{R}\frac{\partial u}{\partial x}\delta w dS \tag{D.7}$$

$$I_2 = \epsilon_2 T_2 = (\frac{1}{R}\frac{\partial v}{\partial\theta}+\frac{w}{R})(\nu\frac{\partial u}{\partial x}+(\frac{1}{R}\frac{\partial v}{\partial\theta}+\frac{w}{R})) = \frac{\nu}{R}\frac{\partial u}{\partial x}(\frac{\partial v}{\partial\theta}+w)+\frac{1}{R^2}(\frac{\partial v}{\partial\theta}+w)^2 = I_{12}+I_{13}+\frac{1}{R^2}(\frac{\partial v}{\partial\theta}+w)^2 \tag{D.8}$$

$$\begin{aligned}\delta I_2 &= \delta\iint \frac{1}{2}\frac{1}{R^2}(\frac{\partial v}{\partial\theta}+w)^2 dxd\theta = \iint \frac{1}{R^2}(\frac{\partial v}{\partial\theta}+w)\delta(\frac{\partial v}{\partial\theta}+w)dxd\theta = \\ &= \int\limits_0^l \frac{1}{R^2}(\frac{\partial v}{\partial\theta}+w)\delta v\Big|_{\theta=0}^{\theta=2\pi}dx - \iint \frac{1}{R^2}(\frac{\partial^2 v}{\partial\theta^2}+\frac{\partial w}{\partial\theta})\delta v dS + \iint \frac{1}{R^2}(\frac{\partial v}{\partial\theta}+w)\delta w dS\end{aligned} \tag{D.9}$$

$$I_3 = \omega S = \frac{1-\nu}{2}(\frac{1}{R}\frac{\partial u}{\partial\theta}+\frac{\partial v}{\partial x})^2 \tag{D.10}$$

$$\begin{aligned}\delta I_3 &= \delta\iint \frac{1}{2}\frac{1-\nu}{2}(\frac{1}{R}\frac{\partial u}{\partial\theta}+\frac{\partial v}{\partial x})^2 dxd\theta = \iint \frac{1-\nu}{2}(\frac{1}{R}\frac{\partial u}{\partial\theta}+\frac{\partial v}{\partial x})\delta(\frac{1}{R}\frac{\partial u}{\partial\theta}+\frac{\partial v}{\partial x})dxd\theta = \\ &= \int\limits_0^l \frac{1}{R}\frac{1-\nu}{2}(\frac{1}{R}\frac{\partial u}{\partial\theta}+\frac{\partial v}{\partial x})\delta u\Big|_{\theta=0}^{\theta=2\pi}dx - \iint \frac{1}{R}\frac{1-\nu}{2}(\frac{1}{R}\frac{\partial^2 u}{\partial\theta^2}+\frac{\partial^2 v}{\partial x\partial\theta})\delta u dS + \\ &\quad + \int\limits_0^{2\pi} \frac{1-\nu}{2}(\frac{1}{R}\frac{\partial u}{\partial\theta}+\frac{\partial v}{\partial x})\delta v\Big|_{x=0}^{x=l}d\theta - \iint \frac{1-\nu}{2}(\frac{1}{R}\frac{\partial^2 u}{\partial\theta\partial x}+\frac{\partial^2 v}{\partial x^2})\delta v dS\end{aligned} \tag{D.11}$$

$$I_4 = \kappa_1 M_1 = -\frac{h^2}{12}\frac{\partial^2 w}{\partial x^2}(-\frac{\partial^2 w}{\partial x^2}-\frac{\nu}{R^2}(\frac{\partial^2 w}{\partial\theta^2}-\frac{\partial v}{\partial\theta})) = \frac{h^2}{12}(\frac{\partial^2 w}{\partial x^2})^2+\frac{h^2}{12}\frac{\nu}{R^2}\frac{\partial^2 w}{\partial x^2}(\frac{\partial^2 w}{\partial\theta^2}-\frac{\partial v}{\partial\theta}) \tag{D.12}$$

$$\begin{aligned}\delta I_{41} &= \delta\iint \frac{1}{2}\frac{h^2}{12}(\frac{\partial^2 w}{\partial x^2})^2 dxd\theta = \iint \frac{h^2}{12}\frac{\partial^2 w}{\partial x^2}\delta\frac{\partial^2 w}{\partial x^2}dxd\theta = \\ &= \int\limits_0^{2\pi} \frac{h^2}{12}\frac{\partial^2 w}{\partial x^2}\delta(\frac{\partial w}{\partial x}) - \frac{h^2}{12}\frac{\partial^3 w}{\partial x^3}\delta w\Big|_{x=0}^{x=l}d\theta + \iint \frac{h^2}{12}\frac{\partial^4 w}{\partial x^4}\delta w dS\end{aligned} \tag{D.13}$$

$$\begin{aligned}\delta I_{42} &= \delta\iint \frac{1}{2}\frac{h^2}{12}\frac{\nu}{R^2}(\frac{\partial^2 w}{\partial\theta^2}-\frac{\partial v}{\partial\theta})\delta\frac{\partial^2 w}{\partial x^2}dxd\theta = \\ &= \int\limits_0^{2\pi} \frac{1}{2}\frac{h^2}{12}\frac{\nu}{R^2}(\frac{\partial^2 w}{\partial\theta^2}-\frac{\partial v}{\partial\theta})\delta(\frac{\partial w}{\partial x}) - \frac{1}{2}\frac{h^2}{12}\frac{\nu}{R^2}(\frac{\partial^3 w}{\partial\theta^2\partial x}-\frac{\partial^2 v}{\partial\theta\partial x})\delta w\Big|_{x=0}^{x=l}d\theta + \\ &\quad + \iint \frac{1}{2}\frac{h^2}{12}\frac{\nu}{R^2}(\frac{\partial^4 w}{\partial\theta^2\partial x^2}-\frac{\partial^3 v}{\partial\theta\partial x^2})\delta w dS\end{aligned} \tag{D.14}$$

$$\delta I_{43} = \delta \iint \frac{1}{2}\frac{h^2}{12}\frac{\nu}{R^2}\frac{\partial^2 w}{\partial x^2}\delta(\frac{\partial^2 w}{\partial \theta^2} - \frac{\partial v}{\partial \theta})dxd\theta =$$

$$= \int_0^l \frac{1}{2}\frac{h^2}{12}\frac{\nu}{R^2}\frac{\partial^2 w}{\partial x^2}\delta(\frac{\partial w}{\partial \theta}) - \frac{1}{2}\frac{h^2}{12}\frac{\nu}{R^2}\frac{\partial^3 w}{\partial x^2 \partial \theta}\delta w\Big|_{\theta=0}^{\theta=2\pi} dx + \iint \frac{1}{2}\frac{h^2}{12}\frac{\nu}{R^2}\frac{\partial^4 w}{\partial x^2 \partial \theta^2}\delta w dS -$$

$$- \int_0^l \frac{1}{2}\frac{h^2}{12}\frac{\nu}{R^2}\frac{\partial^2 w}{\partial x^2}\delta v\Big|_{\theta=0}^{\theta=2\pi} dx + \iint \frac{1}{2}\frac{h^2}{12}\frac{\nu}{R^2}\frac{\partial^3 w}{\partial x^2 \partial \theta}\delta v dS \quad \text{(D.15)}$$

$$a_5 = \kappa_2 M_2 = \frac{h^2}{12}\frac{1}{R^2}(-\frac{\partial^2 w}{\partial \theta^2} + \frac{\partial v}{\partial \theta})(-\nu\frac{\partial^2 w}{\partial x^2} + \frac{1}{R^2}(-\frac{\partial^2 w}{\partial \theta^2} + \frac{\partial v}{\partial \theta})) =$$

$$= \frac{h^2}{12}\frac{1}{R^4}(-\frac{\partial^2 w}{\partial \theta^2} + \frac{\partial v}{\partial \theta})^2 + \frac{h^2}{12}\frac{\nu}{R^2}\frac{\partial^2 w}{\partial x^2}(\frac{\partial^2 w}{\partial \theta^2} - \frac{\partial v}{\partial \theta}) = \frac{h^2}{12}\frac{1}{R^4}(-\frac{\partial^2 w}{\partial \theta^2} + \frac{\partial v}{\partial \theta})^2 + I_{42} + I_{43} \quad \text{(D.16)}$$

$$\delta I_5 = \delta \iint \frac{1}{2}\frac{h^2}{12}\frac{1}{R^4}(-\frac{\partial^2 w}{\partial \theta^2} + \frac{\partial v}{\partial \theta})^2 dxd\theta = \iint \frac{h^2}{12}\frac{1}{R^4}(-\frac{\partial^2 w}{\partial \theta^2} + \frac{\partial v}{\partial \theta})\delta(-\frac{\partial^2 w}{\partial \theta^2} + \frac{\partial v}{\partial \theta})dxd\theta =$$

$$= -\int_0^l \frac{1}{R^4}\frac{h^2}{12}(-\frac{\partial^2 w}{\partial \theta^2} + \frac{\partial v}{\partial \theta})\delta(\frac{\partial w}{\partial \theta}) - \frac{1}{R^4}\frac{h^2}{12}(-\frac{\partial^3 w}{\partial \theta^3} + \frac{\partial^2 v}{\partial \theta^2})\delta w\Big|_{\theta=0}^{\theta=2\pi} dx - \iint \frac{1}{R^4}\frac{h^2}{12}(-\frac{\partial^4 w}{\partial \theta^4} + \frac{\partial^3 v}{\partial \theta^3})\delta w dS +$$

$$+ \int_0^l \frac{1}{R^4}\frac{h^2}{12}(-\frac{\partial^2 w}{\partial \theta^2} + \frac{\partial v}{\partial \theta})\delta v\Big|_{\theta=0}^{\theta=2\pi} dx - \iint \frac{1}{R^4}\frac{h^2}{12}(-\frac{\partial^3 w}{\partial \theta^3} + \frac{\partial^2 v}{\partial \theta^2})\delta v dS \quad \text{(D.17)}$$

$$I_6 = \tau H = \frac{h^2}{12}(1-\nu)\frac{1}{R^2}(-\frac{\partial^2 w}{\partial x \partial \theta} + \frac{\partial v}{\partial x})^2 \quad \text{(D.18)}$$

$$\delta I_6 = \delta \iint \frac{1}{2}\frac{h^2}{12}(1-\nu)\frac{1}{R^2}(-\frac{\partial^2 w}{\partial x \partial \theta} + \frac{\partial v}{\partial x})^2 dxd\theta =$$

$$= \iint \frac{h^2}{12}(1-\nu)\frac{1}{R^2}(-\frac{\partial^2 w}{\partial x \partial \theta} + \frac{\partial v}{\partial x})\delta(-\frac{\partial^2 w}{\partial x \partial \theta} + \frac{\partial v}{\partial x})dxd\theta =$$

$$= \iint \frac{h^2}{12}(1-\nu)\frac{1}{R^2}(\frac{\partial^2 w}{\partial x \partial \theta} - \frac{\partial v}{\partial x})\delta\frac{\partial^2 w}{\partial x \partial \theta}dxd\theta + \iint \frac{h^2}{12}(1-\nu)\frac{1}{R^2}(-\frac{\partial^2 w}{\partial x \partial \theta} + \frac{\partial v}{\partial x})\delta(\frac{\partial v}{\partial x})dxd\theta$$

(D.19)

$$\delta I_{61} = \iint \frac{h^2}{12}(1-\nu)\frac{1}{R^2}(\frac{\partial^2 w}{\partial x \partial \theta} - \frac{\partial v}{\partial x})\delta\frac{\partial^2 w}{\partial x \partial \theta}dxd\theta =$$

$$= \int_0^l \frac{h^2}{12}(1-\nu)\frac{1}{R^2}(\frac{\partial^2 w}{\partial x \partial \theta} - \frac{\partial v}{\partial x})\delta\frac{\partial w}{\partial x}\Big|_{\theta=0}^{\theta=2\pi} dx - \iint \frac{h^2}{12}(1-\nu)\frac{1}{R^2}(\frac{\partial^3 w}{\partial x \partial^2 \theta} - \frac{\partial v}{\partial x \partial \theta})\delta\frac{\partial w}{\partial x}dxd\theta =$$

$$= \frac{h^2}{12}(1-\nu)\frac{1}{R^2}(\frac{\partial^2 w}{\partial x \partial \theta} - \frac{\partial v}{\partial x})\delta w\Big|_{\theta=0}^{\theta=2\pi}\Big|_{x=0}^{x=l} - \int_0^l \frac{h^2}{12}(1-\nu)\frac{1}{R^2}(\frac{\partial^3 w}{\partial x^2 \partial \theta} - \frac{\partial^2 v}{\partial x^2})\delta w\Big|_{\theta=0}^{\theta=2\pi} dx -$$

$$- \int_0^{2\pi} \frac{h^2}{12}(1-\nu)\frac{1}{R^2}(\frac{\partial^3 w}{\partial x \partial \theta^2} - \frac{\partial^2 v}{\partial x \partial \theta})\delta w\Big|_{x=0}^{x=l} d\theta + \iint \frac{h^2}{12}(1-\nu)\frac{1}{R^2}(\frac{\partial^4 w}{\partial x^2 \partial \theta^2} - \frac{\partial^3 v}{\partial x^2 \partial \theta})\delta w dxd\theta$$

(D.20)

Term $\frac{h^2}{12}(1-\nu)\frac{1}{R^2}(\frac{\partial^2 w}{\partial x \partial \theta}-\frac{\partial v}{\partial x})\delta w\Big|_{\theta=0}^{\theta=2\pi}\Big|_{x=0}^{x=l}$ represents "corner" forces, that is known and discussed phenomena in plate theory. For cylindrical shell it is not so well studied and its consideration is far out of scope of this work. It is assumed, that they are not affecting on a value of a total energy potential.

$$\delta I_{62} = \iint \frac{h^2}{12}(1-\nu)\frac{1}{R^2}(-\frac{\partial^2 w}{\partial x \partial \theta}+\frac{\partial v}{\partial x})\delta(\frac{\partial v}{\partial x})dxd\theta =$$
$$= \int_0^{2\pi} \frac{h^2}{12}(1-\nu)\frac{1}{R^2}(-\frac{\partial^2 w}{\partial x \partial \theta}+\frac{\partial v}{\partial x})\delta v\Big|_{x=0}^{x=l} d\theta - \iint \frac{h^2}{12}(1-\nu)\frac{1}{R^2}(-\frac{\partial^3 w}{\partial x^2 \partial \theta}+\frac{\partial^2 v}{\partial x^2})\delta v dxd\theta \tag{D.21}$$

First variation of energy potential can be represented as $\delta U = \delta I_{11} + 2(\delta I_{12} + \delta I_{13}) + \delta I_2 + \delta I_3 + \delta I_{41} + 2(\delta I_{42} + \delta I_{43}) + \delta I_5 + \delta I_{61} + \delta I_{62}$, which can be rearranged as:

$$\begin{aligned}
\delta U = \iint & (-\frac{\partial^2 u}{\partial x^2} - \frac{1-\nu}{2}\frac{1}{R^2}\frac{\partial^2 u}{\partial \theta^2} - \frac{1+\nu}{2}\frac{1}{R}\frac{\partial^2 v}{\partial x \partial \theta} - \frac{\nu}{R}\frac{\partial w}{\partial x})\delta u + \\
& + (-\frac{1+\nu}{2}\frac{1}{R}\frac{\partial^2 u}{\partial x \partial \theta} - \frac{1-\nu}{2}\frac{\partial^2 v}{\partial x^2} - \frac{1}{R^2}\frac{\partial^2 v}{\partial \theta^2} - \frac{h^2}{12}\frac{1-\nu}{R^2}\frac{\partial^2 v}{\partial x^2} - \frac{h^2}{12}\frac{1}{R^4}\frac{\partial^2 v}{\partial \theta^2} - \frac{1}{R^2}\frac{\partial w}{\partial \theta} + \\
& + \frac{h^2}{12}\frac{1}{R^4}\frac{\partial^3 w}{\partial \theta^3} + \frac{h^2}{12}\frac{1}{R^2}\frac{\partial^3 w}{\partial x^2 \partial \theta})\delta v + \\
& + (\frac{\nu}{R}\frac{\partial u}{\partial x} + \frac{1}{R^2}\frac{\partial v}{\partial \theta} - \frac{h^2}{12}\frac{1}{R^4}\frac{\partial^3 v}{\partial \theta^3} - \frac{h^2}{12}\frac{1}{R^2}\frac{\partial^3 v}{\partial x^2 \partial \theta} + \frac{1}{R^2}w + \frac{h^2}{12}\frac{\partial w^4}{\partial x^4} + \frac{h^2}{12}\frac{1+\nu}{R^2}\frac{\partial^4 w}{\partial x^2 \partial \theta^2} + \frac{h^2}{12}\frac{1}{R^4}\frac{\partial^4 w}{\partial \theta^4})\delta w dS + \\
& + \int_0^{2\pi} \Big[(\frac{\nu}{R}w + \frac{\nu}{R}\frac{\partial v}{\partial \theta} + \frac{\partial u}{\partial x})\delta u + (\frac{1-\nu}{2}(\frac{1}{R}\frac{\partial u}{\partial \theta} + \frac{\partial v}{\partial x}) + \frac{h^2}{12}\frac{1-\nu}{R^2}(\frac{\partial v}{\partial x} - \frac{\partial^2 w}{\partial x \partial \theta}))\delta v + \\
& + (\frac{h^2}{12}\frac{1+\nu}{2}(\frac{\partial^2 v}{\partial x \partial \theta} - \frac{\partial^3 w}{\partial x \partial \theta^2}) - \frac{h^2}{12}\frac{\partial^3 w}{\partial x^3})\delta w + (\frac{h^2}{12}\frac{\nu}{R^2}(\frac{\partial^2 w}{\partial \theta^2} - \frac{\partial v}{\partial \theta}) + \frac{h^2}{12}\frac{\partial^2 w}{\partial x^2})\delta(\frac{\partial w}{\partial x})\Big]\Big|_{x=0}^{x=l} d\theta + \\
& + \int_0^{l} \Big[(\frac{1-\nu}{2}\frac{1}{R}(\frac{1}{R}\frac{\partial u}{\partial \theta} + \frac{\partial v}{\partial x}))\delta u + (\frac{\nu}{R}\frac{\partial u}{\partial x} + \frac{1}{R^2}(\frac{\partial v}{\partial \theta} + w) + \frac{h^2}{12}\frac{1}{R^4}(\frac{\partial v}{\partial \theta} - \frac{\partial^2 w}{\partial \theta^2}) - \frac{h^2}{12}\frac{\nu}{R^2}\frac{\partial^2 w}{\partial x^2})\delta v + \\
& + (\frac{h^2}{12}\frac{1}{R^4}(\frac{\partial^2 v}{\partial \theta^2} - \frac{\partial^3 w}{\partial \theta^3}) - \frac{h^2}{12}\frac{1-\nu}{2}\frac{1}{R^2}(-\frac{\partial^2 v}{\partial x^2} + \frac{\partial^3 w}{\partial x^2 \partial \theta})\delta w + \\
& + (-\frac{h^2}{12}\frac{1}{R^4}(\frac{\partial v}{\partial \theta} - \frac{\partial^2 w}{\partial \theta^2}) + \frac{h^2}{12}\frac{\nu}{R^2}\frac{\partial^2 w}{\partial x^2})\delta(\frac{\partial w}{\partial \theta})\Big]\Big|_{\theta=0}^{\theta=2\pi} dx
\end{aligned} \tag{D.22}$$

Kinetic energy potential $T = \frac{1}{2}\rho h \iint ((\frac{\partial u}{\partial t})^2 + (\frac{\partial v}{\partial t})^2 + (\frac{\partial w}{\partial t})^2) R dxd\theta = \frac{1}{2}CR\frac{\rho}{E}\iint ((\frac{\partial u}{\partial t})^2 + (\frac{\partial v}{\partial t})^2 + (\frac{\partial w}{\partial t})^2) dxd\theta$.

Lets consider variation (multiplier CR omitted):

$$\delta\frac{1}{2}\frac{\rho}{E}\int_{t_1}^{t_2}\iint (\frac{\partial u}{\partial t})^2 dtdxd\theta = \frac{\rho}{E}\int_{t_1}^{t_2}\iint \frac{\partial u}{\partial t}\delta\frac{\partial u}{\partial t}dtdxd\theta =$$
$$= \frac{\rho}{E}\iint \frac{\partial u}{\partial t}\delta u\Big|_{t=t_1}^{t=t_2} dS - \frac{\rho}{E}\int_{t_1}^{t_2}\iint \frac{\partial^2 u}{\partial t^2}\delta u dtdxd\theta = -\frac{\rho}{E}\int_{t_1}^{t_2}\iint \frac{\partial^2 u}{\partial t^2}\delta u dtdxd\theta \tag{D.23}$$

Variation $\frac{\rho}{E}\iint \frac{\partial u}{\partial t}\delta u\Big|_{t=t_1}^{t=t_2} dS$ is equal to zero because variation δu can be taken arbitrary and function increment is not dependent on t.

From Eq.D.23 we can obtain value of the variation:

$$\delta \int_{t_1}^{t_2} T dt = -\frac{\rho}{E}\int_{t_1}^{t_2}\iint \frac{\partial^2 u}{\partial t^2}\delta u + \frac{\partial^2 v}{\partial t^2}\delta v + \frac{\partial^2 w}{\partial t^2}\delta w dt dx d\theta \tag{D.24}$$

From Hamilton's principle $\delta H = \delta\int_{t_1}^{t_2}(T-V)dt = 0$ and Eq.D.22, Eq.D.24 we can obtain cylindrical shell vibration equations:

$$\begin{aligned}
&-\frac{\partial^2 u}{\partial x^2} - \frac{1-\nu}{2}\frac{1}{R^2}\frac{\partial^2 u}{\partial\theta^2} - \frac{1+\nu}{2}\frac{1}{R}\frac{\partial^2 v}{\partial x\partial\theta} - \frac{\nu}{R}\frac{\partial w}{\partial x} + \frac{\rho}{E(1-\nu^2)}\frac{\partial^2 u}{\partial t^2} = 0\\
&-\frac{1+\nu}{2}\frac{1}{R}\frac{\partial^2 u}{\partial x\partial\theta} - \frac{1-\nu}{2}\frac{\partial^2 v}{\partial x^2} - \frac{1}{R^2}\frac{\partial^2 v}{\partial\theta^2} - \frac{h^2}{12}\frac{1-\nu}{R^2}\frac{\partial^2 v}{\partial x^2} - \frac{h^2}{12}\frac{1}{R^4}\frac{\partial^2 v}{\partial\theta^2} -\\
&-\frac{1}{R^2}\frac{\partial w}{\partial\theta} + +\frac{h^2}{12}\frac{1}{R^4}\frac{\partial^3 w}{\partial\theta^3} + \frac{h^2}{12}\frac{1}{R^2}\frac{\partial^3 w}{\partial x^2\partial\theta} + \frac{\rho}{E(1-\nu^2)}\frac{\partial^2 v}{\partial t^2} = 0\\
&\frac{\nu}{R}\frac{\partial u}{\partial x} + \frac{1}{R^2}\frac{\partial v}{\partial\theta} - \frac{h^2}{12}\frac{1}{R^4}\frac{\partial^3 v}{\partial\theta^3} - \frac{h^2}{12}\frac{1}{R^2}\frac{\partial^3 v}{\partial x^2\partial\theta} + \frac{1}{R^2}w + \frac{h^2}{12}\frac{\partial w^4}{\partial x^4} +\\
&+\frac{h^2}{12}\frac{1+\nu}{R^2}\frac{\partial^4 w}{\partial x^2\partial\theta^2} + \frac{h^2}{12}\frac{1}{R^4}\frac{\partial^4 w}{\partial\theta^4} + \frac{\rho}{E(1-\nu^2)}\frac{\partial^2 w}{\partial t^2} = 0
\end{aligned} \tag{D.25}$$

And four boundary conditions at $x = 0$ and $x = l$:

$$\begin{array}{ll}
\frac{\nu}{R}w + \frac{\nu}{R}\frac{\partial v}{\partial\theta} + \frac{\partial u}{\partial x} & \text{or} \quad u = 0\\
\frac{1-\nu}{2}\left(\frac{1}{R}\frac{\partial u}{\partial\theta} + \frac{\partial v}{\partial x}\right) + \frac{h^2}{12}\frac{1-\nu}{R^2}\left(\frac{\partial v}{\partial x} - \frac{\partial^2 w}{\partial x\partial\theta}\right) & \text{or} \quad v = 0\\
\frac{h^2}{12}\frac{1+\nu}{2}\left(\frac{\partial^2 v}{\partial x\partial\theta} - \frac{\partial^3 w}{\partial x\partial\theta^2}\right) - \frac{h^2}{12}\frac{\partial^3 w}{\partial x^3} & \text{or} \quad w = 0\\
\frac{h^2}{12}\frac{\nu}{R^2}\left(\frac{\partial^2 w}{\partial\theta^2} - \frac{\partial v}{\partial\theta}\right) + \frac{h^2}{12}\frac{\partial^2 w}{\partial x^2} & \text{or} \quad \frac{\partial w}{\partial x} = 0
\end{array} \tag{D.26}$$

Or four boundary conditions at $\theta = 0$ and $\theta = 2\pi$:

$$\begin{array}{ll}
\frac{1-\nu}{2}\frac{1}{R}\left(\frac{1}{R}\frac{\partial u}{\partial\theta} + \frac{\partial v}{\partial x}\right) & \text{or} \quad u = 0\\
\frac{\nu}{R}\frac{\partial u}{\partial x} + \frac{1}{R^2}\left(\frac{\partial v}{\partial\theta} + w\right) + \frac{h^2}{12}\frac{1}{R^4}\left(\frac{\partial v}{\partial\theta} - \frac{\partial^2 w}{\partial\theta^2}\right) - \frac{h^2}{12}\frac{\nu}{R^2}\frac{\partial^2 w}{\partial x^2} & \text{or} \quad v = 0\\
\frac{h^2}{12}\frac{1}{R^4}\left(\frac{\partial^2 v}{\partial\theta^2} - \frac{\partial^3 w}{\partial\theta^3}\right) - \frac{h^2}{12}\frac{1-\nu}{2}\frac{1}{R^2}\left(-\frac{\partial^2 v}{\partial x^2} + \frac{\partial^3 w}{\partial x^2\partial\theta}\right. & \text{or} \quad w = 0\\
-\frac{h^2}{12}\frac{1}{R^4}\left(\frac{\partial v}{\partial\theta} - \frac{\partial^2 w}{\partial\theta^2}\right) + \frac{h^2}{12}\frac{\nu}{R^2}\frac{\partial^2 w}{\partial x^2} & \text{or} \quad \frac{\partial w}{\partial\theta} = 0
\end{array} \tag{D.27}$$

Appendix E

Spring equipment sketch

Equipment designed such that if radius of tube is changed, periodicity pattern will be preserved.

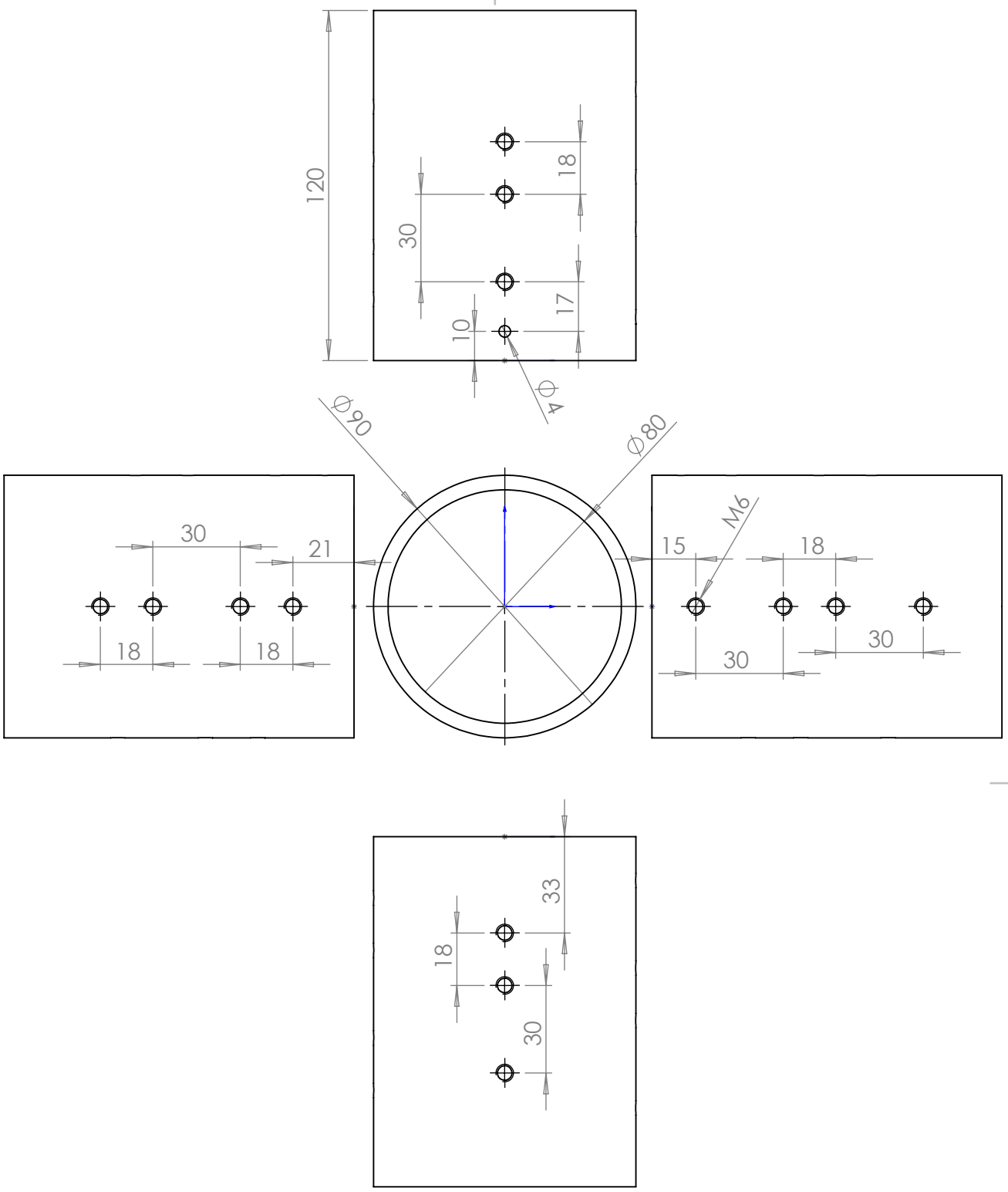

UNLESS OTHERWISE SPECIFIED: DIMENSIONS ARE IN MILLIMETERS SURFACE FINISH: TOLERANCES: LINEAR: ANGULAR:	FINISH:	DEBURR AND BREAK SHARP EDGES	DO NOT SCALE DRAWING / REVISION

	NAME	SIGNATURE	DATE			
DRAWN	A.Khvatov				22822399	
CHK'D						
APPV'D						
MFG						
Q.A						

TITLE: Spring Equipment

MATERIAL: Steel

WEIGHT:

DWG NO. Cylinder

A4

SCALE:1:2

SHEET 1 OF 1

Appendix F

Experiments data (magnesium-lithium alloy)

Here shown results obtained in all experiments done in acoustics lab with magnesium-lithium prototypes. Experiment are presented in order, which used in Ch.3. Here uni-axial loading is denoted by loading(I) and torque loading denoted by loading(II) for brevity.

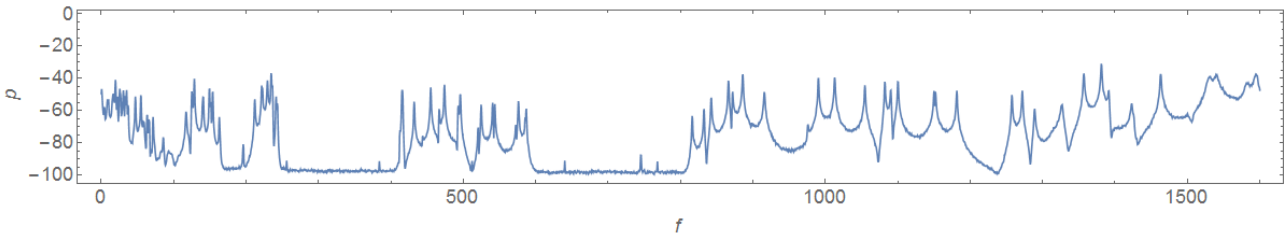

Figure F.1: Loading(I), LR

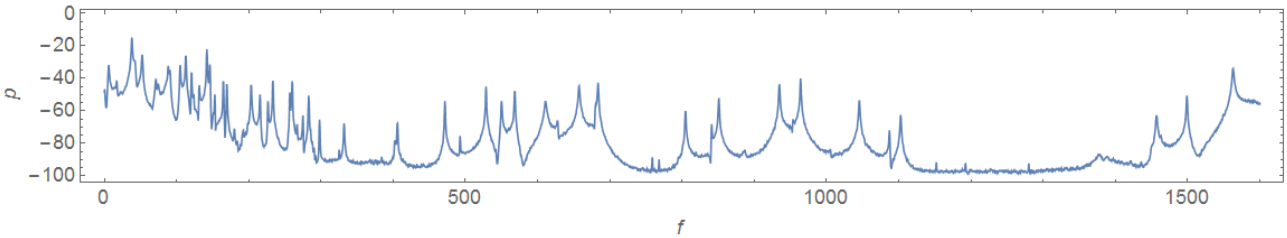

Figure F.2: Loading(I), SR

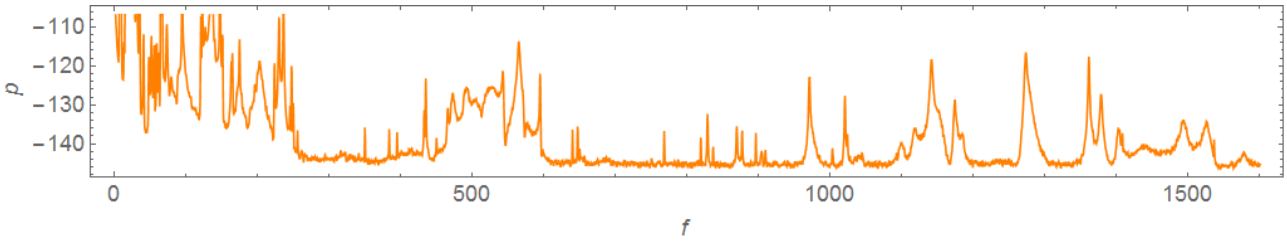

Figure F.3: Experiment 1, loading(II) , LR

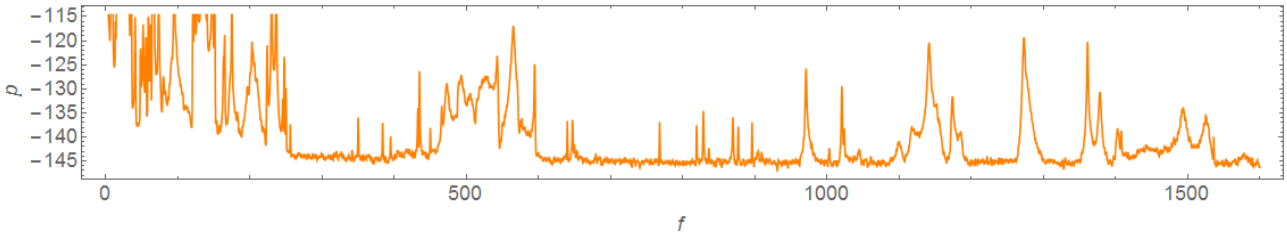

Figure F.4: Experiment 2, loading(II) , LR

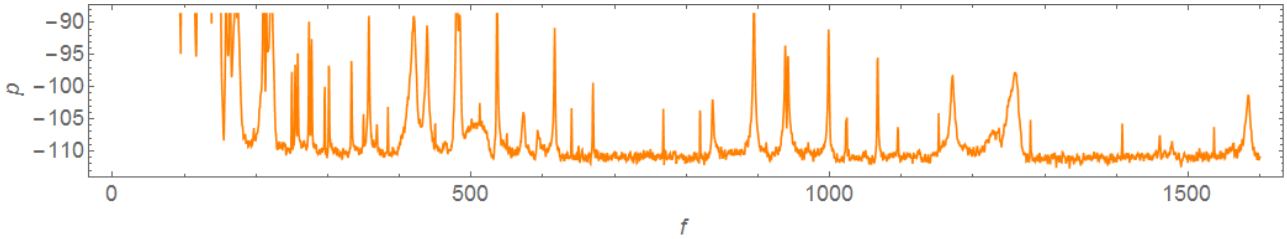

Figure F.5: Loading(II), SR

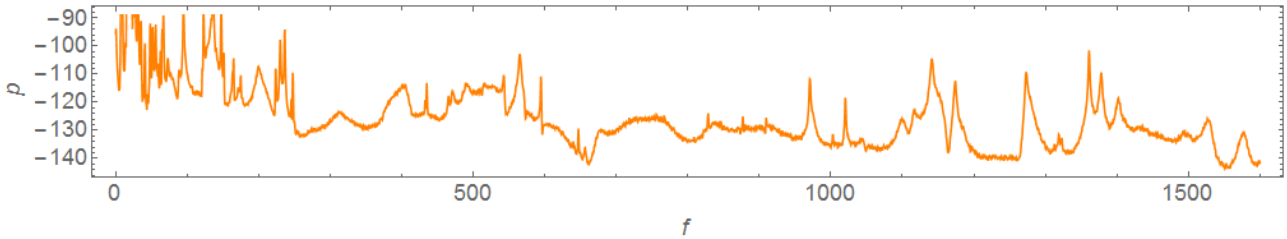

Figure F.6: Loading(II), higher force amplitude, LR

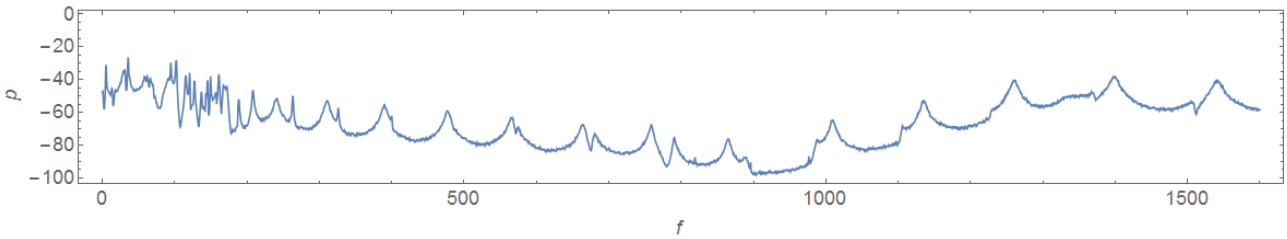

Figure F.7: Helical spring , loading(I), SR

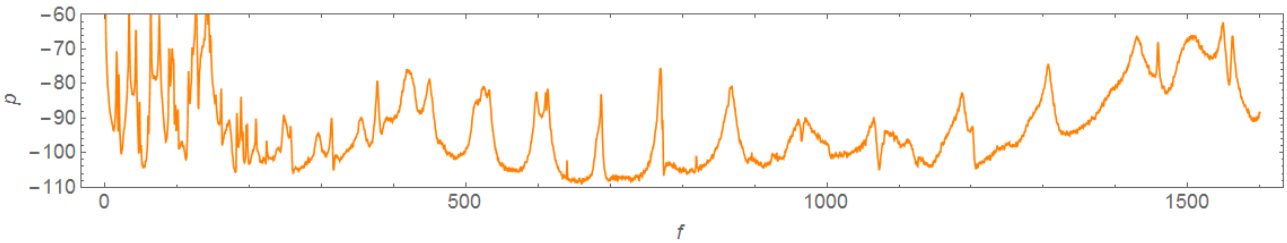

Figure F.8: Helical spring , loading(II), SR

Appendix G

Experiments data (steel)

Here shown results obtained in all experiments done in acoustics lab with steel prototypes. Experiment are presented in order, which used in Ch.3. Here uni-axial loading is denoted by loading(I) and torque loading denoted by loading(II) for brevity.

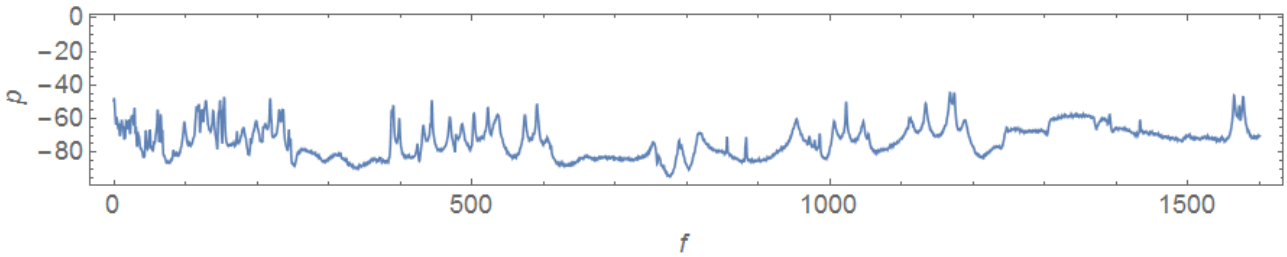

Figure G.1: Experiment 1, loading(I), LR

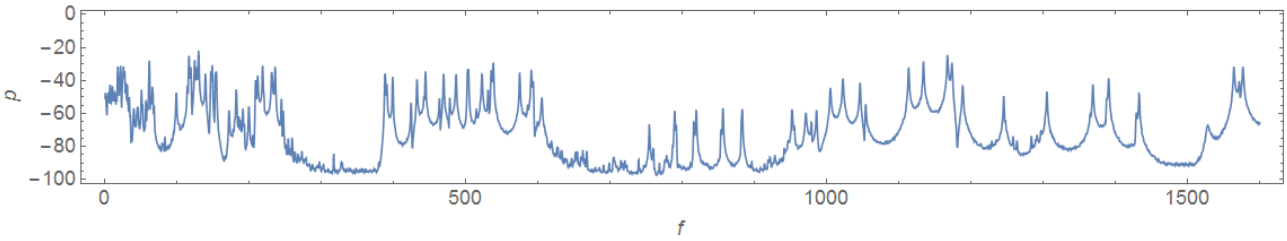

Figure G.2: Experiment 2, loading(I), LR

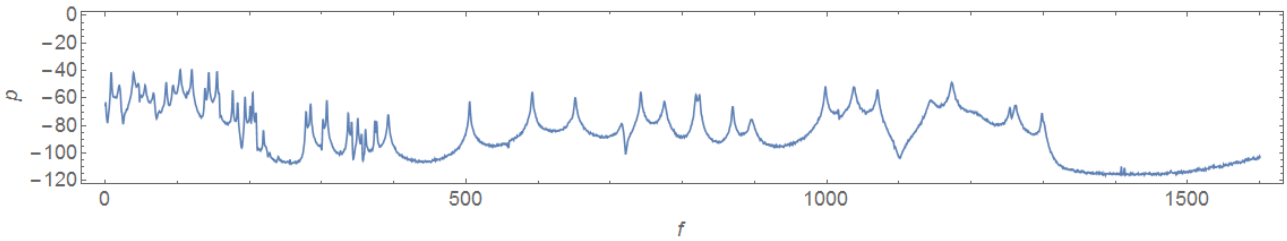

Figure G.3: Loading(I), SR

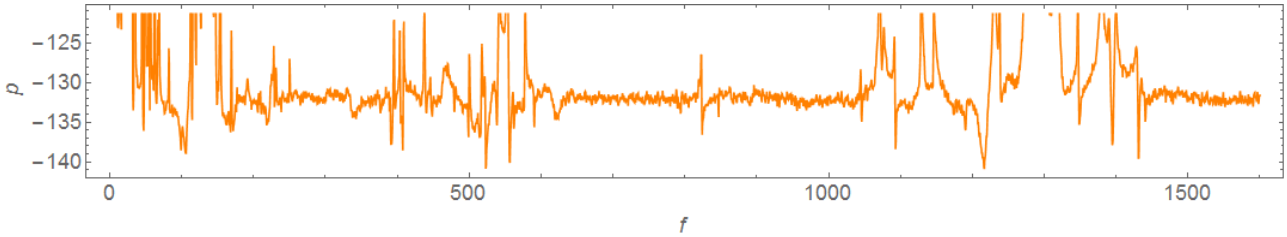

Figure G.4: Experiment 1, loading(II), LR

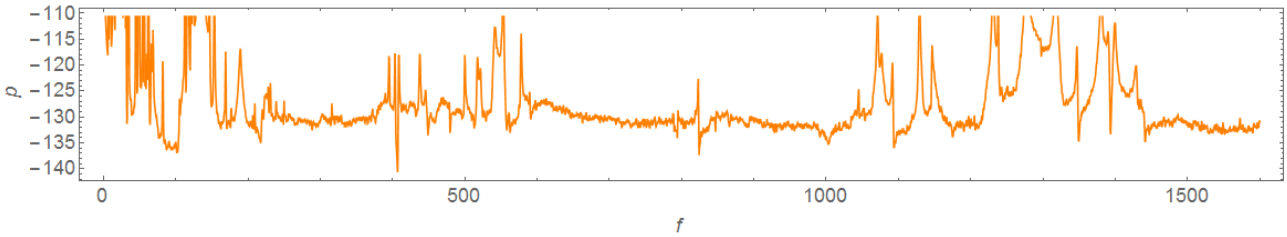

Figure G.5: Experiment 2, loading(II), LR

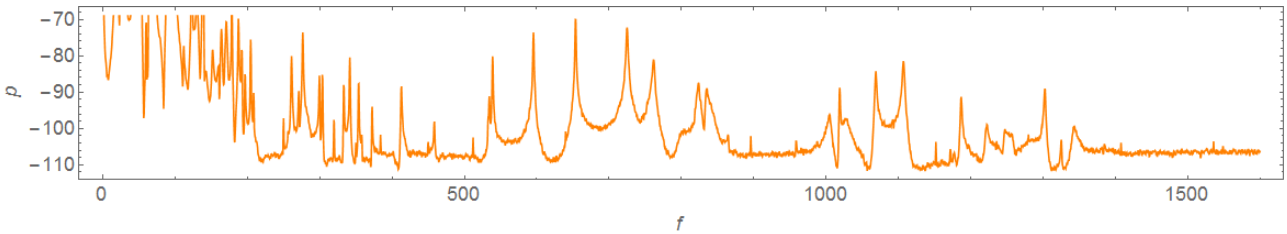

Figure G.6: Loading(II), SR

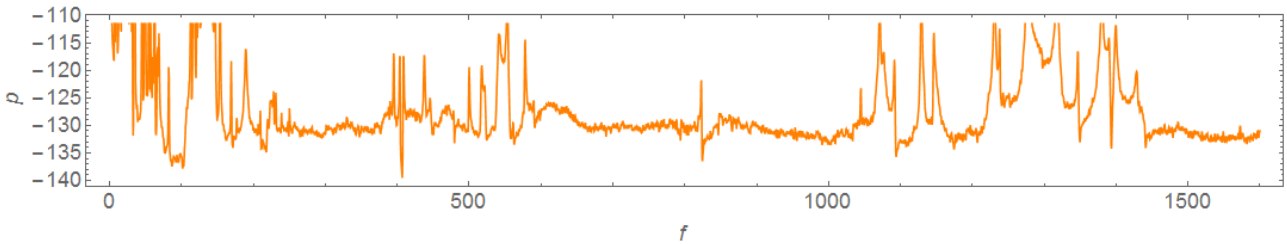

Figure G.7: Loading(II), higher force amplitude, LR

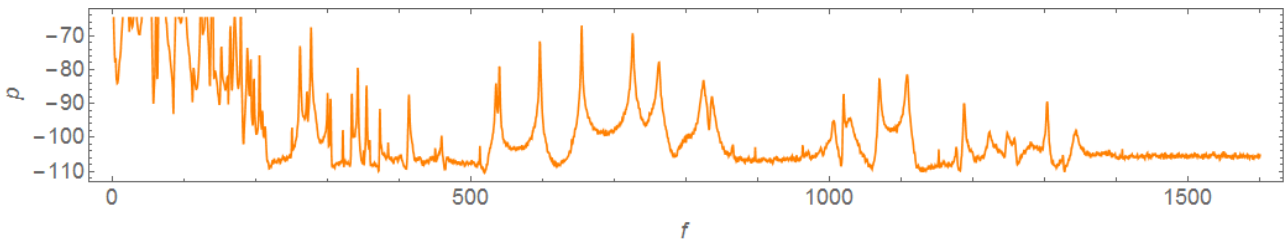

Figure G.8: Loading(II), higher force amplitude, SR

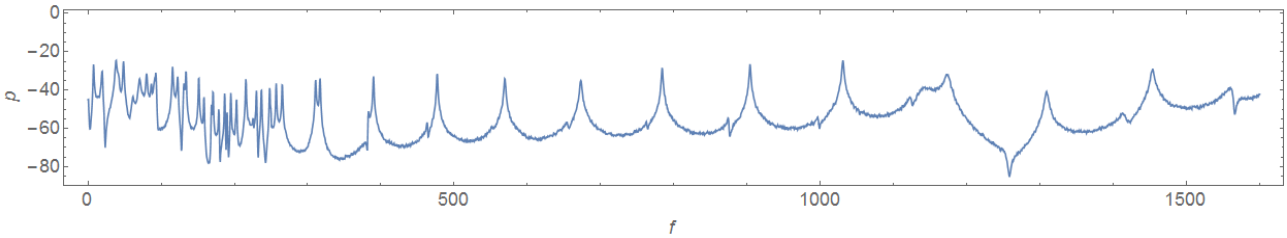

Figure G.9: Helical spring, loading(I), SR

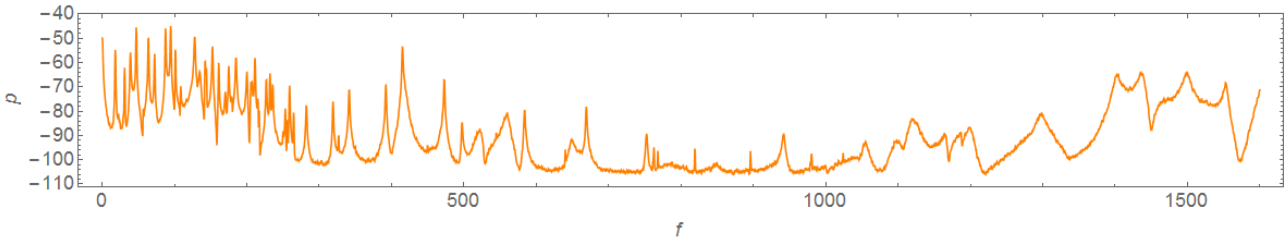

Figure G.10: Helical spring, loading(II), SR

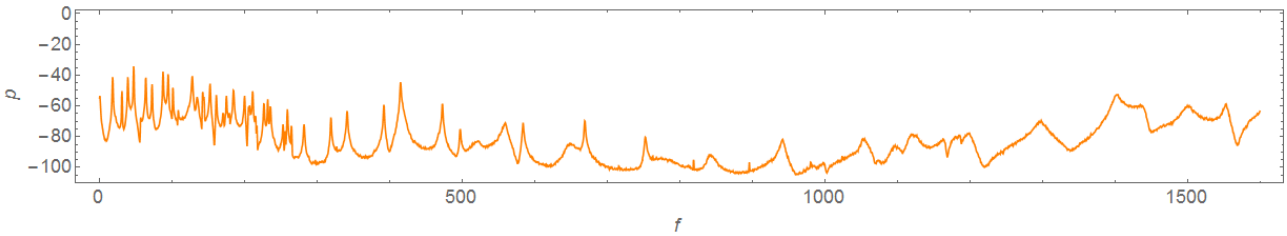

Figure G.11: Helical spring, loading(II), higher force amplitude, SR